2011

An experimental and numerical study of secondary flows and film cooling effectiveness in a transonic cascade

James C. Kullberg
University of Central Florida

AN EXPERIMENTAL AND NUMERICAL STUDY OF SECONDARY FLOWS AND FILM COOLING EFFECTIVENESS IN A TRANSONIC CASCADE

by

JAMES C. KULLBERG

A thesis submitted in partial fulfillment of the requirements
for the Honors in the Major Program in Mechanical Engineering
in the College of Engineering and Computer Science
and in the Burnett Honors College
at the University of Central Florida
Orlando, Florida

Spring 2011

Thesis Chair: Dr. Jayanta Kapat

ABSTRACT

In the modern world, gas turbines are widely used in aircraft propulsion and electricity generation. These applications represent a massive use of energy worldwide, so even a very small increase in efficiency would have a significant beneficial economic and environmental impact. There are many ways to optimize the operation of a gas turbine, but a fundamental approach is to increase the turbine inlet temperature to increase the basic thermodynamic efficiency of the turbine. However, these temperatures are already well above the melting temperature of the components.

A primary cooling methodology, called film cooling, creates a blanket of cool air over the surface and is an effective way to help protect these components from the hot mainstream gasses. This paper focuses on the effect of the film holes upstream of the first row of blades in the turbine because this is the section that experiences the highest thermal stresses. Many factors can determine the effectiveness of the film cooling, so a complete understanding can lead to effective results with the minimum flow rate of coolant air.

Many studies have been published on the subject of film cooling, but because of the difficulty and expense of simulating turbine realistic conditions, many authors introduce vast simplifications such as low speed conditions or linear cascades. These simplifications do not adequately represent the behavior of a turbine and therefore their results are of limited use. This study attempts to eliminate many of those simplifications.

The test rig used in this research is based on the NASA-GE E^3 design, which stands for Energy Efficient Engine. It was introduced into the public domain to provide an advanced platform from which open-literature research could be performed. Experimental tests on a transonic annular rig are time-consuming and expensive, so it is desirable to use experimental results to validate a computational model which can then be used to extract much more information. The purpose of this work is to create a numerical model that can be used to simulate many different scenarios and then to apply these results to experimental data.

DEDICATION

To My Wife

Who Humors My Research Efforts

ACKNOWLEDGEMENTS

I would like to thank my wife and family who help give me love and support and to our bird who did his best to hinder my research efforts.

I would like to thank Dr. Jayanta Kapat, my advisor, who taught me much about engineering, research, and dedication. I would like to thank my committee members: Dr. Weiwei Deng, Dr. Ali Gordon, and Dr. Ratan Guha for their time and support.

I would like to thank Tim Casey for mentoring me and for working with me on the experimental portions of this research and Sri Krishna for also mentoring me and working with me on the computational portions of this research. I would also like to thank all the members of CATER for helping me learn, develop, and grow.

Lastly, I would like to thank NASA for creating the E^3 model and FCAAP for providing funding. For computing resources, I would like to thank Dr. Guha for providing the Ariel cluster and Dr. Brian Goldeiz for providing the Stokes cluster to compute the solution. I would also like to thank the Star-CCM+ university program and Dr. Kapat for providing me with software licenses.

TABLE OF CONTENTS

LIST OF FIGURES

NOMENCLATURE

5HP	Five Hole Probe	
BR	Blowing ratio	
$CATER$	Center for Advanced Turbines and Energy Research	
CCD	Charge coupled device	
DR	Density ratio	
E^3	Energy Efficient Engine	
FCE	Film cooling effectiveness	
h	Heat transfer coefficient (HTC)	[W/m^{2}K]
HTC	See "h"	
ID	Inner Diameter	
MR	Momentum ratio	
η	Adiabatic FCE / cycle efficiency	
$\bar{\eta}$	Laterally averaged FCE	
$\bar{\bar{\eta}}$	Spatially averaged FCE	
nm	Nanometer	
OD	Outer Diameter	
ρ	Density	[kg/m^3]
P	Static Pressure	[N/m^2]
P_o	Total Pressure	[N/m^2]

PS	Pressure side (concave) of a turbine blade	
PSP	Pressure sensitive paint	
$q"$	Heat flux	[W/m^2]
$RANS$	Reynolds-Averaged Navier-Stokes	
SS	Suction side (convex) of a turbine blade	
T	Temperature	[K]
TSP	Temperature sensitive paint	
v	Velocity	[m/s]

CHAPTER 1: INTRODUCTION

1.1 Introduction to Turbines

Gas turbines are used throughout the world to provide efficient power in many applications, such as electrical power generation and aircraft propulsion. These applications represent significant energy usage worldwide, which dictates that turbines be run as efficiently as possible for economical and environmental reasons. Gas turbines can be designed to be more efficient by increasing turbine inlet temperatures, increasing component life, and decreasing energy losses.

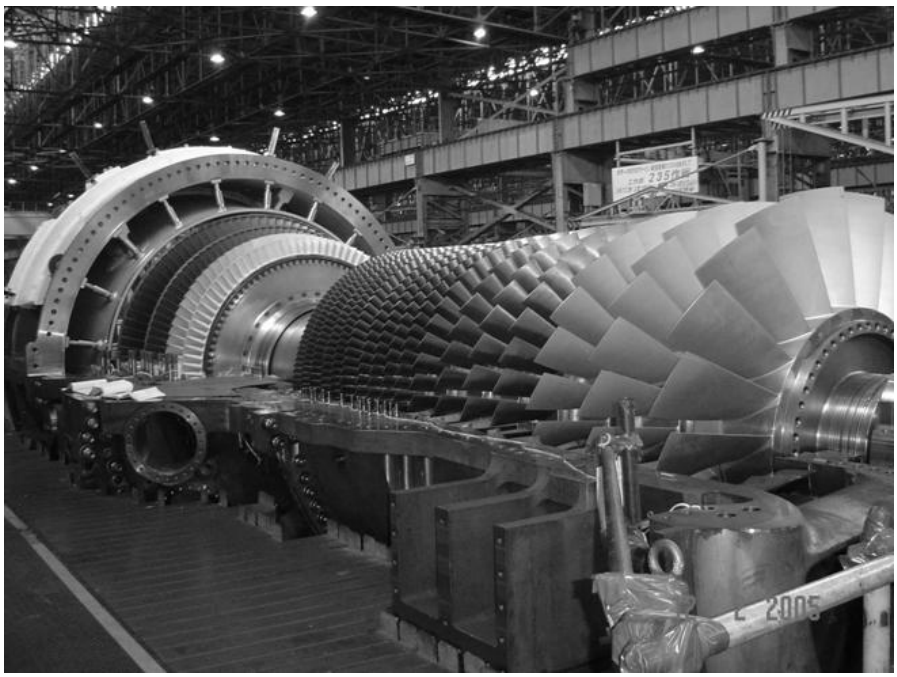

Figure 1: View of a partially disassembled power-generation turbine [1].

Increasing the turbine inlet temperatures can make a turbine more efficient because it operates on the thermodynamic Brayton cycle. The efficiency of this cycle is limited by the turbine inlet temperature as derived in Chapter 2. Increasing component life can make a turbine more efficient from an economic perspective. Turbine repair is expensive and time consuming, so a longer life can significantly reduce repair costs and downtime. Downtime for repair is very important because with a price that can range from $5-50 million (USD), it is unlikely that many entities have more than the minimum required.

The challenge of trying to achieve both higher temperatures and longer life simultaneously is difficult to overcome because the higher the temperature of the material becomes, the more the life of the components is reduced. The operational temperatures of turbine components, such as blades, are as close to the melting point as possible. At these temperatures, the components exhibit creep, deformation due to high temperatures and loads for an extended period of time. Under these conditions, an increase in component temperature of 25°C could halve its operational life.

Turbine inlet temperatures are not the same as material temperatures. Currently, temperatures inside turbines well exceed the melting temperatures of the components. Such high temperatures are made workable by using thermal barrier coatings, film cooling, and internal blade cooling. This thesis is focused on two major aspects of film cooling, namely (i) the effects of film cooling on the aerodynamic losses and (ii) the effects of secondary flows on the film cooling effectiveness. Further advances in film cooling will permit higher inlet temperatures

while still maintaining component life. The figure shown below illustrates the rise in the turbine inlet temperature over time.

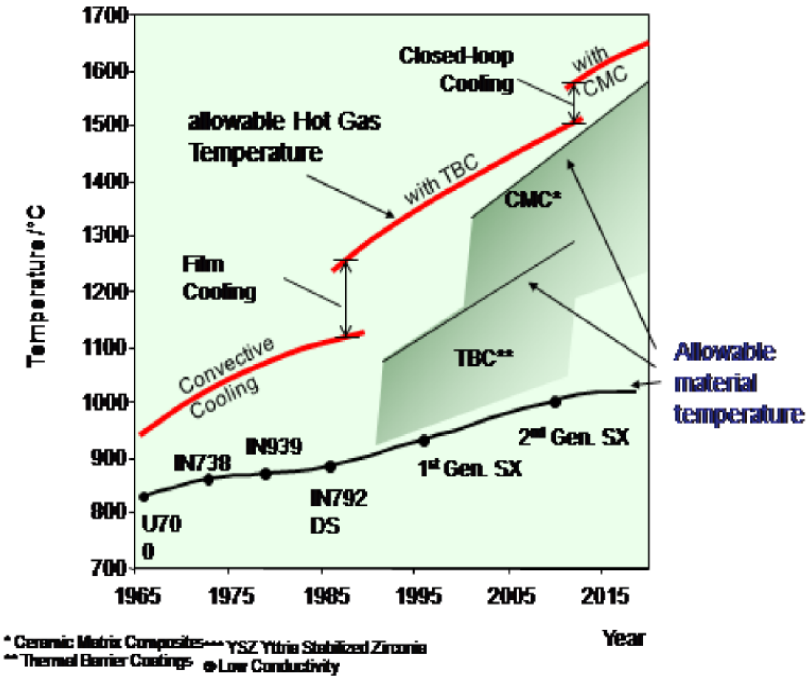

Figure 2: Illustration showing increase in turbine inlet temperature over time. [1]

1.2 Introduction to Film Cooling

Film cooling involves extracting relatively cool air, approximately 900 K, from the compressor stage of the turbine and injecting it onto the surface of components in the turbine. This effectively creates a protective blanket of cool air that protects the surface from the extremely hot gases.

In the early days of film cooling, cooling air was introduced through wide slots. However, this approach created stress concentrations and weakened the turbine structurally.

Because of this, research has been mainly focused on other types of film cooling. The most notable has been discrete-hole film cooling. This approach started out as being much less effective than slot cooling, but has been extensively refined over the last 40 years, notably pioneered by Goldstein and Eckert [2]. Now, discrete-hole film cooling uses complicated geometries such as shaped holes and trenched film cooling that provide relatively efficient cooling.

Film cooling is used in many regions of the turbine assembly and each blade can contain hundreds of holes to ensure full film coverage. Even small defects could result in a high temperatures that would lead to decreased component life and possibly even catastrophic failure. Simply overcompensating with high safety factors is not sufficient because this increased coolant bleed from the compressor would negatively affect the turbine's efficiency and offset the potential benefits of film cooling. Also, excessive amounts of coolant may simply lift off from the surface and not provide any cooling effect. The possible scenarios are shown below.

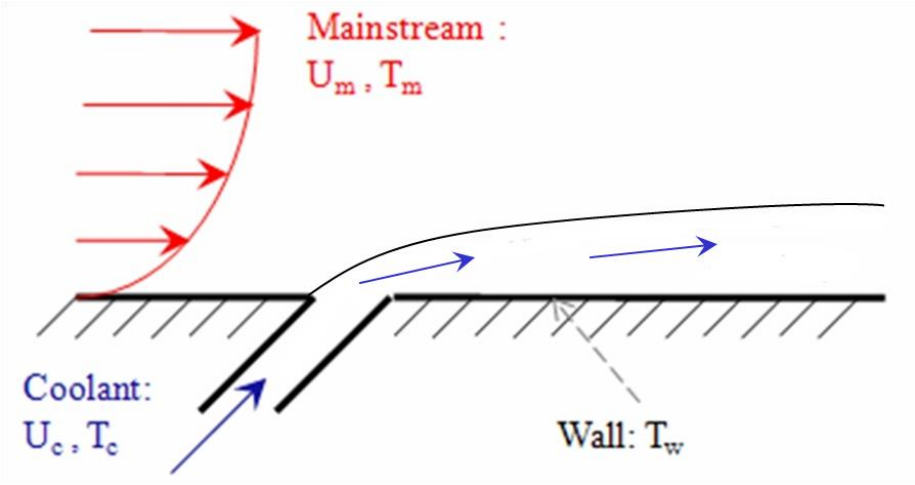

Figure 3: Film cooling properly attached to wall, good cooling.

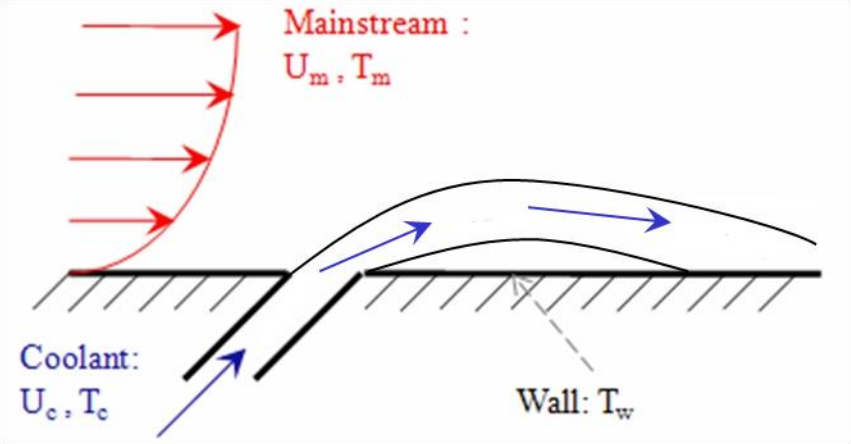

Figure 4: Film cooling reattached to wall, less cooling.

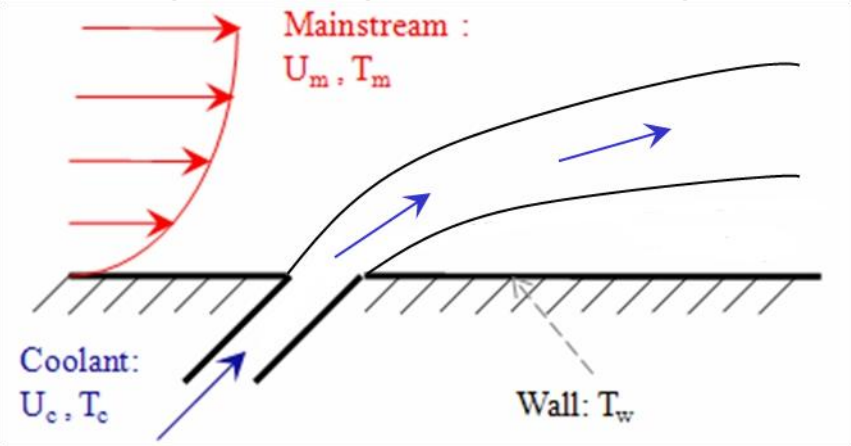

Figure 5: Film cooling separated from wall, no cooling.

The motivation for this study of film cooling is to gain an understanding of how the complicated secondary flows inside a turbine disrupt the coolant blanket discharged from the holes. These flow conditions are complex and cannot be perfectly represented with modern technology yet. However, engineers still need to be able to produce reliable and efficient turbines, so further research is needed to understand how to compensate for these flows and protect the components as efficiently as possible.

CHAPTER 2: PROBLEM DEFINITON

2.1 General Problem

Around the world, people are consuming more energy per capita than any previous time in history while inexpensive supplies of energy are being depleted quickly. Many alternative sources of energy are being explored, such as wind and solar power, but in the near future, they will still be prohibitively expensive and only provide a tiny fraction of the global energy usage. Many steps are being taken on the consumer level to increase the efficiency of appliances and climate control, but a large energy need still exists. This issue is best dealt with at the source, where almost all electric power is produced by power-generation turbines.

Gas turbines are one of the main types of power-generation turbines and they also power the majority of air transportation and some large marine propulsion systems. They operate on the thermodynamic Brayton cycle, which is illustrated in below in Figures 2 and 3. A cross-sectional view of a turbine is provided in Figure 4 to show how the Brayton cycle is practically implemented. The first stage of the cycle occurs in the compressor where air is taken in from the environment and compressed to a high pressure. The next stage occurs in the combustor, where the heat is added while the compressor air is maintained at constant pressure. Finally, these hot gases expand through the turbine, producing power.

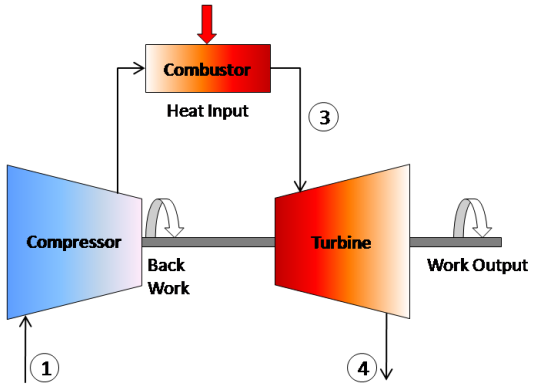

Figure 6: Brayton cycle illustration.

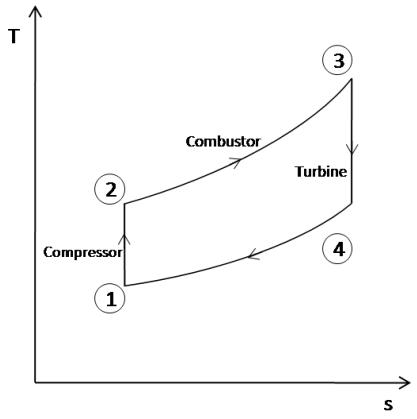

Figure 7: Brayton cycle shown on T-s diagram.

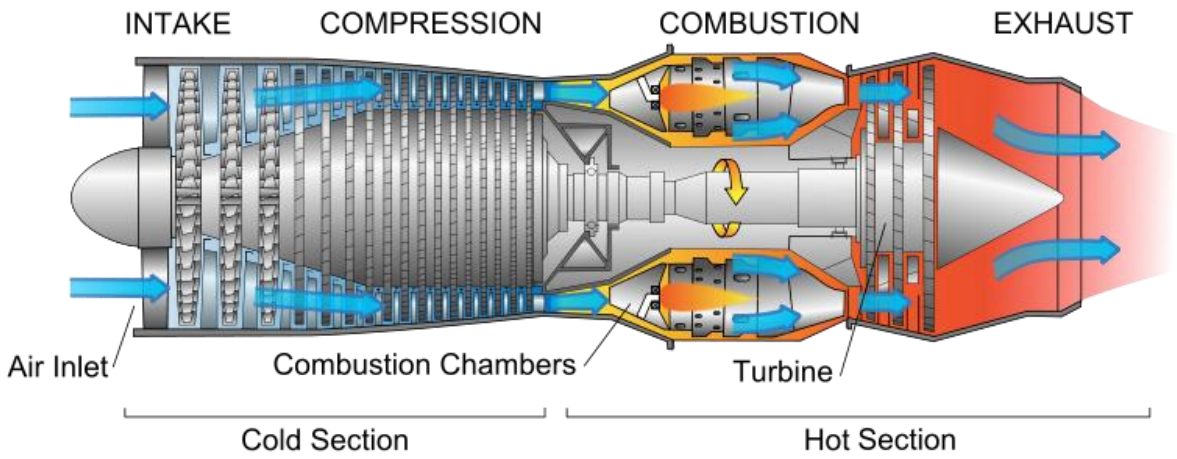

Figure 8: Aircraft-propulsion gas turbine illustration with labels [3].

The need for high efficiencies in the modern world is apparent and because turbines are so widespread, they are a very productive target. Even an efficiency increase of only a fraction of a percent can save millions of dollars worldwide. This demonstrates the importance of the work of turbine designers who seek to discover new technologies to achieve higher efficiencies. These can be attained by increasing the cycle efficiency, decreasing energy losses, or increasing

component life. One of the most fundamental techniques used to raise cycle efficiency is to raise the turbine inlet temperature. The efficiency of the Brayton cycle is derived below for an isentropic process.

$$\eta_{Brayton} = \frac{Q_{in} - Q_{out}}{Q_{in}} = 1 - \frac{T_4 - T_1}{T_3 - T_2} = 1 - \frac{T_4\left(1 - \frac{T_1}{T_4}\right)}{T_3\left(1 - \frac{T_2}{T_3}\right)} \quad (1)$$

$$Isentropic: \frac{T_1}{T_4} = \frac{T_2}{T_3} \qquad \eta_{Brayton\ \ Isentropic} = 1 - \frac{T_4}{T_3} \quad (2)$$

The efficiency is closer to 100% when the fractional term is equal to zero. If T_3 is raised, it will bring the fractional term closer to zero and increase the isentropic efficiency of the Brayton cycle. However, $T_{3,}$ or the turbine inlet temperature, is already well in excess of the component melting temperature, so a delicate balancing act must be carried out.

Components are cooled by film cooling; the cooler these metal surfaces are, the higher component life is. However, if these surfaces are sufficiently cooled, the inlet temperature of the turbine can be raised slightly to improve efficiency and then component life is decreased again. Any amount of excessive coolant that is injected into the mainstream flow represents an inefficiency that should be removed because this leeches a greater fraction of air from the compressor that could be utilized to produce power. This means that this area must be studied in depth to provide the maximum balance of efficiency and component life.

2.2 Specific Problem

One of the most widely used techniques used to cool a turbine's surface is film cooling. This involves a flow of cool air that acts as a blanket and protects the surface from the hot gasses. This cool air is bled from the compressor stage of the turbine and selectively injected into the turbine stage to cool components exposed to high temperatures. The manner in which this coolant is injected requires much study because of the complex flow conditions.

However, film cooling comes at a price. When air is removed from the compressor stage and utilized for film cooling, this results in an efficiency loss because back work had been used to compress it, but additional energy was not able to be extracted from it in the turbine stage. If too much of this valuable air is used in film cooling, the overall efficiency of a turbine could be significantly lowered through film cooling.

This occurs to some extent in modern gas turbines because highly complex secondary flows inside the turbine disrupt the cooling blanket and tears it off the surface of the turbine components. Because the flow conditions are turbulent and highly complex, a mathematical model has yet to be proposed. However, engineers still need to produce reliable and efficient turbines, so turbine designers must overcompensate with high factors of safety to ensure turbine life is maintained. However, as the world continually pushes for higher efficiencies and less carbon production, this is not satisfactory. The flows inside a turbine need to be understood intimately so that film cooling can be as efficient as possible.

Even though these secondary flows are very important and need to be understood, their characteristics have not been extensively studied in turbine realistic conditions. The cost of recreating these conditions is very high, so many researchers vastly simplify their models. Most often, the choice is made to use two-dimensional blades and a linear endwall. However, research has shown that an annular endwall can lead to different secondary flows. The model studied in this thesis uses an annular endwall, high-speed conditions, and a three-dimensional NASA-GE E^3 blades to represent turbine conditions as close as possible. This cascade has been validated to ensure that periodicity has been achieved in this cascade.

The usefulness of a film cooling scheme can be evaluated in several ways. One of these is referred to as film cooling effectiveness (FCE) which is defined as:

$$\eta(x,y) = \frac{T_{adiabatic\ \ wall}\,(x,y) - T_{recovery}}{T_{coolant} - T_{recovery}} \tag{3}$$

However, this determines the effectiveness at a given point, which is not useful when determining trends or the entire effectiveness over the surface. Because of this, equations 4 and 5 were created to determine laterally and spatially averaged effectiveness respectively.

$$\bar{\eta}(x) = \frac{\int \eta(x,y)\,dy}{\int dy} \tag{4}$$

$$\bar{\bar{\eta}} = \frac{\int \eta(x,y)\,dxdy}{\int dxdy} \tag{5}$$

Another method that is used is referred to as the heat transfer coefficient (HTC). This is based on the convective definition of heat transfer where "h" represents the HTC. This is useful

because sometimes the surface can be well covered in the FCE definition, but the injection created so much mixing that the surface is no more protected. The HTC definition is defined as:

$$q" = h(T_{fluid} - T_{wall}) \tag{6}$$

In order to study this effectiveness and its relation to the coolant flow, a definition must be created to describe the coolant flow rate. The first method simply compares the density of the coolant to the density of the mainstream, which is referred to as the density ratio (DR). The major method used in literature compares the mass flux of the coolant with the mass flux of the mainstream flow, called the blowing ratio (BR). An alternate method that is useful for determining penetration compares the momentum fluxes of the coolant and mainstream flow and is called the momentum ratio (MR).

$$DR = \frac{\rho_c}{\rho_m} \tag{7}$$

$$BR = \frac{(\rho V)_c}{(\rho V)_m} \tag{8}$$

$$MR = \frac{(\rho V^2)_c}{(\rho V^2)_m} \tag{9}$$

2.3 Research Questions

To create efficient film cooling in gas turbines, both the effects of the film cooling parameters and their interaction with secondary flows must be well understood. Film cooling is governed by a number of factors such as flow conditions: blowing ratio, density ratio, or momentum ratio, and geometric parameters: inclination angle, compound angle, length to diameter ratio, and pitch to diameter ratio. It is desirable to determine relations between the various parameters so that turbine designers can make informed decisions. Much research has been carried out in low-speed, linear, two-dimensional cascades, but these do not adequately represent turbine conditions. These models can be occasionally used to predict trends, but (i) differences in compressible and incompressible flow and (ii) differences in secondary flows between two and three-dimensional test cases can be very significant and cause very different trends.

The NASA-GE E^3 transonic cascade at the CATER facility is a solution to some of these issues. This experimental rig can operate at turbine realistic speeds and contains annular endwalls and three-dimensional blades. However, obtaining experimental results from this rig is a time-consuming and expensive process. In many cases, it would be unrealistic to obtain a full understanding of the flow and heat transfer because of uncertainties and instrumentation access and resolution. Therefore, it is desirable to create a detailed computational model of the experimental setup and validate it using experimental results. Accomplishing this could help reduce the cost of future research and help provide new insights that would not have been observable in the experimental flow field alone.

2.4 Thesis Objectives

The objective of this thesis is to develop a detailed and flexible computational model of the NASA-GE E^3 experimental rig in the CATER facility that can be used in the current study and for many variations to come such as shaped holes, various inclination and compound angles, and purge cooling, cooling from the rotor-stator clearances. Next, several cases will be solved numerically, which will be used to compare with experimental data to predict the performance of future tests. This study will focus on the effectiveness of film cooling on the cascade endwall, the pressure distribution along the endwall and blade surface, the pressure distribution along the inner and outer endwalls, and the total pressure losses at the exit of the cascade with and without film cooling.

While extensive research has been performed on the subject of film cooling, this thesis is novel, significant, and useful. This thesis is novel because few publications in the open literature have studied film cooling in a high-speed, annular, three-dimensional cascade. This means that the results of this study will be more realistic than previous research. This research is significant because it may lead to improvements in film cooling, which would extend the life of gas turbines and let them operate more efficiently. Because turbines represent a significant part of the world economy, such as power generation and aircraft propulsion, this would have important effects. Finally, this work is useful because it may lead to film cooling improvements which will allow turbine designers to develop a greater understanding of how to effectively use film cooling and help guide further research in this field.

CHAPTER 3: LITERATURE REVIEW

3.1 Background (Early Literature to 1999)

Film cooling was originally developed as a technique used to de-ice airplane wings. However, the idea soon took hold in other areas such as rockets and turbines. Some of the earliest papers in film cooling available, Goldstein et al. [2] and Knuth [4], deal with film cooling in the combustion chamber of rockets. Unfortunately, much of the research conducted in rocketry deals with supersonic flows, helium, and changing phases, which are not applicable to gas turbines.

Some of the most basic work in film cooling on turbines was pioneered by Goldstein and Eckert et al. [5]. They experimented with various types of holes and concluded that their shaped holes were superior to standard cylindrical holes because the larger mouth lowered the momentum ratio and helped the jet remain attached to the wall. One note to remember from this study is that there seems to be a discontinuity in the literature. Some literature states that lower blowing rates are more effective while others state that higher blowing rates are more effective. It is the author's opinion that this is likely because of the level of turbulence in the flow, the angle of the injection hole, or simply different delineations of blowing rate. The fundamental agreement of all these papers has been that blowing rates and angles that cause the coolant to separate and enter the main-flow are ineffective. The other important difference, which will be referenced further on is that turbulent flows seem to have a resistance to penetration by the

coolant steam and therefore higher blowing rates can be effective in turbulent flows that would cause separation and lift-off in a more laminar flow.

One of main concerns in gas turbine film cooling is secondary flows in turbine cascade passages. By definition, these flows do not follow the path of the main-flow and are often manifested as vortices that cause high heat transfer to occur on turbine components. Much literature is dedicated to understanding and compensating for these flows. Langston [6] wrote a fundamental paper on these secondary flows in which he found that there are strong crossflows that make traditional assumptions about the boundary layer invalid. As shown in Figure 7, there are large crossflows on the suction side of the vane, including the passage vortex crossing the passage toward the suction side, while there are some small vortices on the pressure side of the vane, not pictured. These are some of the reasons that a blade passage is so difficult to model theoretically. Fitt et al. [7] attempted to approach the topic of film cooling analytically, but was forced to make a great number of assumptions to sufficiently simplify his equations.

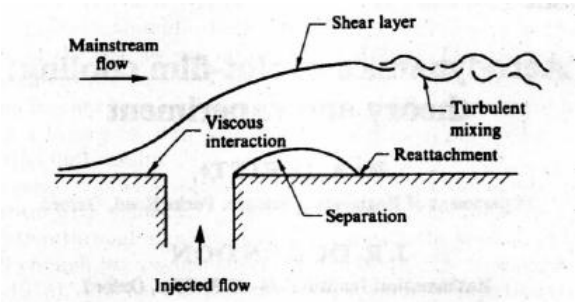

Figure 9: Basic film cooling diagram [7].

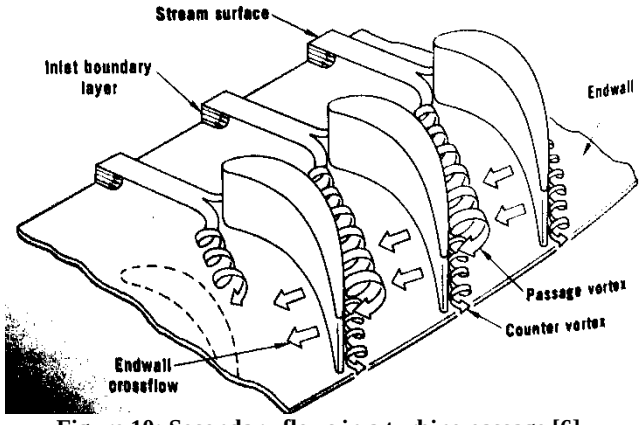

Figure 10: Secondary flows in a turbine passage [6].

Friedrichs et al. [8][9], also studied endwall film cooling and used a method with oil and dye to visualize the effect of these secondary flows on the endwall, shown below. He also mapped the total pressure due to the addition of film cooling, which is an important comparison for the pressure losses examined in this study, even though his work only involved a two-dimensional cascade.

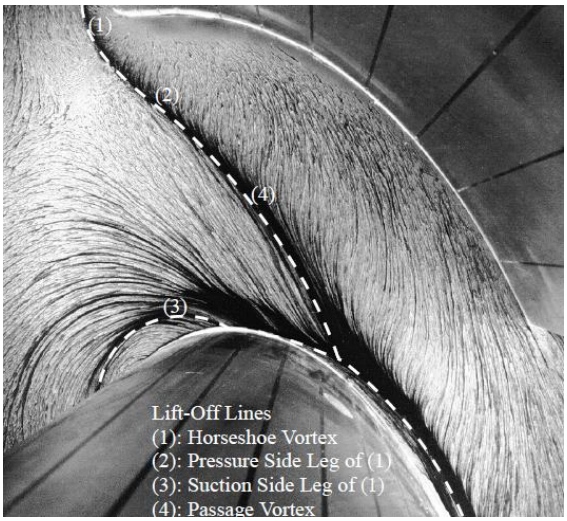

Figure 11: Secondary flow visualization without film cooling [8].

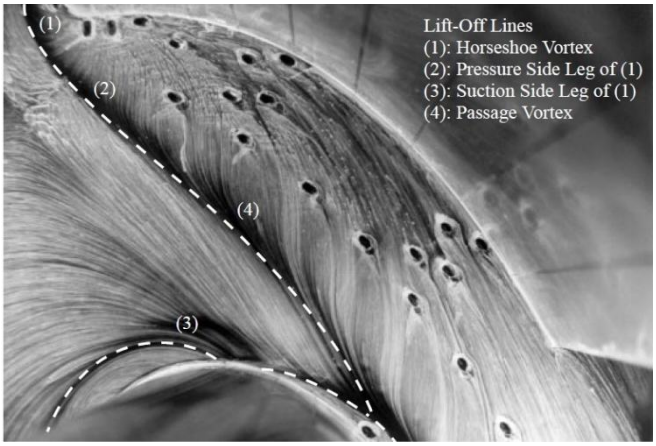

Figure 12: Secondary flow visualization with film cooling [8].

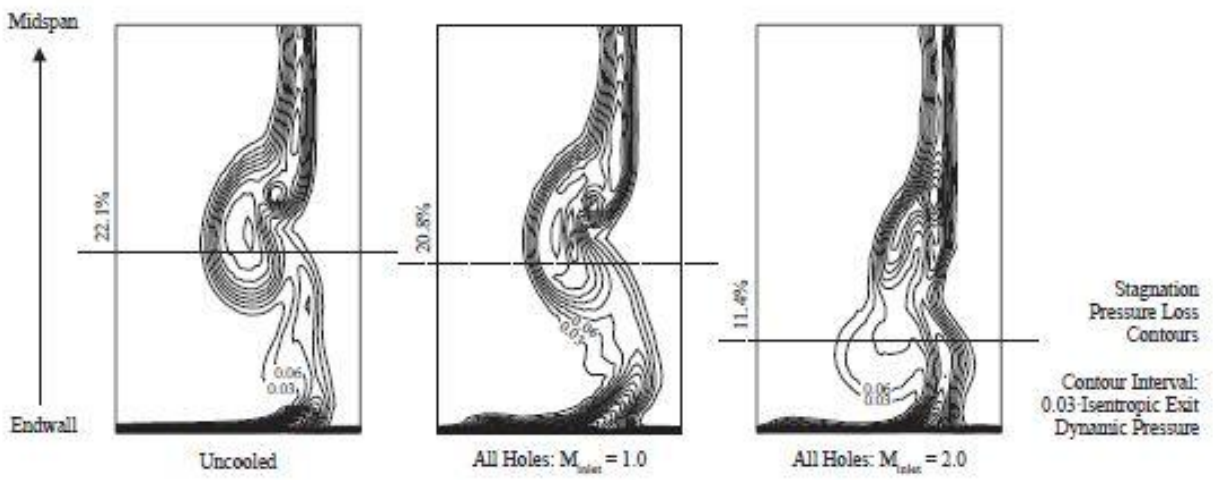

Figure 13: Total pressure loss contours based on the addition of film cooling [9].

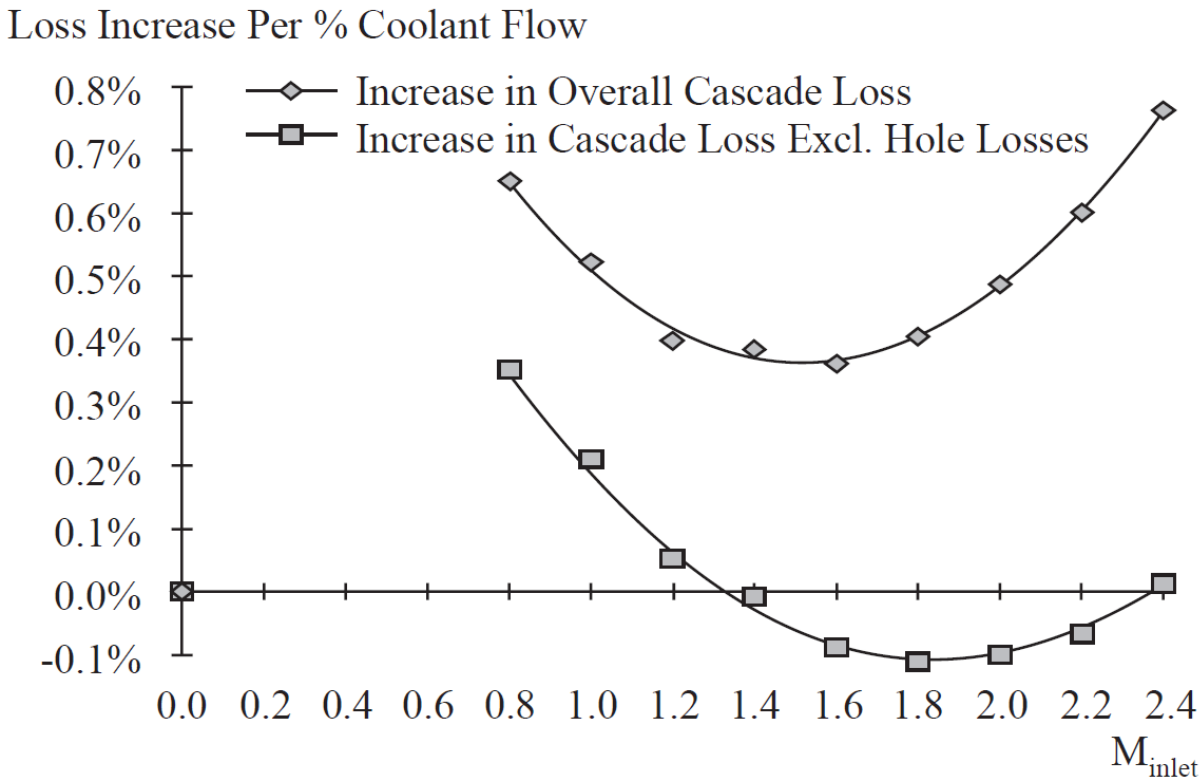

Figure 14: Percentage loss increase per percentage of coolant flow [9].

Sinha et al. [10] studied the effect of density ratio in conjunction with blowing ratio and determined that density ratio is an important parameter in determining the effectiveness of film cooling and that momentum flux is a factor that controls how well the coolant jet will adhere to the surface. Another author, Ammari et al. [11][12], also focused on density ratios, but also varied the coolant injection angle. He noted that many authors use density ratios of close to 1.0 in their experiments, while a turbine experiences ratios of closer to 1.5 or 2.0. The author found that the HTC increased with injection, but higher density ratios helped to decrease this trend. Other findings were that higher injection angles caused higher HTC close to the hole while lower injection angles caused higher HTC further downstream from the hole. Acceleration in the mainstream flow also helped to reduce the HTC from the coolant by suppressing injection-induced turbulence. These findings indicate that a turbine will experience higher effectiveness values than predicted by studies because of the high accelerations and density ratios. This means that if the blowing rates for film cooling in turbines were selected from previous studies that did not take these effects into account, the blowing ratio will not be high enough and cooling would not be as effective as expected.

An important paper was written by Bons et al. [13] which described the impact of high turbulence on film cooling effectiveness which has a significant effect that is often ignored in low speed experiments. In this study, the authors found that high turbulence lowered the effectiveness of low blowing ratios because it was swept away from the surface. High blowing ratios were very effective because the turbulence trapped it near the wall and was not able to disperse it. Additionally, this was done with a density ratio of 1.0, so it would be even more

effective with more realistic conditions. This study opposes earlier and more simplistic studies that found the opposite outcome. This shows the importance of simulating turbine conditions as closely as possible.

One important facet of film cooling is the shape of the hole. A particular study carried out by Grirsch et al. [14] tested various shapes in discrete-hole film cooling and found several geometrics much more effective than a normal cylindrical hole. Similar geometries should be studied with slot cooling to see if they can help increase effectiveness. The authors also showed that a transonic flow produced more effective results than subsonic flow, confirming the results of other literature.

Kohli et al. [15] studied the effects of high turbulence on film cooling. Unlike previous studies [14] where the turbulence helped anchor the high blowing ratios streams to the wall, this study found that very turbulent conditions caused the main-flow to pass through the coolant and reach the wall. The differences in these studies are probably based on varying levels of turbulence and thickness of the coolant blanket. It appears from these studies that at any given turbulence level, there is a corresponding optimum blowing rate that needs to be determined experimentally.

For completeness, it should be noted that turbines experience pulsations in the flow. This study will not pursue this added complexity, but it is an important area in turbine research that needs have its effect tested alongside film cooling. Dr. Ligrani has done a significant amount of work in this field. He collaborated in the studies of Bell et al. [16] and Ligrani and Bell [17],

which test the effects of pulsations on various film cooling setups. The authors found that these pulsations have significant effects that disrupt the cooling from its normal steady state behavior.

3.2 State of the Art Review (2000-2011)

This portion of the literature review focuses on more recent and directly relevant literature. The most relevant studies to this thesis are Nguyen et al. [18], Casey [1], Casey et al. [19], and Nguyen [20]. All of these studies are based on experimental and computational results previous carried out on the NASA E^3 cascade at the CATER facility. Nguyen et al. [18] records preliminary validation data for the cascade which includes the pressure distributions along the inner and outer endwalls and across the inlet and exit of the cascade. Casey [1] measured the pressure loss data at the exit of the cascade using a five hole probe (5HP) to determine the pressure losses and behavior of the secondary flows and how they were affected by the addition of film cooling. Casey et al. [19] studied the effectiveness of film cooling along the inner endwall of the cascade using the temperature sensitive paint technique. Nguyen [20] performed a computational study of the interaction between film cooling and secondary flows in two and three-dimensional conditions. The results of this paper important, but they do not model the experimental setup used in the CATER facility, so they which are of limited use for the purposes of this study. A plot comparing Nguyen's study to a previous 2D cascade test is shown below that is compared to the work of Kopper et al [21]. Relevant work that does not directly pertain to the experimental setup at the CATER facility is discussed after.

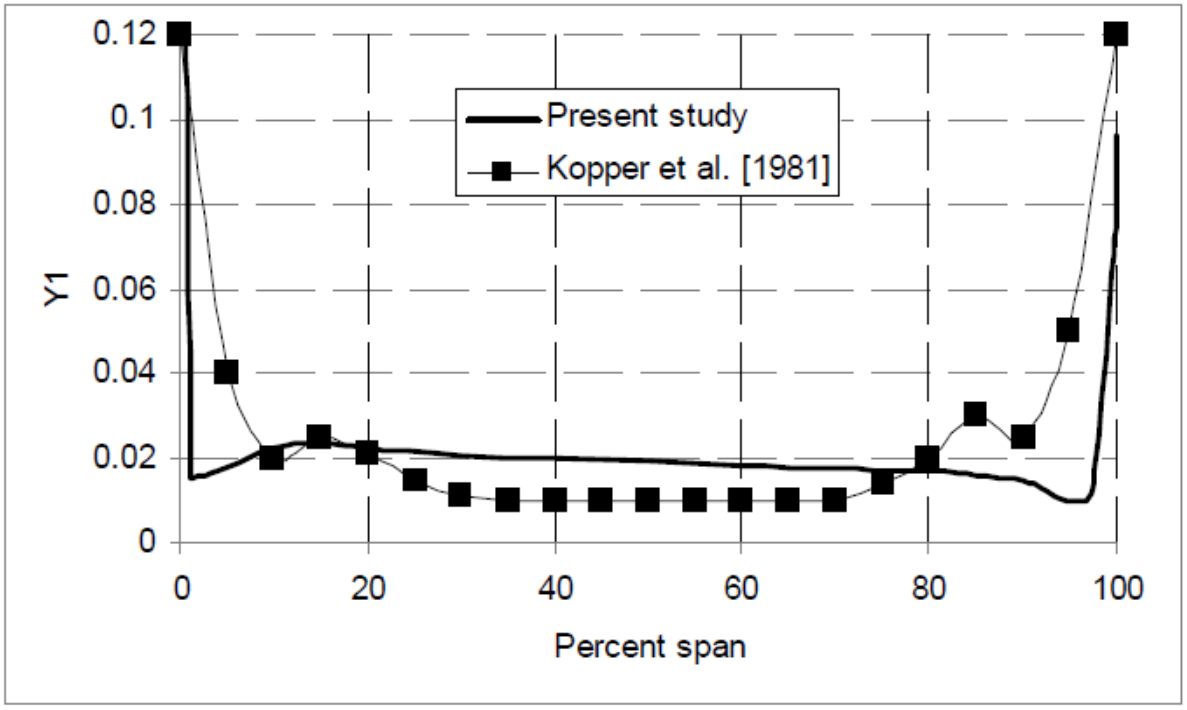

Figure 15: Pressure Loss Coefficient plotted spanwise in E^3 cascade [20].

Kost [22] and Nicklas [23] wrote a two-part paper that explores film cooling on an endwall under transonic flow. Kost's work focused on aerodynamics, utilizing a test setup that consisted of 19 film holes per passage arrayed in three rows and angled at 35°. He found that the coolant coverage of the endwall varied significantly from the expected values due to the average blowing ratio. This was because on the suction side where the flow has high kinetic energy, the local blowing ratio was relatively low and the coolant was forced against the wall. However, near the pressure side, the flow had low kinetic energy and therefore the local blowing ratio was very high and the coolant lifted off of the surface. The images below illustrate these effects well. The author suggested that the coolant coverage was poor on the suction side because of limitations of the measurements system and the effects of the suction side leg of the horseshoe

vortex. These images also demonstrate the important effect that the coolant flow decreases the endwall crossflow because it adds mass to and thickens the endwall boundary layer, allowing it resist the effects of the pressure gradient in the passage. This study shows that film cooling can be used effectively to provide effective cooling even in unfavorable areas such as the pressure side of the passage.

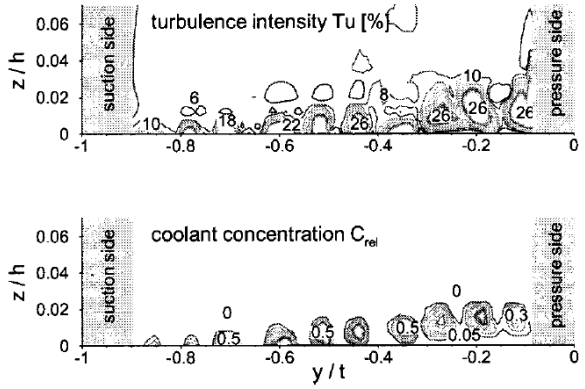

Figure 16: L2F measurements at 10% chord [21].

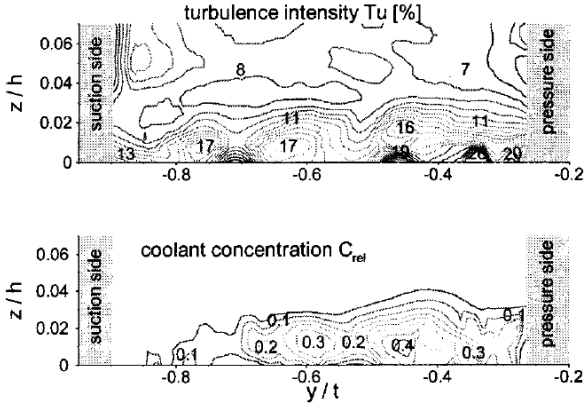

Figure 17: L2F measurements at 35% chord [21].

Nicklas [23] focused on heat transfer and film cooling effectiveness using the same film cooling setup as Kost [22]. He showed that the heat transfer increased 300% compared to a no film ejection case because the purge flow behind the film holes strengthened the horseshoe vortex and reduced the effectiveness of the film cooling. This demonstrates the need for research to not simplify experimental setups or critical flow-field patterns may be overlooked. Nicklas also verified the findings of Kost that even in this case, the coolant was able to decrease the strength of the passage vortex, probably due to the strengthening of the boundary layer on the endwall. Like Kost, he also found that the injection of coolant increased the turbulence of the flow, which results in total pressure loss and should be observable at the cascade exit.

Zhang and Jaiswal [24] studied film cooling on an endwall using pressure sensitive paint (PSP). This technique is similar to future approach that is planned to be implemented at the CATER facility. The mass transfer technique in this paper is different from the heat transfer approach shown in previous studies. This provides a good comparison case because it avoids certain errors, such as heat conduction through the endwall. The authors found that for low blowing rates, the normal endwall secondary flows dominated, but higher blowing rates the secondary flows are suppressed by the coolant flow. This verifies previous works and provides a good expectation of how blowing rates will affect post-cascade exit losses.

Thole and Knost [25] performed a study using both film and slot cooling in a linear, low speed cascade. The authors found that using both types of cooling at higher flow rates overcooled the endwall and suggested removing the film cooling holes and only relying on purge cooling. This is an interesting finding that suggests that current turbine designs may be overcooling the endwall if they are using the sufficient purge cooling to prevent the entrainment of mainstream gases. However, previous studies such as Nicklas seem to contradict this because in that case, the purge flow enhanced the horseshoe vortex and intensified the need for film cooling. This difference is likely due to the low-speed cascade conditions used in this study, which is not turbine representative.

Hung and Chen [26] studied film cooling over a curved endwall with film cooling at various compound angles. This study is useful because it can be used to understand the behavior of a coolant stream on a curved endwall when not affected by blades. The authors show that expanded geometry at the film hole exit leads to better performance because this lowers the

momentum flux, allowing the flow to stay attached to the surface. This is significant on a turbine's inner endwall, which is convex in shape. Hung states that when lift-off occurs on convex surfaces, cooling effectiveness is significantly reduced because the flow is unlikely to reattach. Another finding of the authors was that compound angle injection also increases the film cooling coverage, but this approach does cause increased mixing with the mainstream and therefore increases turbulence. The net result of this interaction is the same as injection in-line with the flow, which suggests that there are few benefits to compound angle injection. The figures below illustrate this effectively where Models A and B have no compound angle and A is a simple hole while B has a shaped geometry. Models C and D are both shaped and have a compound angle.

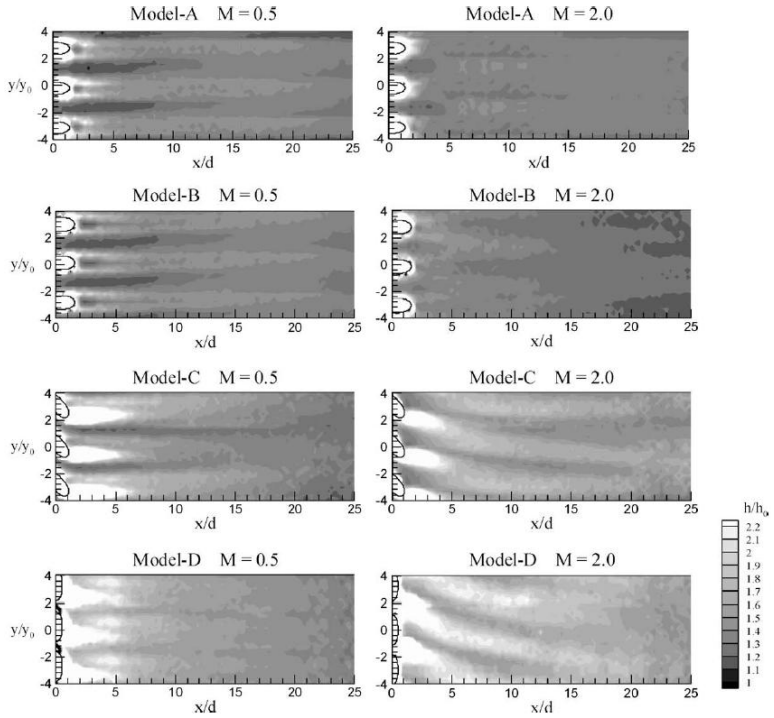

Figure 18: HTC ratio on a convex surface with various hole geometries [25].

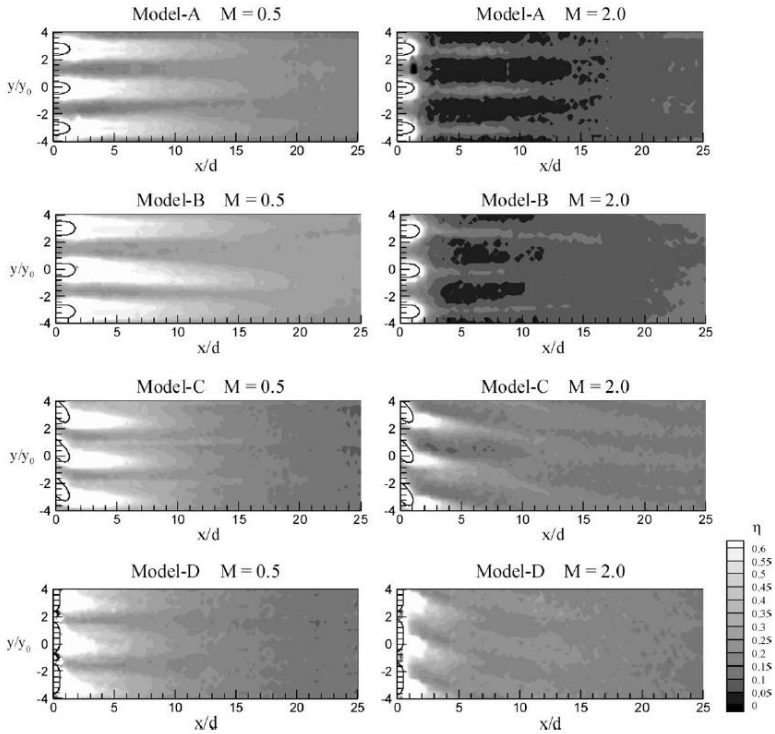

Figure 19: Film effectiveness ratio on a convex surface with various hole geometries [25].

Bogard and Thole [26] published a strong overview of film cooling in gas turbines that covers many important research topics. They discuss how many studies focus only on cooling effectiveness, while the HTC must be closely studied to ensure that the heat flux through the surface is decreased. This is especially important with compound angle holes and supports the work of Hung and Chen [27]. They also discuss how many tests are carried out at low turbulence values, which lead to incorrect conclusions. In a gas turbine, where mainstream turbulence levels are much higher, an optimal momentum flux ratio is an order of magnitude higher than it was shown to be in the experiment. This shows the need for more realistic studies to ensure that turbine designers have accurate resources. The authors also provided a set of images that illustrate the various attachment conditions that film coolant can experience. As discussed previously, Case (a) is the desired state, while Case (c) is usually damaging due to the higher HTC caused by the additional mixing.

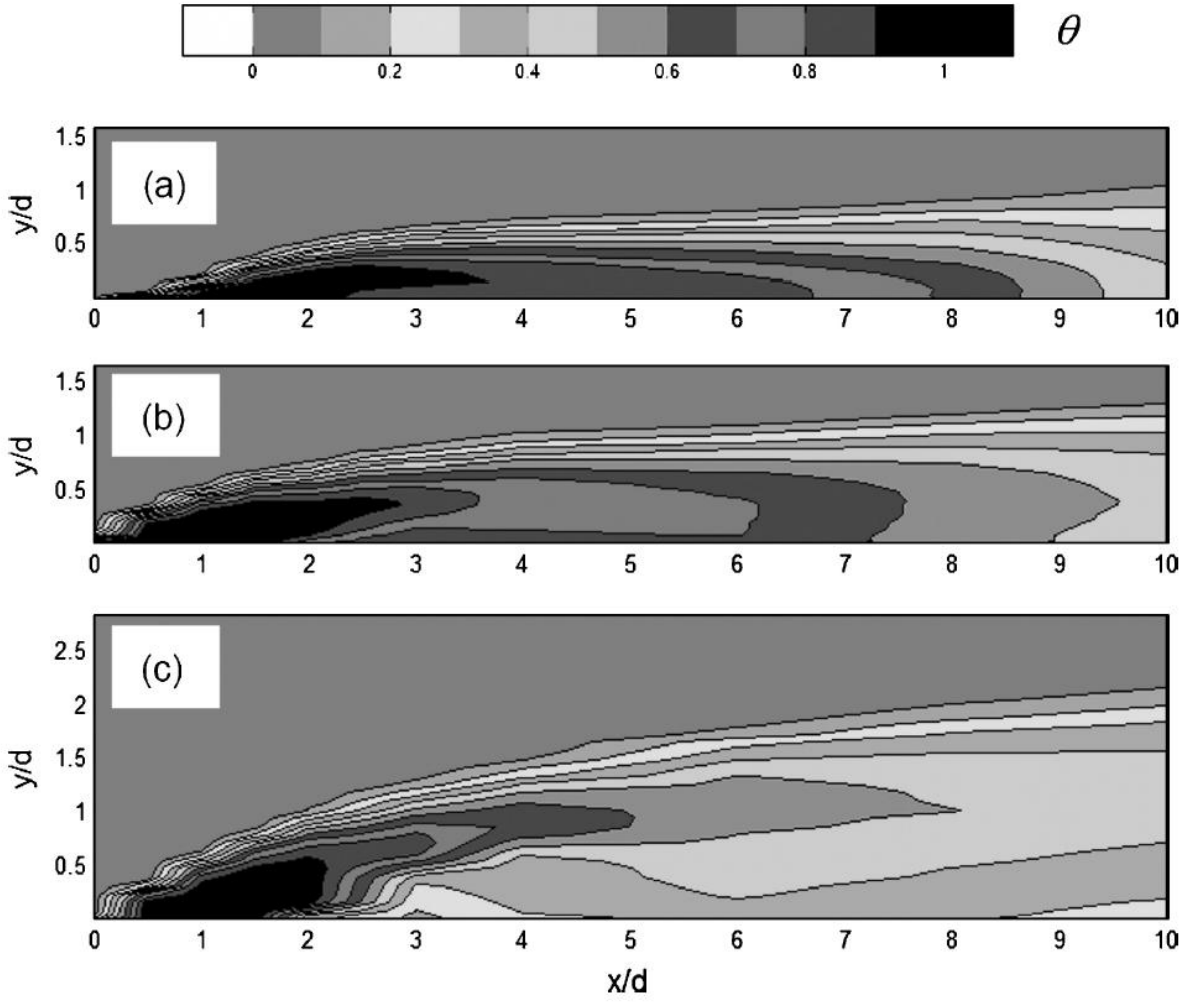

Figure 20: Various film cooling cases: (a) fully attached, (b) reattached, (c) fully separated [26].

CHAPTER 4: EXPERIMENTAL SETUP AND PROCEDURE

4.1 History of the Energy Efficient Engine Project

The current study is based on the NASA-GE E^3 cascade of first stage turbine blades at the CATER facility. E^3, or the Energy Efficient Engine project, was a General Electric (GE) project commissioned by the National Aeronautical and Space Administration (NASA). The original purpose of the design was to improve the efficiency of propulsion systems in the late 1980s and early 1990s. The research was later released into the public domain to provide a relatively advanced starting point for open literature research efforts. NASA has several publications available that describe this project, but the most relevant to this topic is a report by Timko [27]. Several figures from the report are shown below to illustrate the highlights of the project.

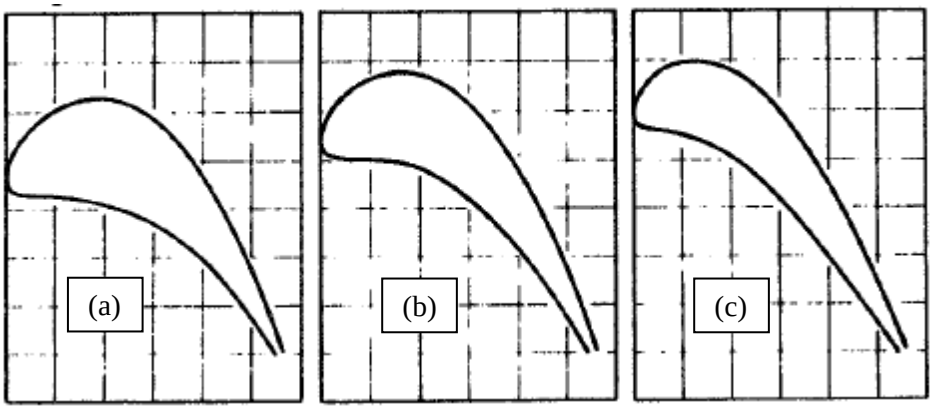

Figure 21: Profile for a E3 Stage 1 Blade: (a) Hub, (b) Pitch, and (c) Tip [26].

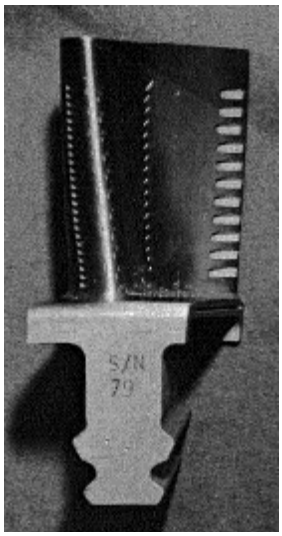

Figure 22: Photograph of individual E^3 Stage 1 Blade [26].

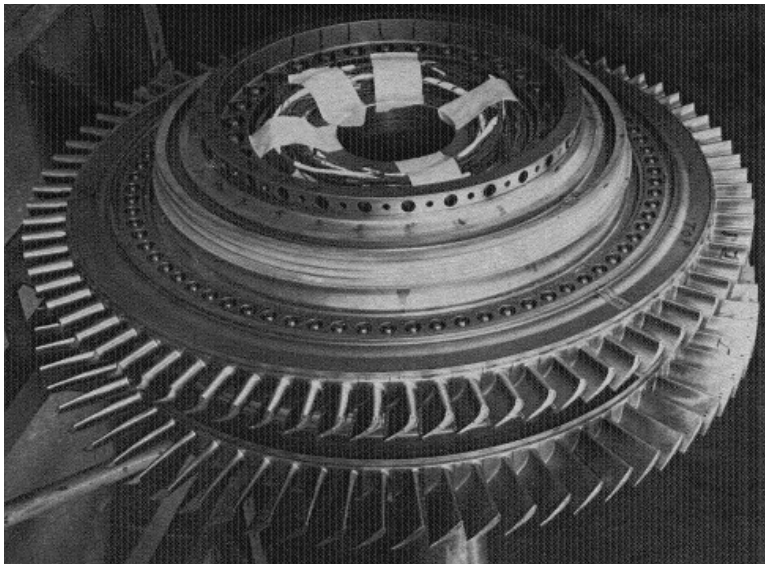

Figure 23: Photograph two-stage rotor assembly for E^3, with Stage 1 Blades shown on top [26].

4.2 E^3 Cascade at the CATER Facility

4.2.1 Experimental Model

NASA, through FCAAP, has funded a research project at CATER to study the E^3 geometry. A three-times scaled version of the first stage E^3 turbine blade has been utilized to create a five passage cascade and implemented in a wind tunnel at the CATER facility. The tunnel is powered by a 440V 3-phase 350HP electric motor and blower that can produce transonic flow, with speeds up to Mach 0.7 at the throat of the cascade. The tunnel can operate in both open and closed-loop conditions. In the closed loop configuration, a heat exchanger is used to maintain the air at a steady state temperature of approximately 80˚ C [20]. After the heat exchanger, a turning duct with vanes to guide the air in line with the test section. Next, a flow conditioning section is placed after the heat exchanger to break down turbulent eddies in the flow. The section was designed within space limitations according to the work of Mehta and Bradshaw [28] with a section of honeycomb and two screens. A nozzle with an area ratio of 3.3 is used after this section to compress the boundary layer before the air passes down a special rectangular to annular nozzle with an area ratio of 2.9. After this, the flow enters the film cooling section which was added upstream of the cascade in order to enable a wide variety of new research topics to the cascade. Some sample images are shown below of the implementation.

Figure 24: Downstream view of the E^3 blades [20].

Figure 25: Upstream view of the E^3 blades [20].

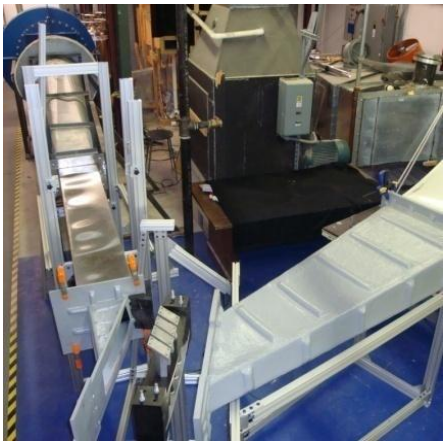

Figure 26: Overview of the entire E^3 setup [20].

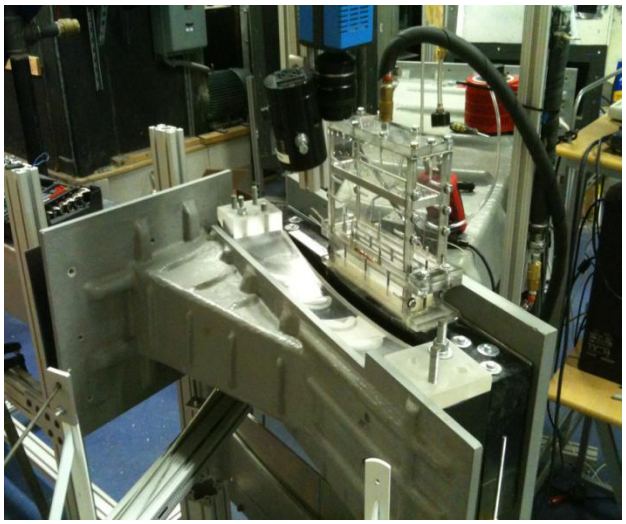

Figure 27: Film cooling section installed in cascade [1].

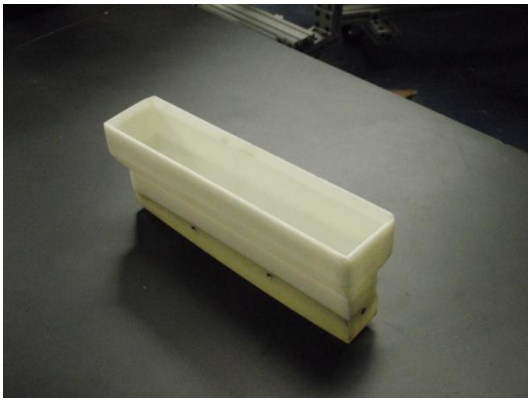

Figure 28: View of film cooling coupon assembly.

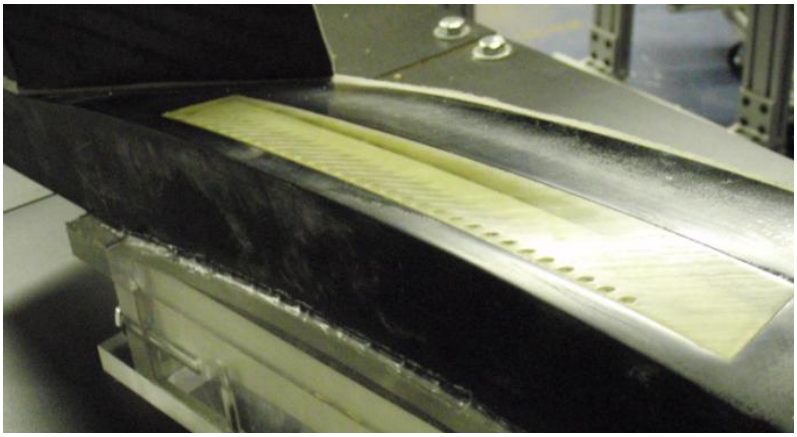

Figure 29: Close-up of film cooling coupon.

4.2.2 Overall Solid Model

Now that the realization of the experimental setup has been shown, a solid model will be used to show additional levels of detail. Below is pictured a fully labeled model of the wind tunnel in closed-loop condition. The open-loop configuration does not need additional description because it is simply truncated at the expansion duct after the blower and at the flow conditioning section. It can be seen that the wind tunnel is built with general purpose rectangular adapters so two annular to rectangular adapters were implemented to address this issue. Not shown on the diffuser section before the heat exchanger is an atmospheric inlet to ensure a known total pressure to the cascade and to allow mass flow as the air is heated and cooled.

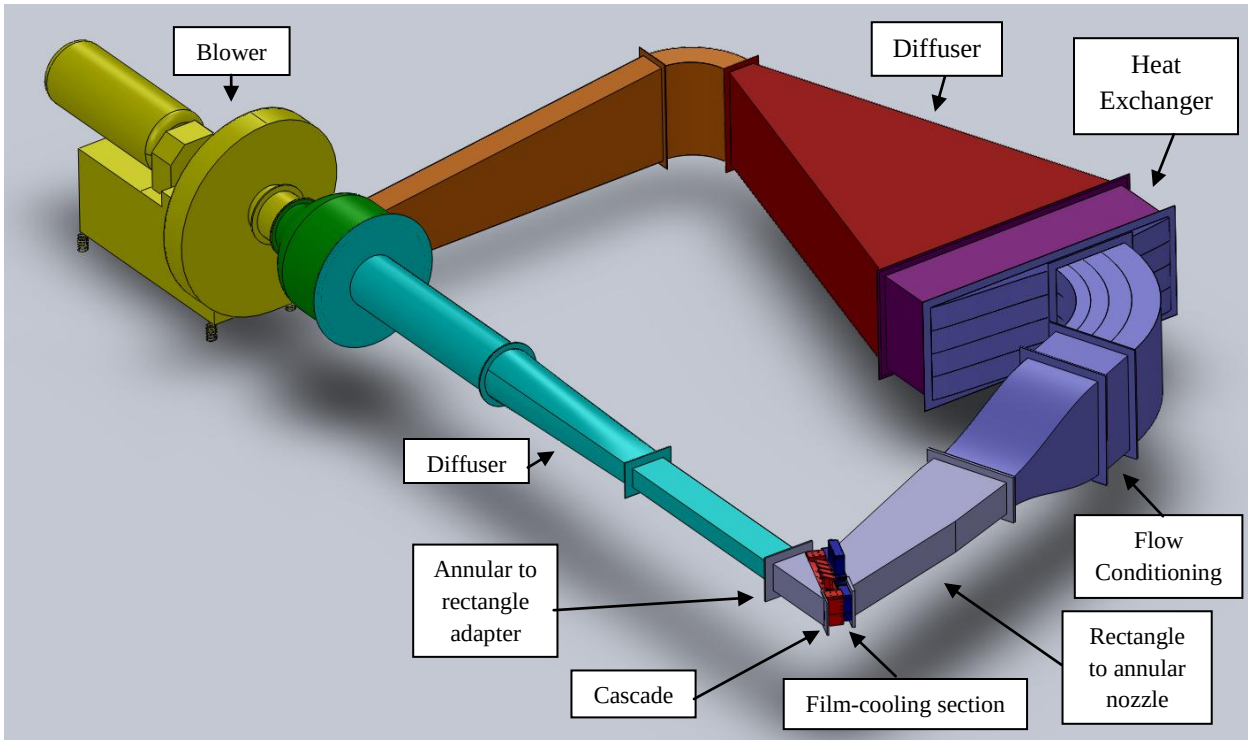

Figure 30: Overview of the E^3 solid model wind tunnel in close-loop configuration.

4.2.3 Cascade Solid Model

The experimental cascade consists of five passages with four E^3 stage one turbine blades at a scale of three times actual size. The inlet and exit ducts to this section were designed to model the airstream through the blade in turbine conditions which involves a turning angle of 69.9˚ with incoming flow at a 43.2˚ angle and outgoing flow at a 66.9˚ angle with respect to a reference axis normal to the inlet and outlet planes. Several views of the solid model are provided below.

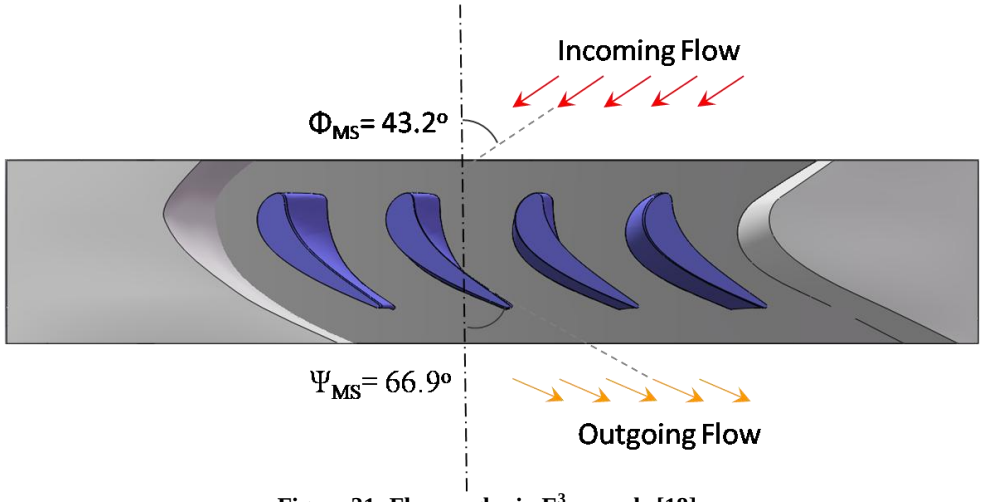

Figure 31: Flow angles in E^3 cascade [18].

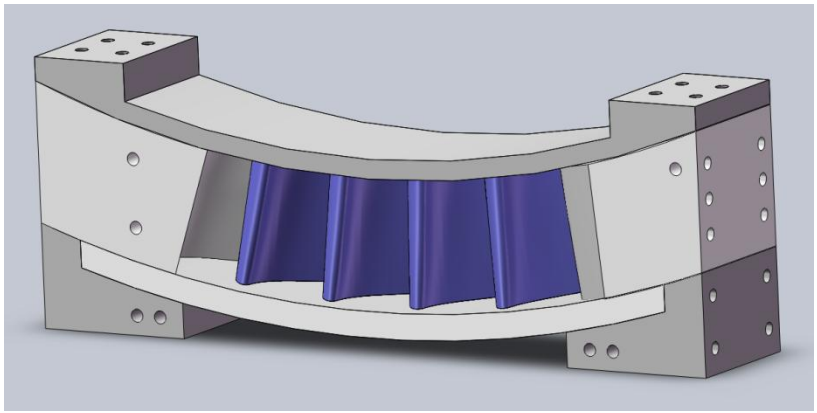

Figure 32: Upstream view of airfoil cascade.

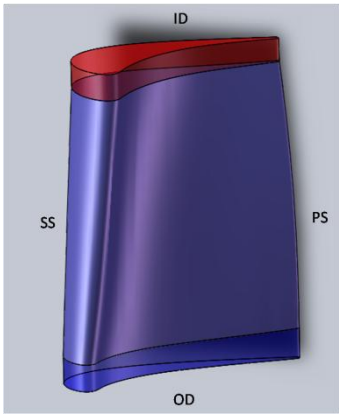

Figure 33: Single airfoil model.

4.2.4 Film Cooling Section Solid Model

A section was included directly upstream of the cascade section so that various film cooling configurations could be applied. A two-piece coupon was created so that only a small, inexpensive piece would have to be manufactured each time a new test configuration was desired. The current configuration has a small hole for a coupon that covers one and a half blade pitches, but the top of the section is modular so that a larger hole for a full coverage coupon can be implemented later. The specifications of the current coupon are shown in the table below and several views of the film cooling section and coupon are provided below.

Table 1: Coupon Film Hole Geometrical Parameters [1]

Hole shape	Round (cylindrical hole)
Diameter, *D* [mm]	2
Number of film hole per passage	14
Pitch-to-diameter, *p/D*	1.5
Film hole distance, from LE δ	1.5d (*d* =13 mm)
Film jet Inclination angle, α [degree]	30
Film jet compound angle, β [degree]	0

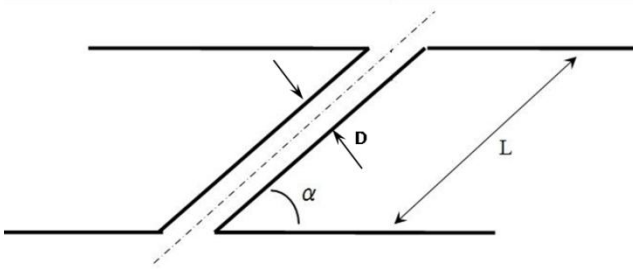

Figure 34: Film hole parameters side view

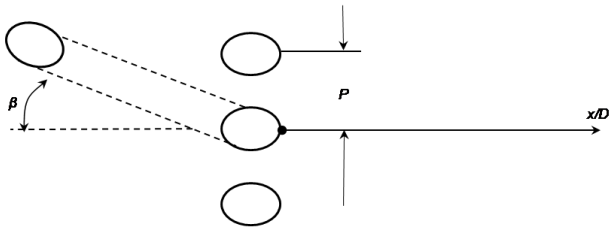

Figure 35: Film hole parameters top view.

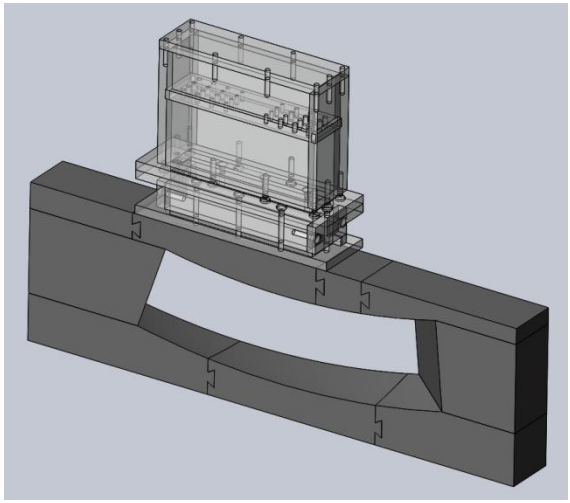

Figure 36: Overall view of film cooling assembly.

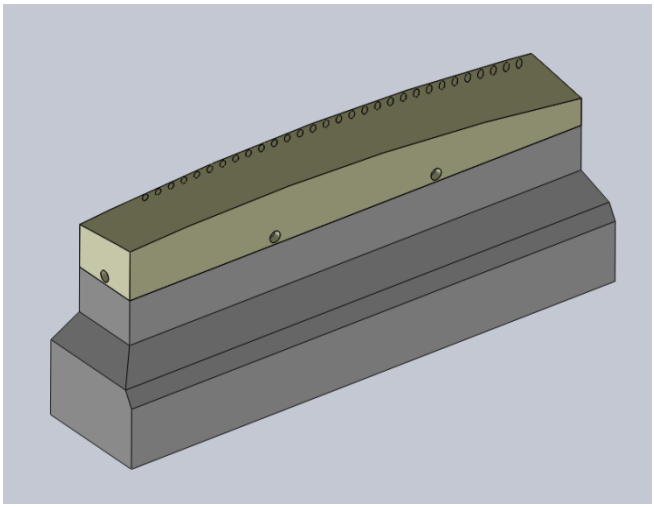

Figure 37: Close-up view of coupon assembly.

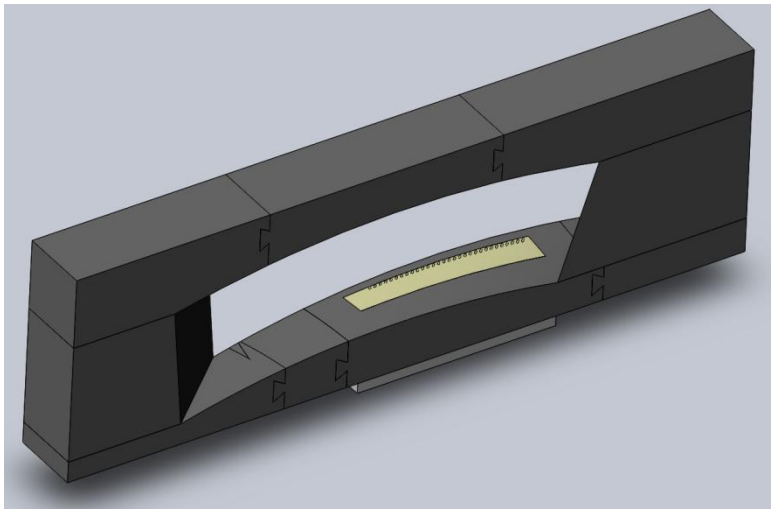

Figure 38: Close-up view of coupon in place.

4.3 Five Hole Probe

A five hole probe is a relatively rugged and cost effective method of examining components of a flow such as velocity vectors and total and static pressures. This probe is much superior to a pitot probe because it can accurately measure velocity vectors up to 60˚ from the probe axis. This probe is designed with a cone shaped tip with one hole in the center like a pitot probe, but instead of static pressure holes, it has four additional holes on the sides of the cone. This allows the probe to measure pressure from several different planes. This capability combined with the Multiprobe software allows all the parameters of the flow to be extracted such as the flow angles, static and total pressures, and all velocity components. This capability is very useful in a cascade where the direction of the flow is uncertain. When in use, the flow angle capability of the probe is used to point the probe into the flow within one to two degrees. This is referred to as nulling the probe and it is done because small inaccuracies have been noted at the higher angles. The probe was manufactured by the Aeroprobe Corporation. A diagram and several images of the probe are shown below [29].

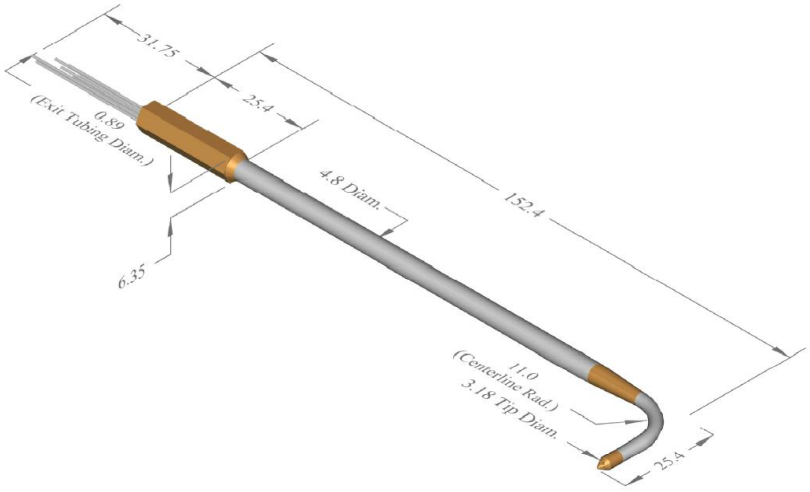

Figure 39: Diagram of five hole probe [29].

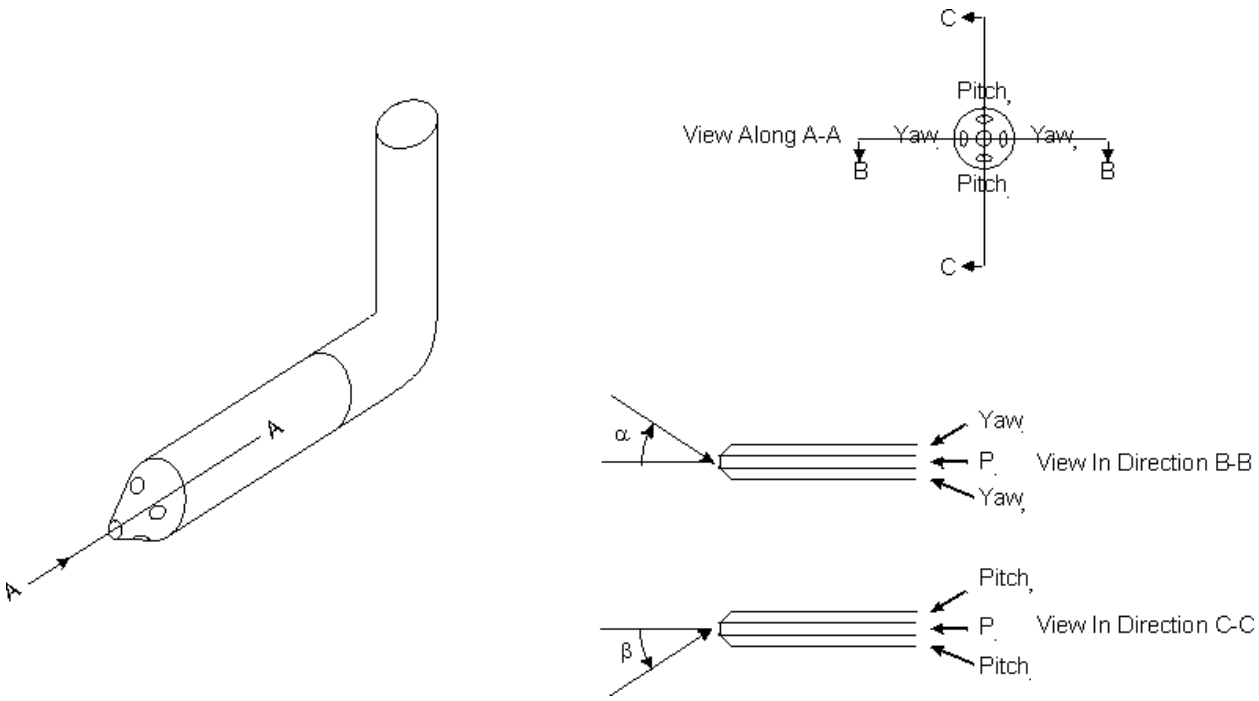

Figure 40: Close-up diagram of five hole probe tip [30].

Figure 41: Overall image of five hole probe.

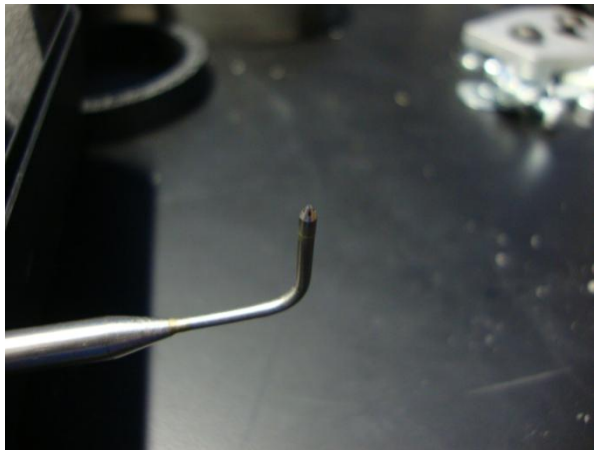

Figure 42: Close-up of five hole probe head.

The angle of a five hole probe needs to be precisely controlled. Several tools used for this purpose were a Velmex rotary table and an in-house traversing system. Finally, a pressure transducer multiplexer system from the Scanivalve Corporation was used to collect the data from the probe.

Figure 43: Close-up of velmex rotary table [1].

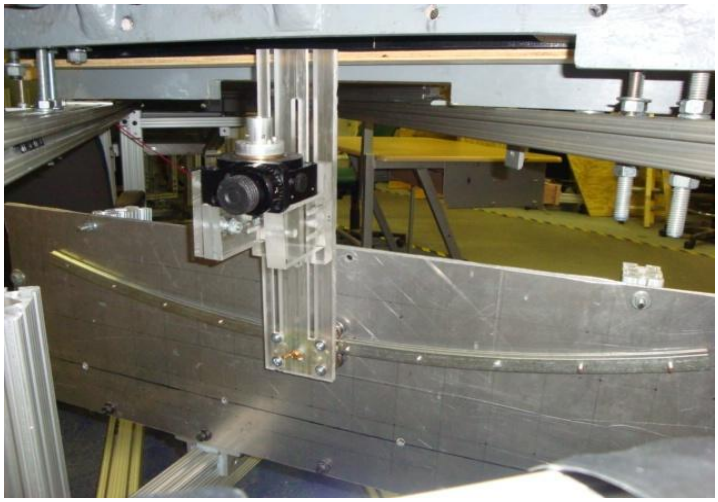

Figure 44: In-house traversing system [1].

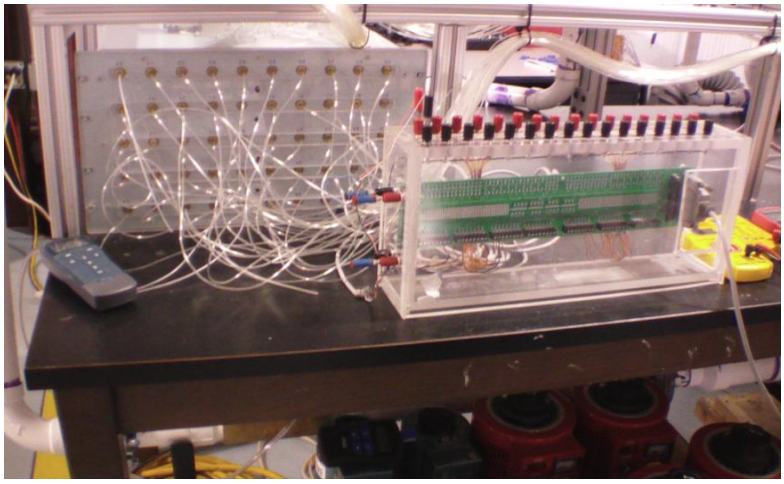

Figure 45: Pressure multiplexer and DAQ setup [1].

4.4 Temperature Sensitive Paint

A measurement technique called temperature sensitive paint (TSP) can be used to determine the film cooling effectiveness on the inner endwall. The TSP contains probe molecules that are excited by light at a certain frequency, in this case 460 nm. When the probe molecules are excited, there are several methods by which they can release the energy while returning to the ground state. The first is by luminescence at a specific wavelength, which can be detected by a filtered charge coupled device (CCD) camera. The second would be oxygen molecules, but the specific binder in TSP is impermeable to oxygen. The last way is through thermal quenching. The ratio of thermal quenching to luminescence can be correlated to temperature through calibration

There are many factors unique to each individual test such as excitation light intensity, ambient light, variations in paint thickness, and other irregularities. However, these can be compensated for by taking two images, one at a known temperature, called the reference image and one of the test case, called the signal image. The ratio of reference and signal images can be computed, and it will remove many of these irregularities, while careful post-processing can eliminate the remainder of the issues that may occur. A detailed study of TSP was carried out by Liu [31]. Once this ratio between images has been determined, a calibration curve can be used to convert this to a difference in temperature between the signal and reference images. The temperature of the reference pictures is known, so the actual temperatures in the signal image can be determined.

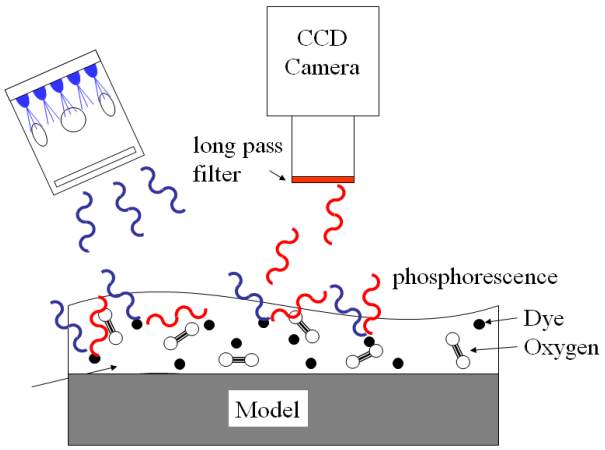

Figure 46: Experimental setup with TSP [30].

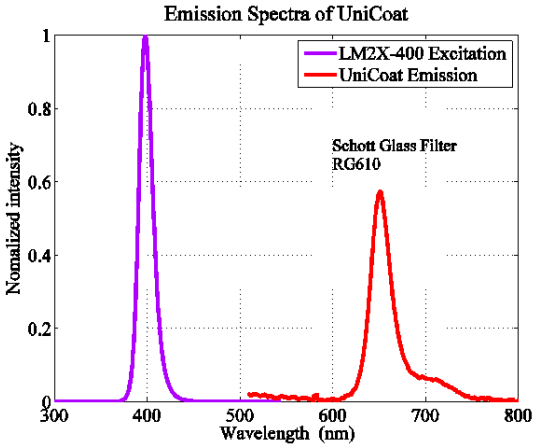

Figure 47: Representative TSP emission spectra [30].

To implement the use of this on the E^3 cascade, a clear inner endwall was fabricated from a urethane-based material and TSP was applied to one passage. Due to experimental constraints, the wind tunnel was run in open loop configuration with a heated coolant flow. This is not an ideal setup, so various modifications will be made in the future to allow a closed loop configuration with a cooled coolant flow.

Figure 48: TSP setup on E^3 cascade [1].

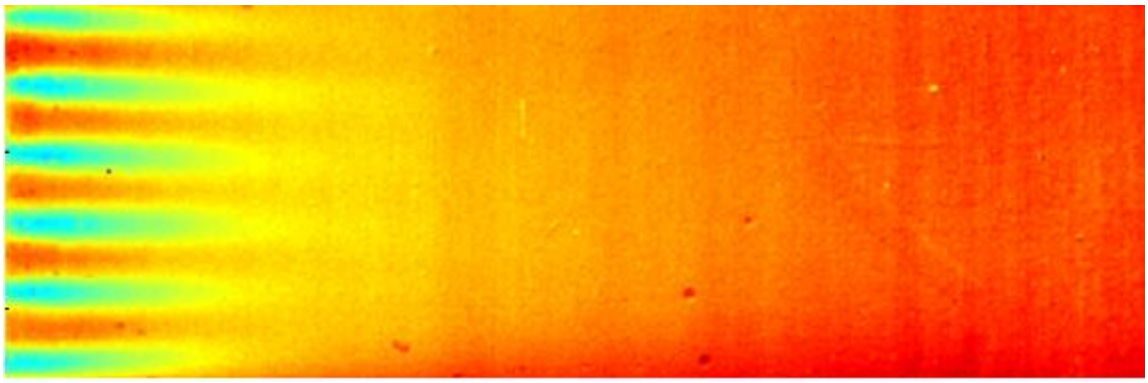

Figure 49: Sample film cooling image using TSP technique. [20]

4.5 Numerical Approach

4.5.1 Overview and Goals

A main goal of this work is to develop a numerical model that will closely model the experimental conditions. When this is complete, the limited experimental results that can be gathered will be used to calibrate the model so that many difficult to obtain parameters can be determined from the numerical approach.

To limit the computational domain, many works simply model one blade with periodic conditions. However, while the experimental rig is periodic, there are other geometric factors that could lead to differences between this idealized setup and the physical experiment. Because of this, a numerical model was created that simulates the entire experimental setup, from the inlet of the rectangular to annular nozzle to the outlet of the annular to rectangular adapter. Air models were created in Solidworks based on the original part drawings and were carefully adapted to ensure high quality surfaces and perfect alignment between connecting sections. The full solid air model is shown below with the nozzle (red and purple), film cooling section (orange), cascade (yellow), and adapter (green). The nozzle was separated into two sections because the flow behavior was studied and it was determined that the red section was required to be meshed with the test section to obtain quality results.

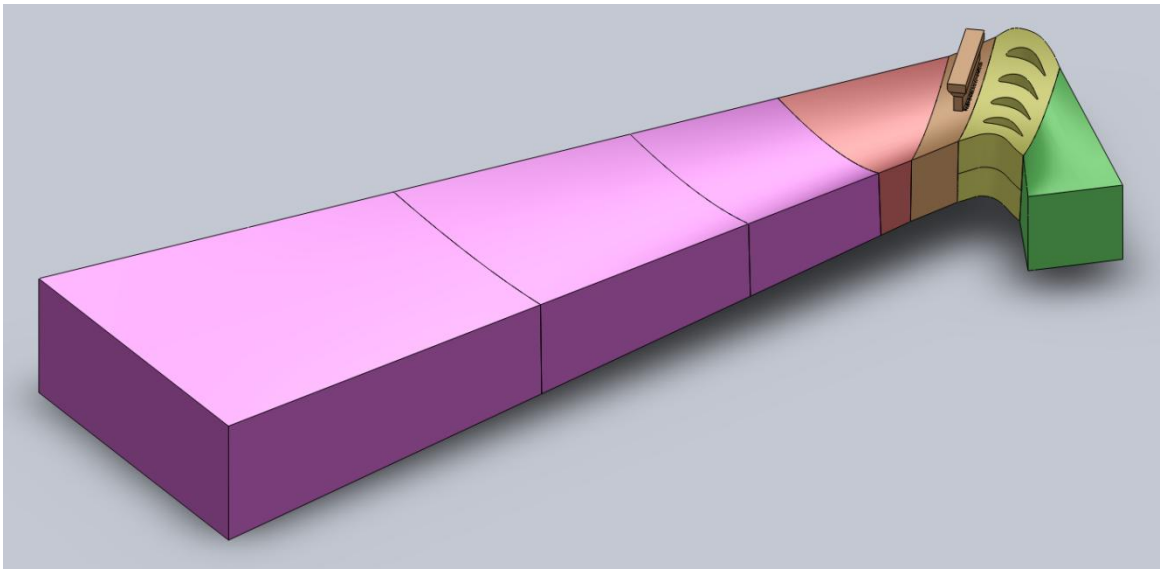

Figure 50: Overview of the full E^3 air model.

For the numerical models, similar physics models were chosen for consistency. Steady Reynolds-Averaged Navier-Stokes (RANS) was chosen to simply calculations because of the high number of cells. The realizable K-Epsilon model was chosen for accuarate turbulence modeling and a two-layer, all y+ treatment was used to ensure that the viscous sublayer and heat transfer were modeled carefully. Because much of the flow is compressible, air was treated with the ideal gas model. Coupled flow modeling was chosen for all the sections because of the compressible nature of the flow. This choice greatly increased the computational requirements of this model, but this was necessary because segregated flow modeling is incapable of finding the solution and simply oscillates.

4.5.2 Developed Flow Section

For the purposes of this work, it was determined that the inlet to the nozzle would be treated as a fully developed profile even though this is not exactly what occurs in the physical model. In the experimental model, there is a flow conditioning section and two-dimensional nozzle before the annular nozzle. This simplification was chosen because it was impractical to model sections far upstream of a nozzle when the nozzle would highly compress the boundary layer and remove the effect of those upstream components. A simple rectangular duct geometry with the same cross section as the nozzle inlet was created with periodic boundary conditions and a specified pressure drop. A mass flow condition was more ideal, but the solution would not converge quickly on this setting, so the pressure drop condition was utilized to obtain the desired mass flow rate.

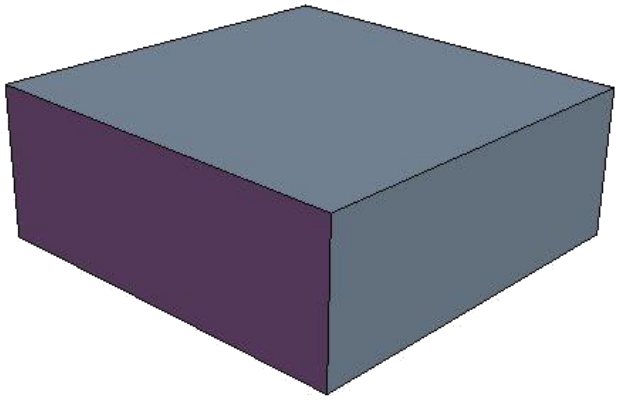

Figure 51: Developed flow section geometry.

The geometry was meshed with a medium fineness mesh that contained approximately 716,000 cells and the mesh is shown below. Only aerodynamic factors were important in this case, so 6 prism layers were used on the walls.

Figure 52: Developed flow section mesh.

The solution was allowed the converge and a total pressure plot is provided to demonstrate the flow characteristics. The velocity components, turbulent kinetic energy and turbulent dissipation rate were output in a table for use in the nozzle inlet conditions.

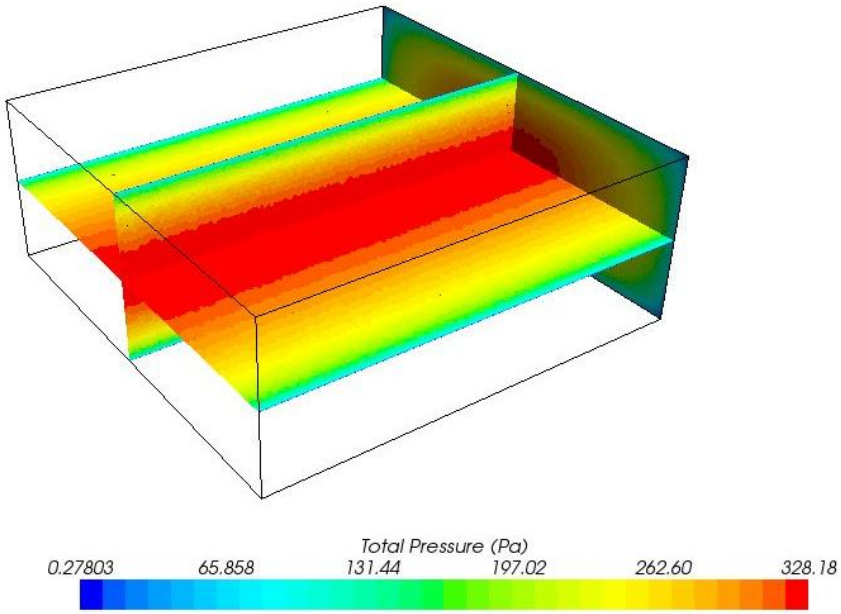

Figure 53: Total pressure contours in developed flow section.

4.5.2 Nozzle Section

For this work, the nozzle section was computed separately from the film cooling and cascade sections. This was done to reduce the computational domain so that a finer mesh could be used for the film cooling and cascade sections. Also, Nguyen [20] computed a variation of domain that did not contain the film cooling section with a coarse mesh and determined that the profile as far upstream as the nozzle exit was unaffected by the blades. However, for future flexibility, the nozzle was split into several sections so that they could be meshed with the full test section if that capacity was desired.

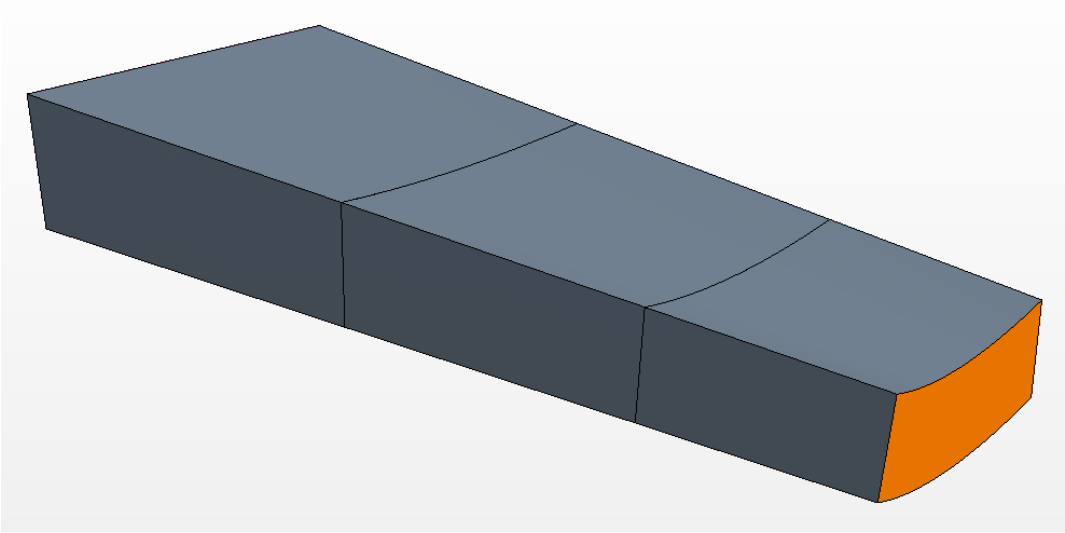

Figure 54: Nozzle section geometry.

The meshing for the section was done at various fineness levels. The inlet was done with a rather coarse mesh while the outlet section was done with a fine mesh and the middle section was done with a medium mesh. This helped reduce the computational complexity while maintaining a quality profile at the outlet. The total number of cells was approximately 3.1

million cells with 6 prism layers on each surface. A pressure outlet was assigned to the outlet of the nozzle because this result was found in the work of Nguyen [20].

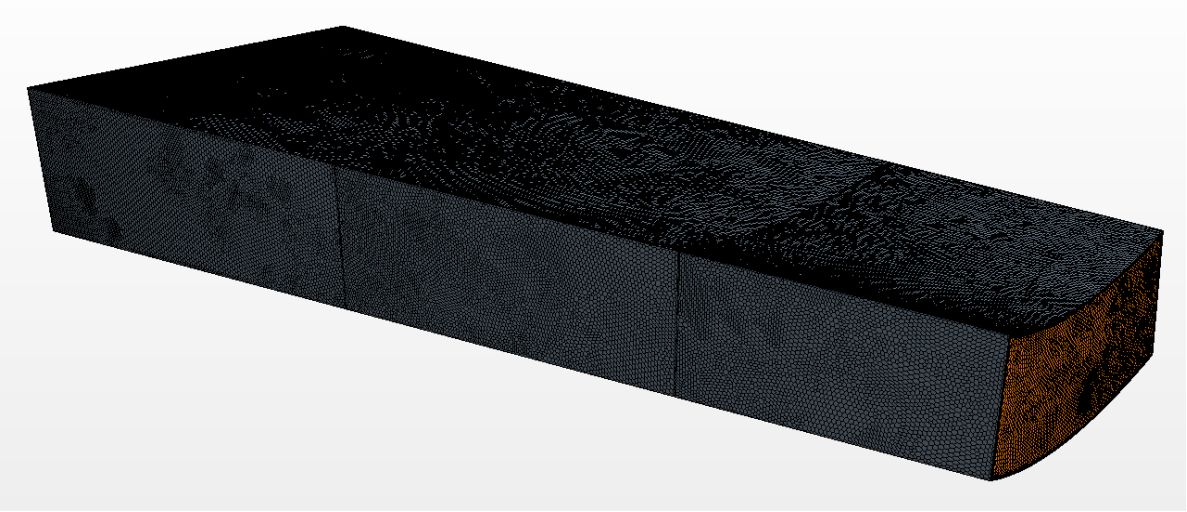

Figure 55: Nozzle section mesh.

The solution was allowed to converge and a total pressure plot is provided to demonstrate the flow characteristics. As with the previous section, the velocity components, turbulent kinetic energy, and turbulence dissipation rate were output to a table to use as the inlet conditions for the test section.

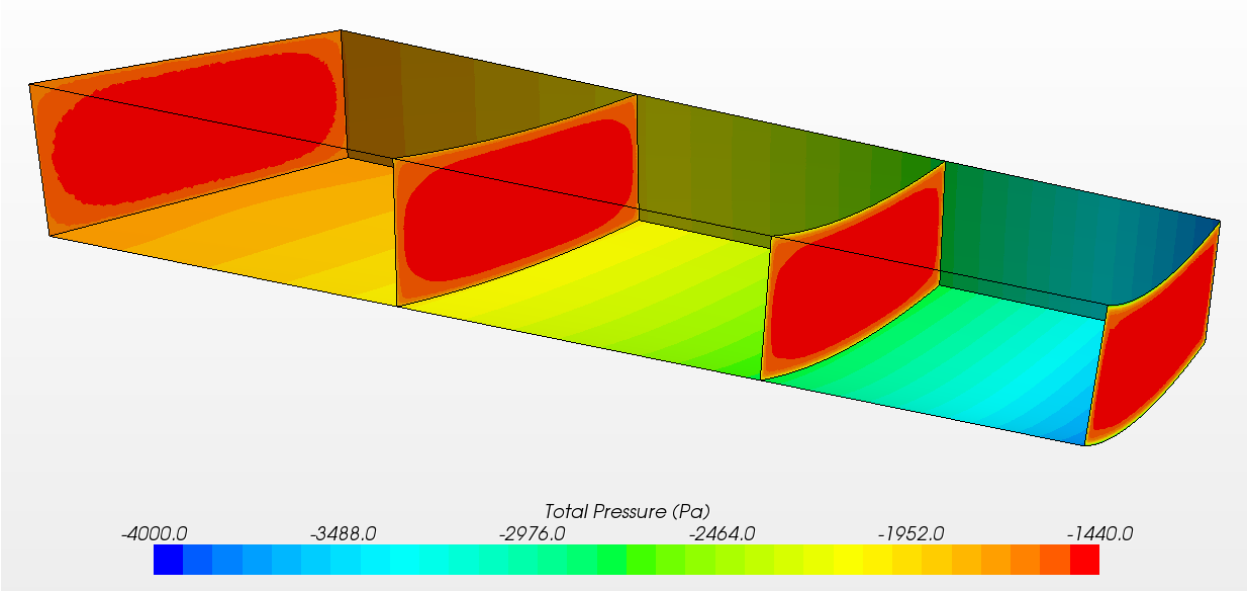

Figure 56: Total pressure contours in nozzle section.

4.5.3 Film Cooling and Cascade

The film cooling, cascade, and annular-to-rectangular adapter sections were assembly as the main area of investigation for this study. This was done because each component has a significant impact on the adjacent parts and cannot be separated. The film cooling coupon currently in use on the experimental rig has an inclination angle of 30˚ and a compound angle of 0˚. This design was matched in the computational model, however this can be altered later to reflect new designs.

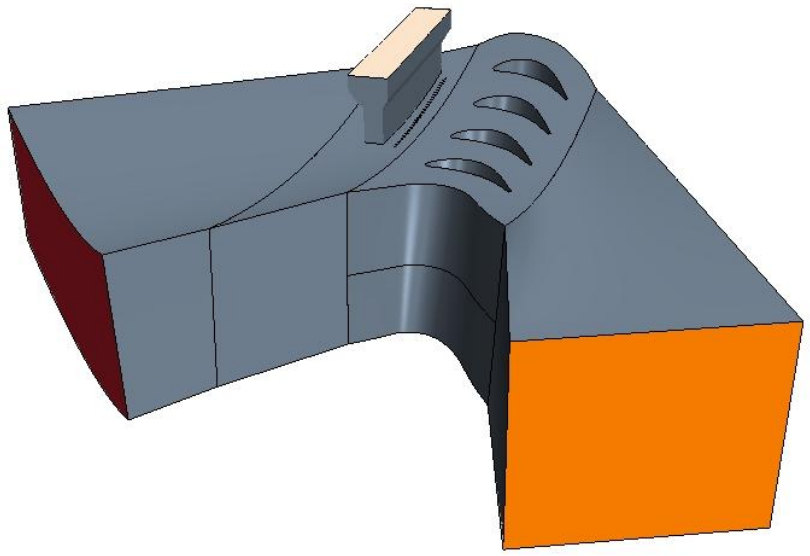

Figure 57: Test section geometry.

The film cooling and cascade sections were meshed at a high fineness level, especially on the inner diameter surface over which the coolant passes. The adapter section was meshed with a coarser mesh because it has a limited effect on the final solution. The mesh was optimized in all sections to limit skewed cells. Care was taken on the inner diameter section to ensure that the

inner-most prism layer was at a y+ distance of less than one so that the heat transfer could be accurately computed. To ensure a quality boundary layer profile, 12 prism layers were used on the inner diameters. Several levels of fineness of the mesh were created for the purpose of a grid-independence study. A pressure outlet was also used as the outlet condition for this mesh because it occurs at a point where the flow exits into a larger duct and this was a condition that could easily be correlated to experimental conditions. A mesh with 4.2 million cells is shown below to illustrate the characteristics of the mesh. Next is shown the skewness results from 85˚ and it can be seen that there a few skewed cells and they do not occur in areas of significance.

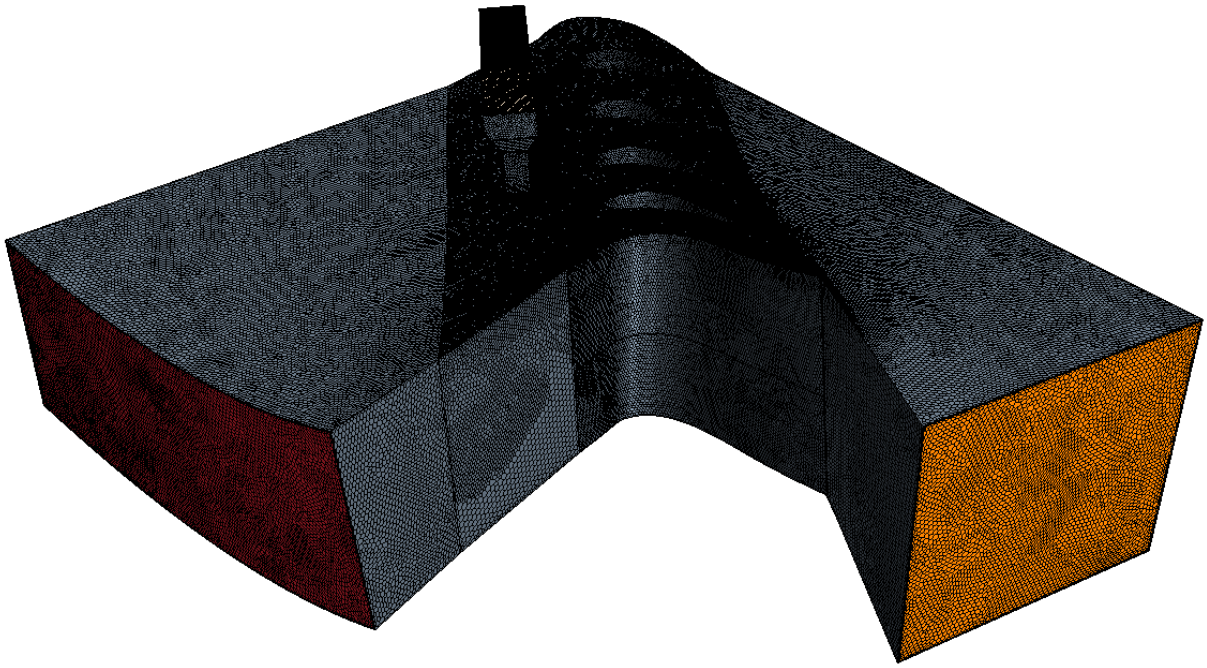

Figure 58: Test section sample mesh.

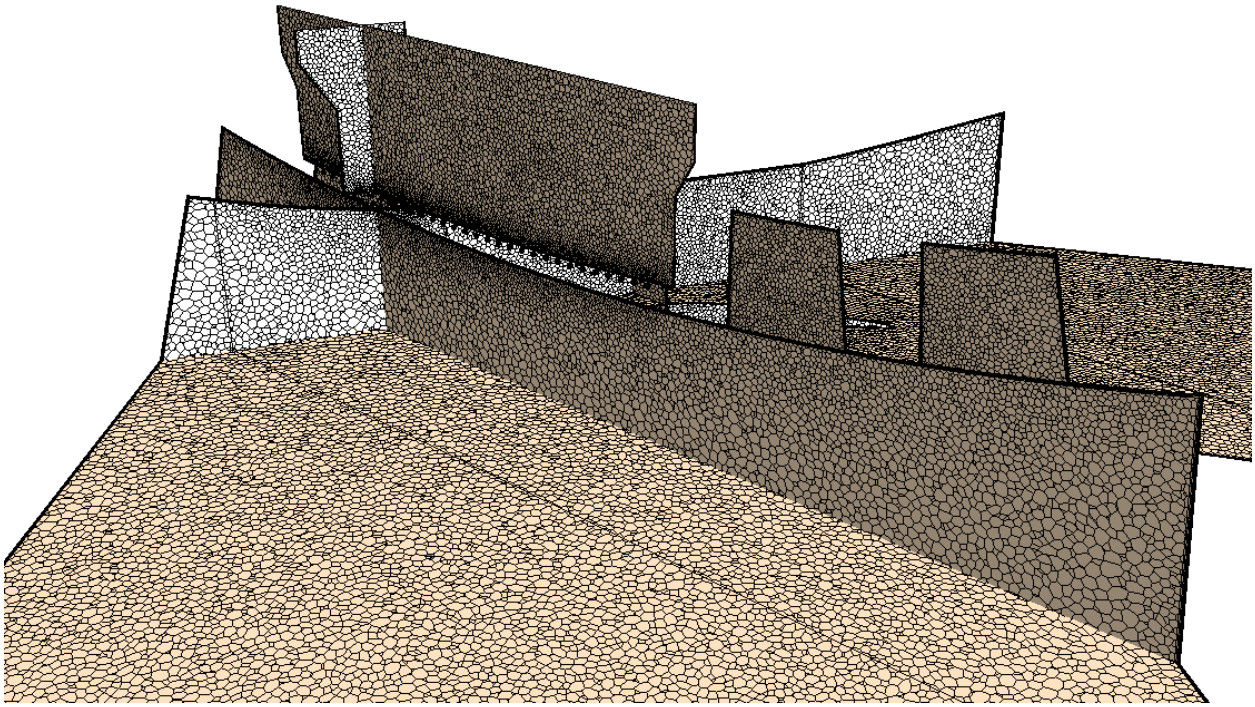

Figure 59: Cross-sectional mesh views of test section.

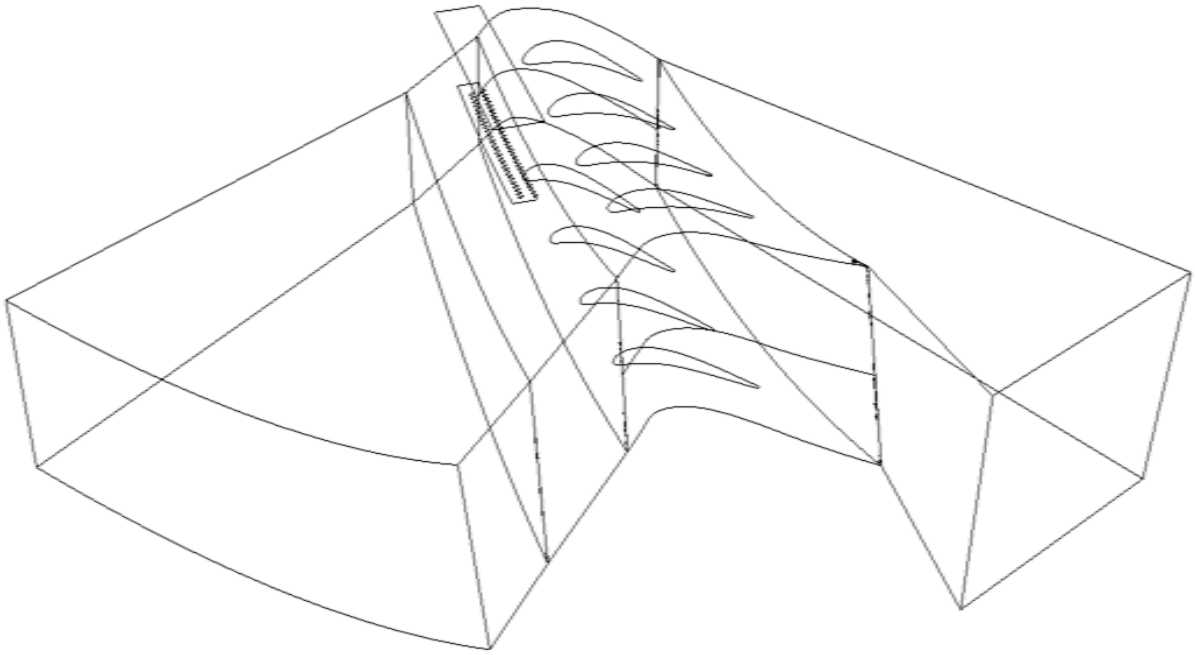

Figure 60:Graph of skewness angle in cascade.

A grid study was performed on various meshes from 0.7 million to 4.2 million. Larger grid sides would have been beneficial to include to increase the confidence of this study, but the large computational resources required by these meshes and solutions placed a limit on the amount of large tests that could be solved. It can be noted that there are more low number tests cases than necessary. This occurred because the author wanted to have a good understanding of the trends between grid size and convergence and could solve these small grid sizes with relative ease. Various parameters were compared between these cases and a summary is shown in the graphs of the total pressure loss coefficient as defined below with all components mass-averaged over the inlet and outlet of the test section respectively.

$$\zeta = \frac{P_o inlet - P_o outlet}{P_o inlet - P\ outlet} \tag{10}$$

To compare the various cases, criteria were established and the highest cell case was treated as the ideal or asymptotic value and the other grids were compared to this case. The author acknowledges that these grids have not achieved full grid independence, but they appear to be within a percent of the asymptotic value, so it is reasonable to treat the highest case as ideal. Further research could explore this issue further and verify that this conclusion is correct. However, it is unlikely that larger grid sizes would be practically used in future analysis because of the high computational cost, so it is reasonable to not study higher grids.

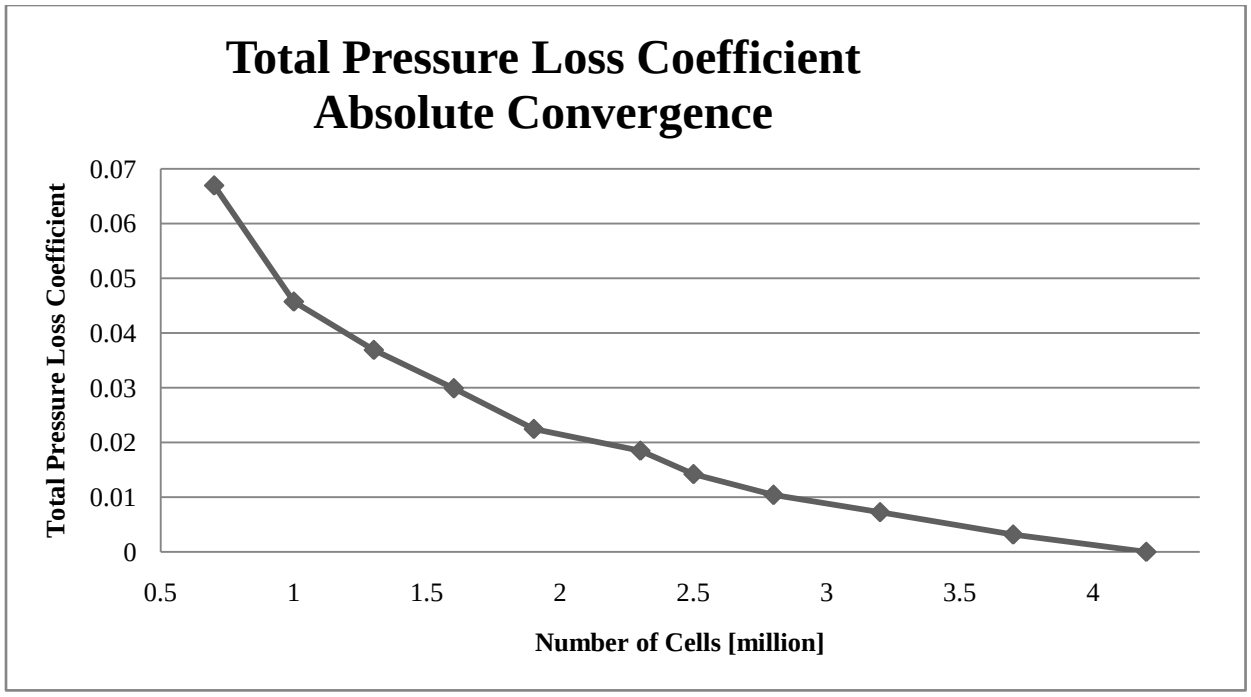

Figure 61: Absolute convergence of total pressure loss coefficient.

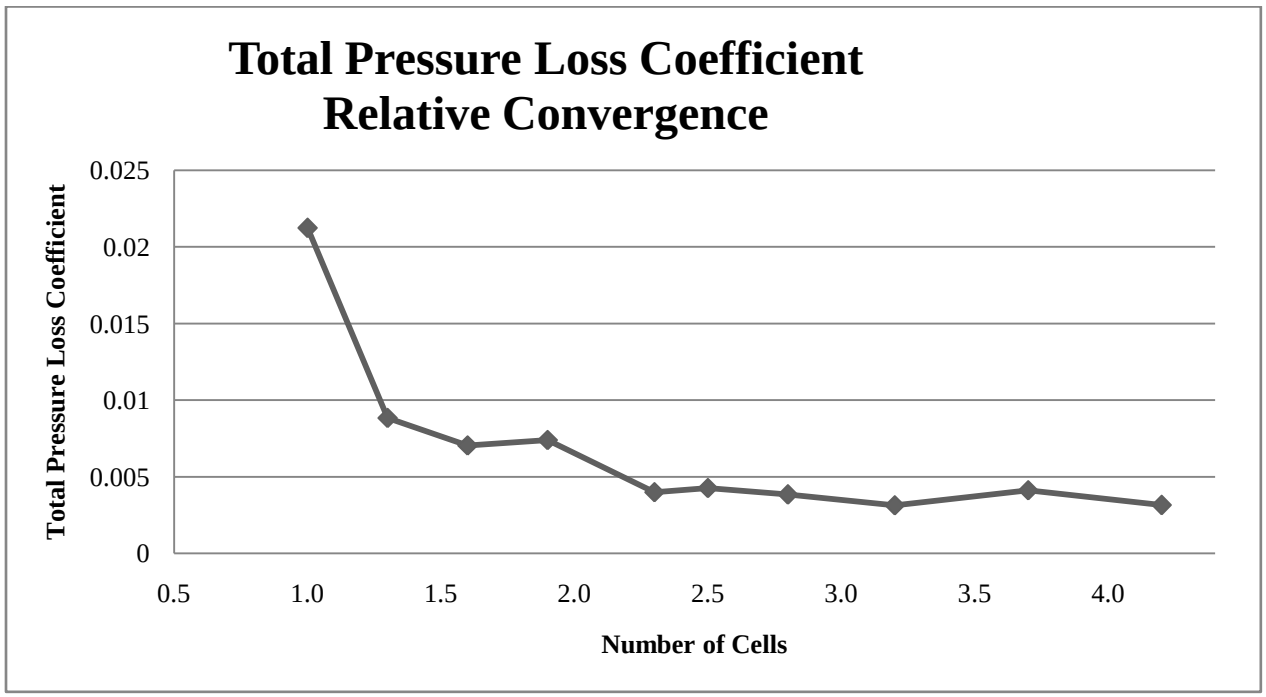

Figure 62: Relative convergence of total pressure loss coefficient.

CHAPTER 5: RESULTS AND DISCUSSION

5.1 Experimental Parameters and Validation

The solution to the CFD simulations were obtained and the data will be presented here and compared to the relevant work on the E3 cascade. Careful observations were taken of the solution to ensure that a realistic outcome occurred. When creating the simulation, care was taken to match measured rig conditions and data from previous works. The conditions used in this simulation are listed below.

Table 2. The experimental parameters.

Mainstream Condition	
Mach number at the cascade inlet	0.25
Mach number at the exit	0.45
Temperature, T_m [^{o}C | K]	27 | 300
Test section inlet gage total pressure, P_{t_inlet} [kPa]	-4.822
Test section inlet gage static pressure, P_{s_inlet} [kPa]	-6.996
Test section outlet gage static pressure, P_{s_outlet} [kPa]	-13,900
Mass flow rate, m_s [kg/s]	3.85 (0.77 each passage)
Coolant Flow Condition (when applicable)	
Temperature, T_c [^{o}C | K]	77 | 350
Density ratio, *DR*	0.86 (0.93/1.09)
Blowing ratio, *BR*	0.5
Coolant plenum mass flow rate, m_c [kg/s]	0.00

This work will be compared to the work of Nguyen [20] because it was a similar simulation, however, due to a few significant differences that will be discussed, this work is not intended to closely match the work of Nguyen. His work used a much more coarse mesh because he was not studying the full cascade. Additionally, his work did not include the film cooling section and his inlet conditions were not able to be simulated due to differences in software and lack of the relevant data. However, as many parameters were matched to Nguyen as possible, such as the mass flow and temperatures were matched along with measured values at the inlet and outlet of the cascade. As expected, some differences occurred, but in some cases, they were larger than anticipated. For some aspects, this is understandable because Nguyen did not use the same experimentally measured parameters that this study did. A few differences also occurred with the experimental rig. The controlling parameter in the simulation was the measured static outlet pressure measured on the rig. This led to a result about 2 kPa different than the inlet static pressure measured on the rig. It is known that there are some non-ideal portions of the experimental rig which probably caused this result. This caused the pressure values to be somewhat different than those of Nguyen, so while the absolute values were not matched, the trends were. Also, the mass flow set by Nguyen was matched, but his velocity was also higher. It is unknown how Nguyen obtained higher velocities in addition to higher pressures while maintaining the set mass flow rate. Because of this issue, the velocity trend has also been matched. Losses 27% of the chord length downstream of the blades were also matched to the work of Nguyen and Kopper et al. [21]. The trends and values are very similar for these cases and the slightly differences are probably accounted for due to the fact that Nguyen did not

specify the other location of this plot in the theta direction. In all of these graphs, 0% span represents the ID and 100% span represents the OD.

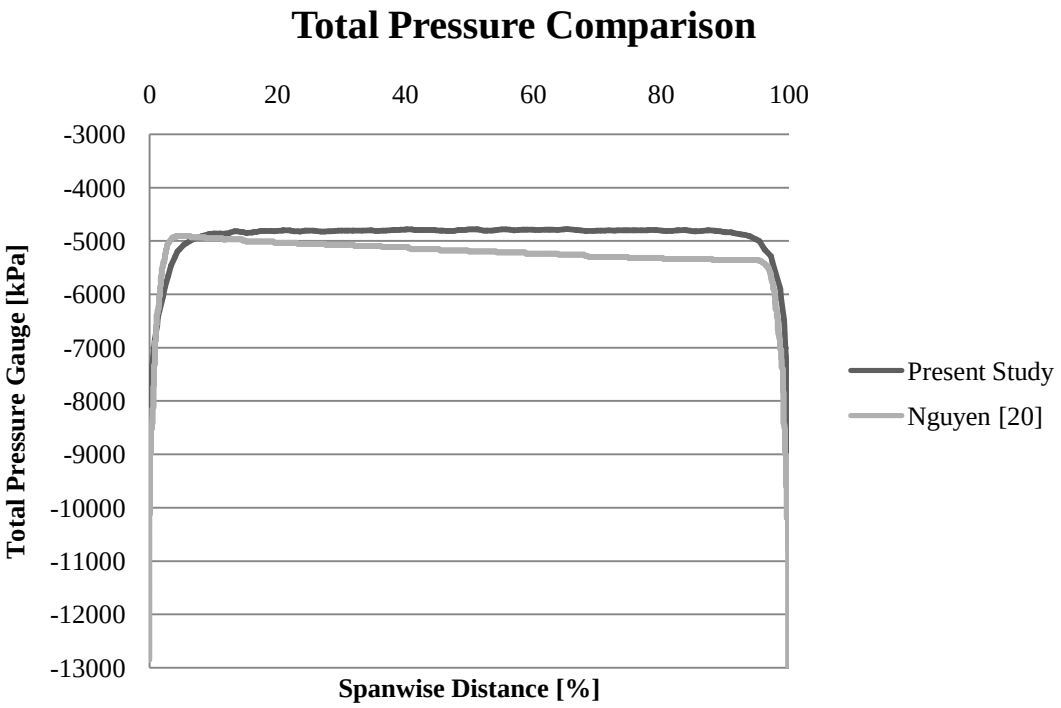

Figure 63: Total Pressure Comparison with Nguyen [20].

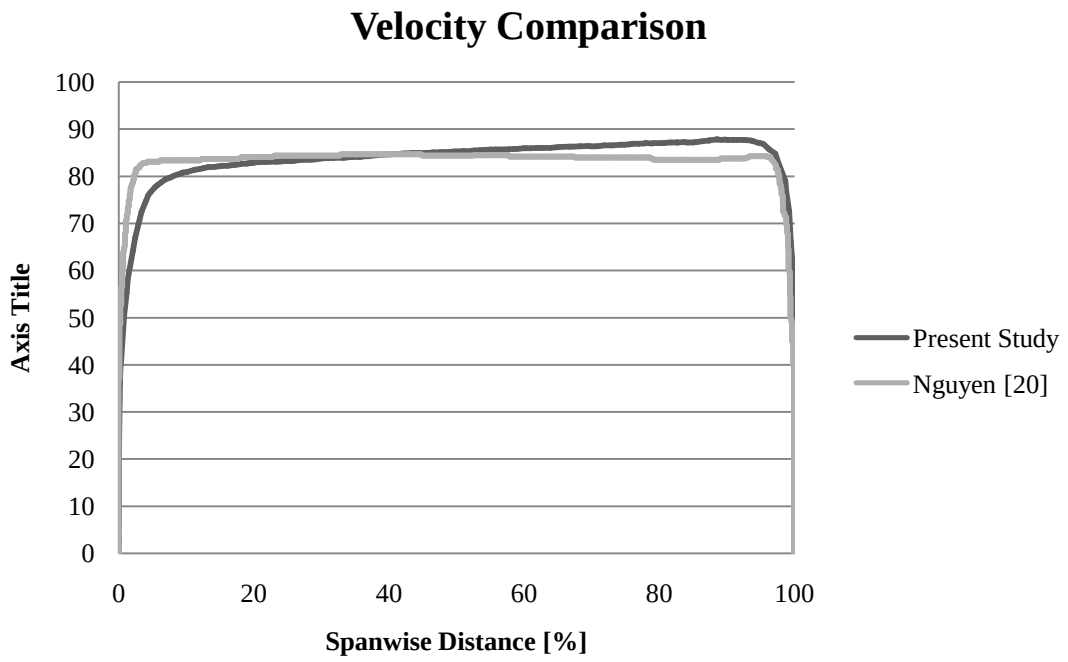

Figure 64: Velocity comparison with Nguyen [20].

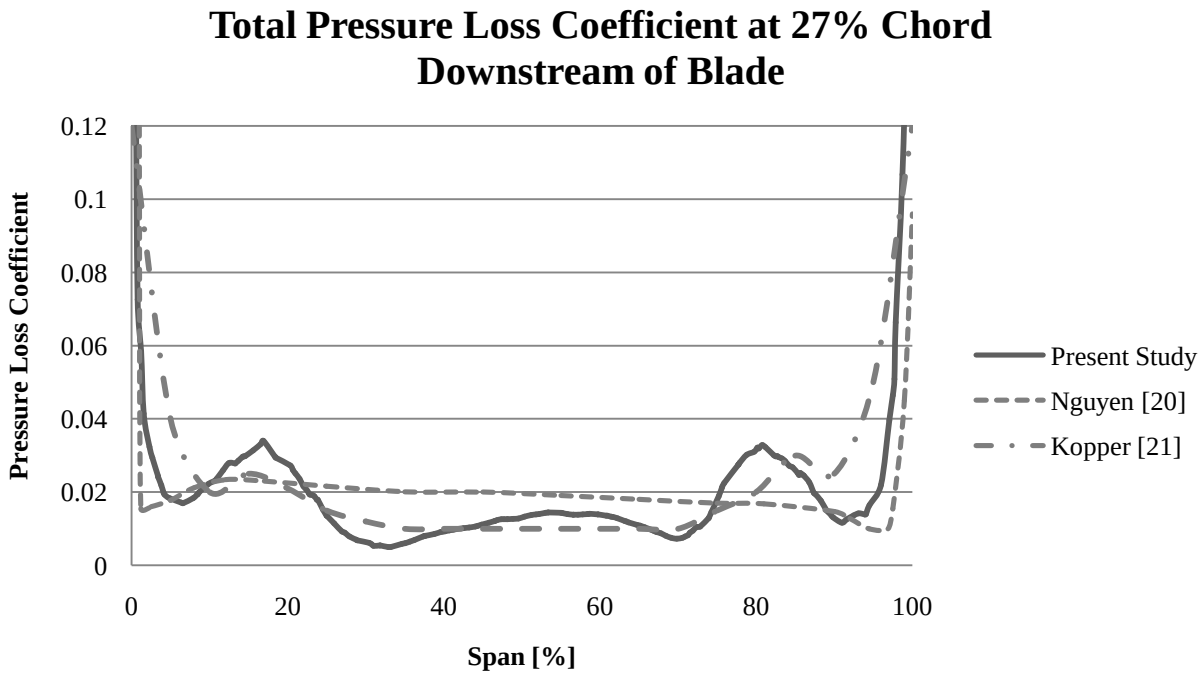

Figure 65: Total Pressure Loss Coefficient comparison with previous literature.

5.2 Endwall Static Pressure Comparison

One of the parameters that will compared with the experimental rig is static pressure in the cascade along the endwalls. Measurements were taken when the cascade was first assembled along the inlet and outlet on the ID and OD of the cascade to ensure periodicity. These studies only compared the three middle passages and later numerical data will illustrate why the outer passages are not periodic and therefore should be avoided for experimental purposes. First the numerical data will be shown alongside numerical data and then full numerical plots will be shown of the endwall to illustrate the full distribution that causes the values seen by the taps and to illustrate what should be expected when PSP will be implemented onto the experimental rig. The experimental data shown here was implemented before the film cooling section had been created, was run under different conditions than this simulation, and had a more losses because of non-ideal portions, so only the trends will be matched, not the exact pressure and the data will be slightly offset to illustrate this. It can be seen from these images that the numerical model have a very similar trend, but the numerical model seems to under-predict the results. This may simply be an effect of the different conditions between the models or it may represent that additional corrections need to be added to the numerical model. Further research would need to be carried out on the current experimental rig in open-loop conditions to ensure these measurements are still valid.

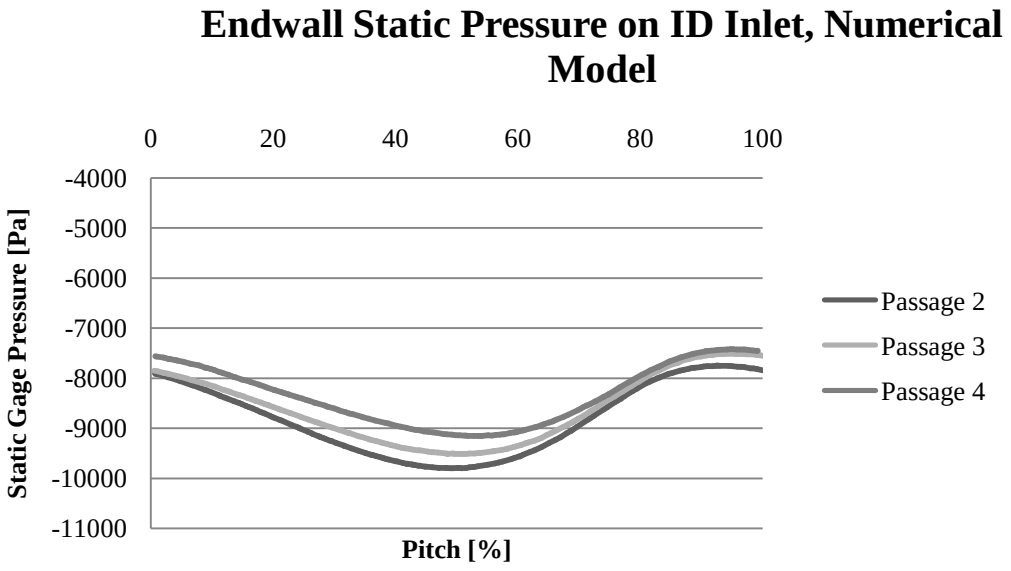

Figure 66: Endwall static gage pressure on ID inlet from numerical model.

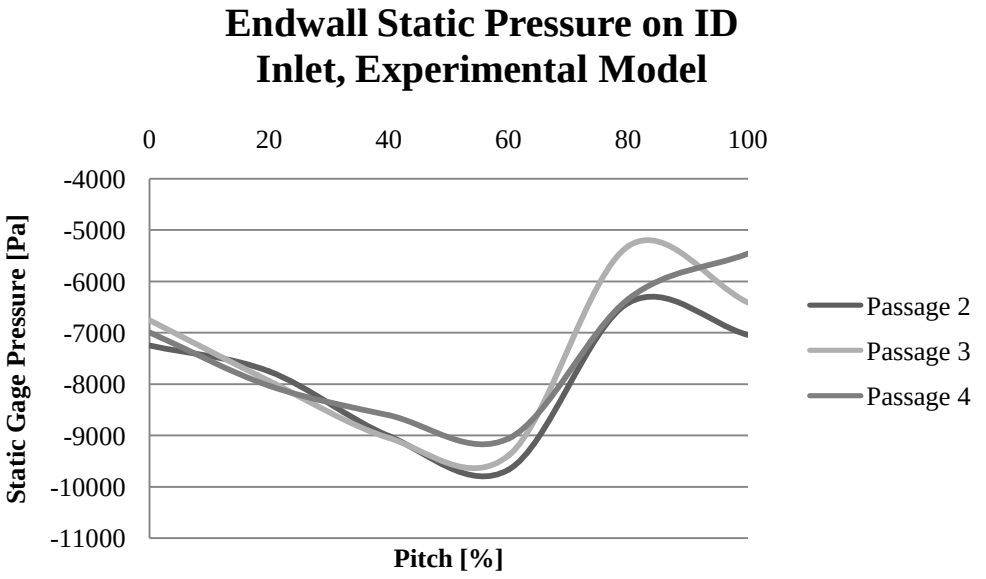

Figure 67: Endwall static gage pressure on ID inlet from experimental model.

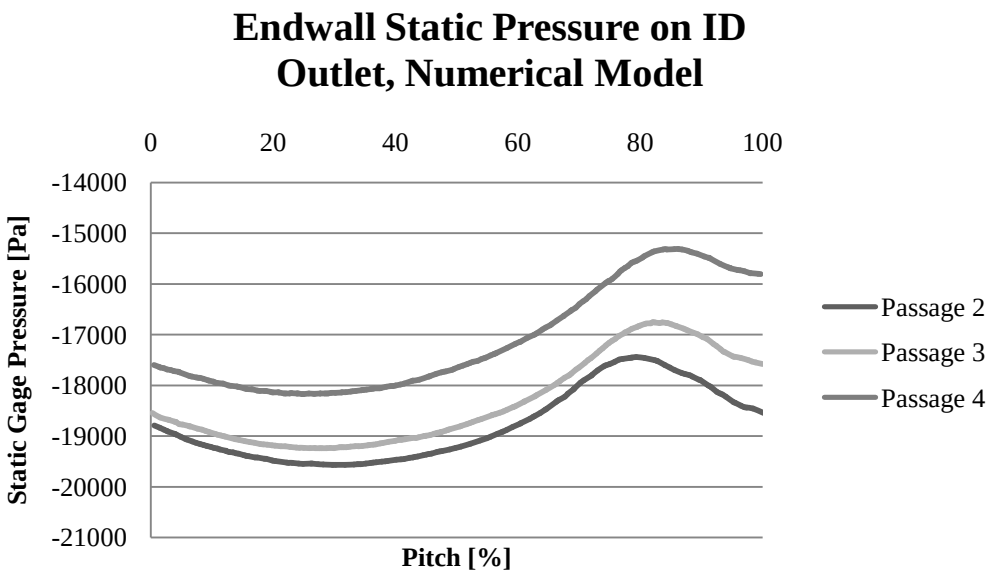

Figure 68: Endwall static gage pressure on ID outlet from numerical model.

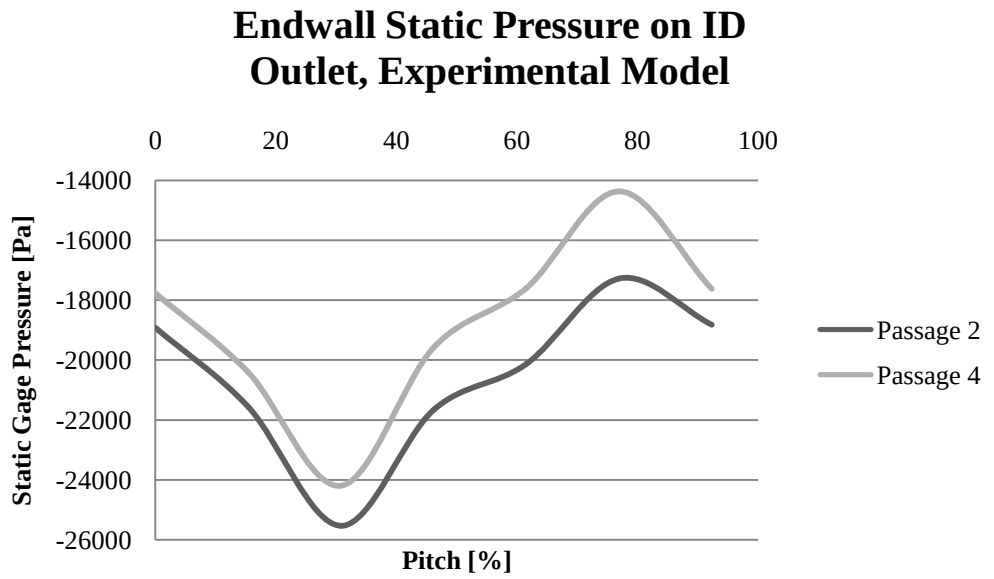

Figure 69: Endwall static gage pressure on ID outlet from experimental model.

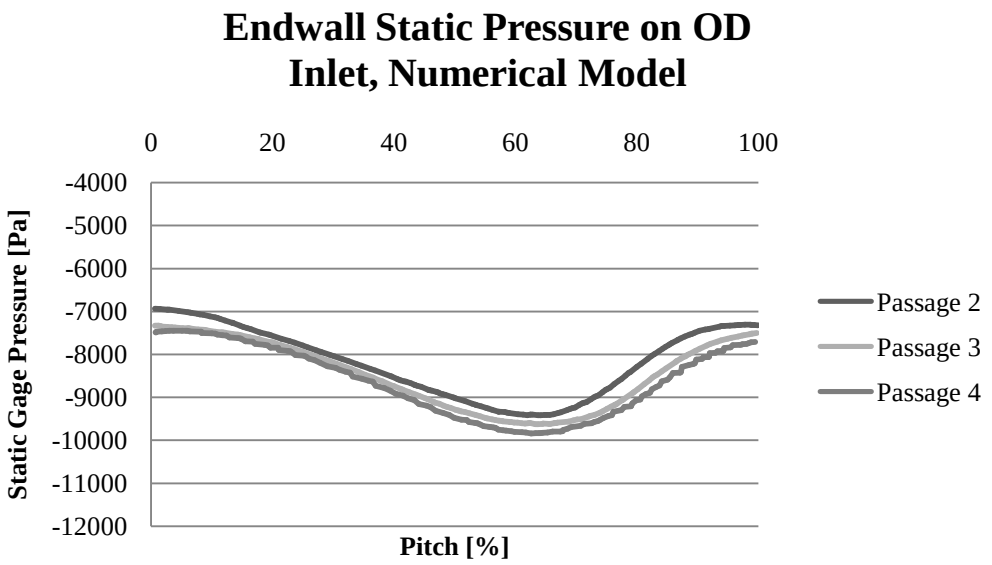

Figure 70: Endwall static gage pressure on OD inlet from numerical model.

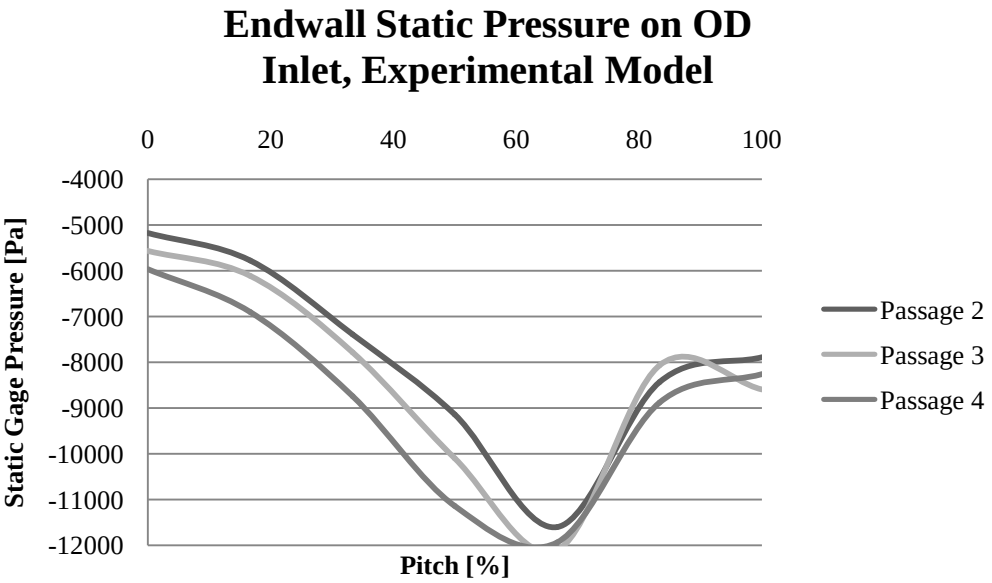

Figure 71: Endwall static gage pressure on OD inlet from experimental model.

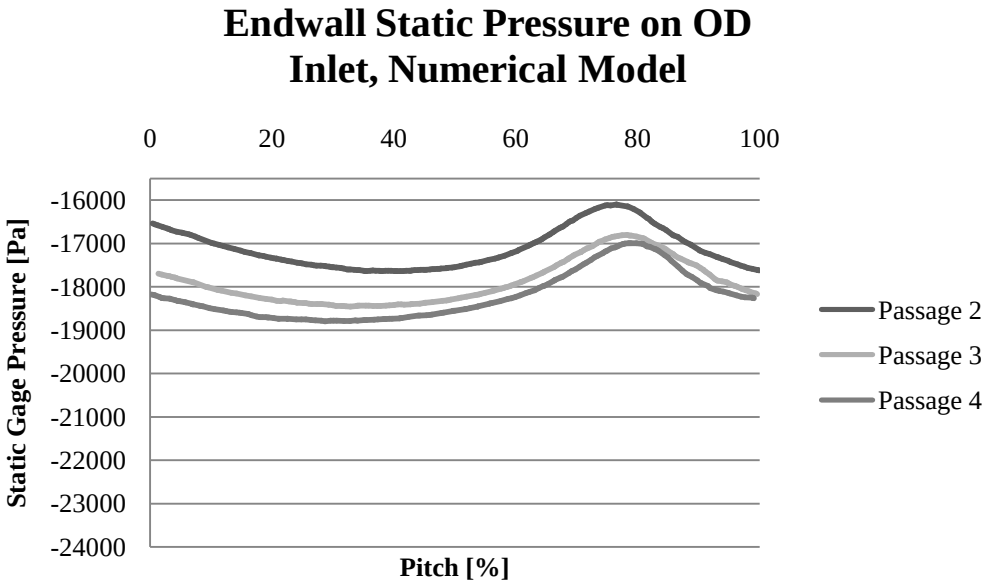

Figure 72: Endwall static gage pressure on OD outlet from numerical model.

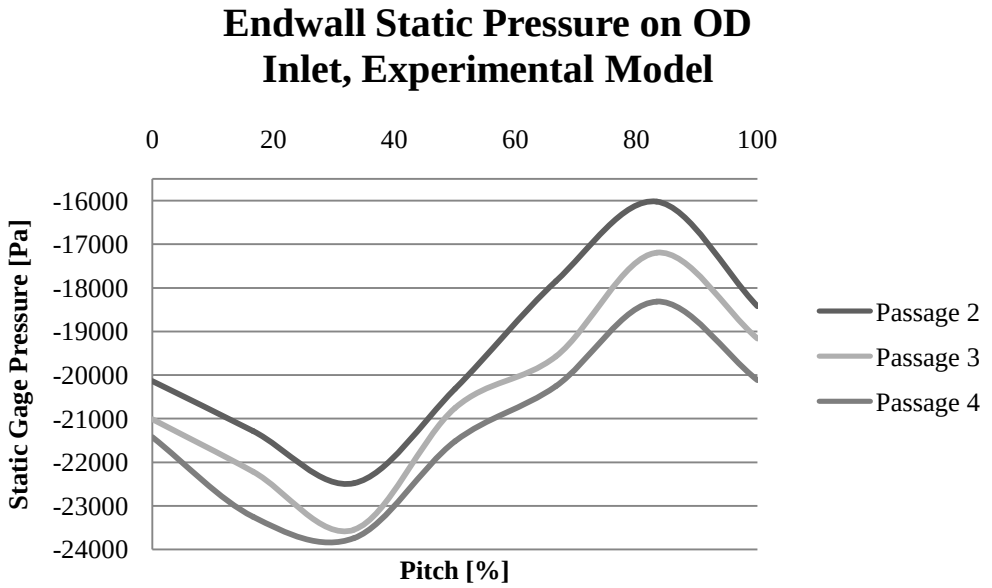

Figure 73: Endwall static gage pressure on OD outlet from experimental model.

Now that the endwall comparisons have been shown, static pressure contours on the inner and outer endwalls as well as those at 25, 50, and 75% will be displayed to assist in future research. These additional views are shown because this passage is annular and the blades are three-dimensional in shape, so each plane of the passage should be unique and provide additional insight into the flow structure. From the conclusions previously noted in this work, the differences in static pressure should be greater than shown in the numerical model, either because it under-predicts the solution or because the assumed mass flow in the simulation was lower than that of the real model. It can be seen from these models that the three center passages are similar, but that the two end passages do not have similar flow patterns.

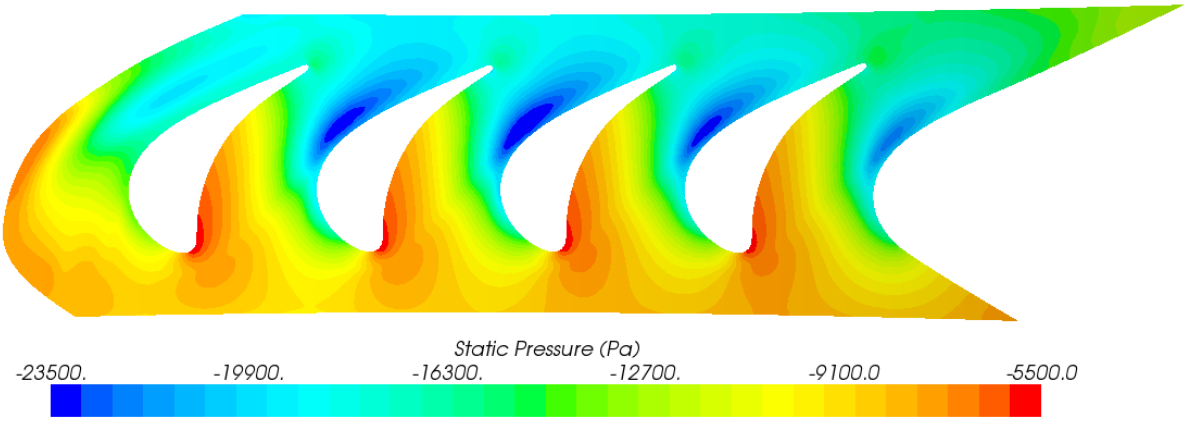

Figure 74: Static pressure distribution on the ID surface, numerical simulation.

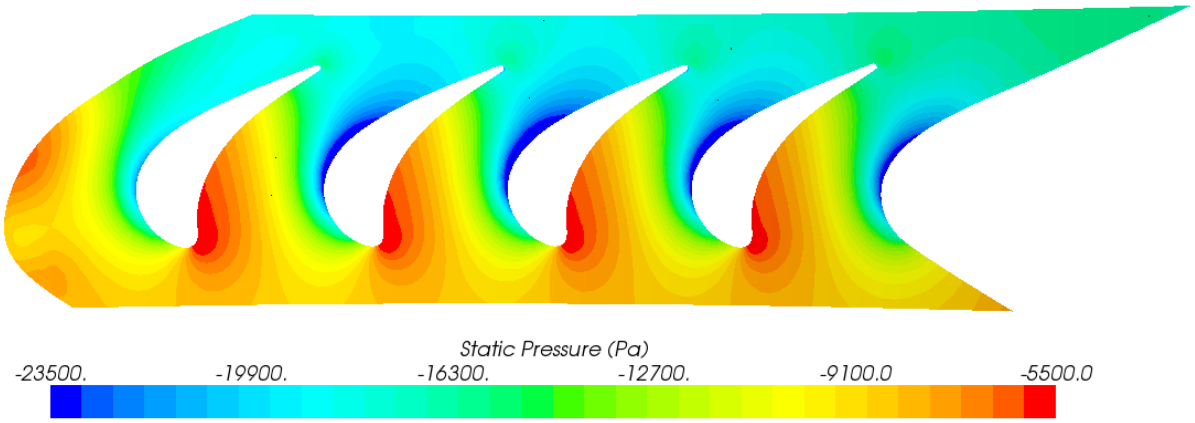

Figure 75: Static pressure distribution on 25% radial cut, numerical simulation.

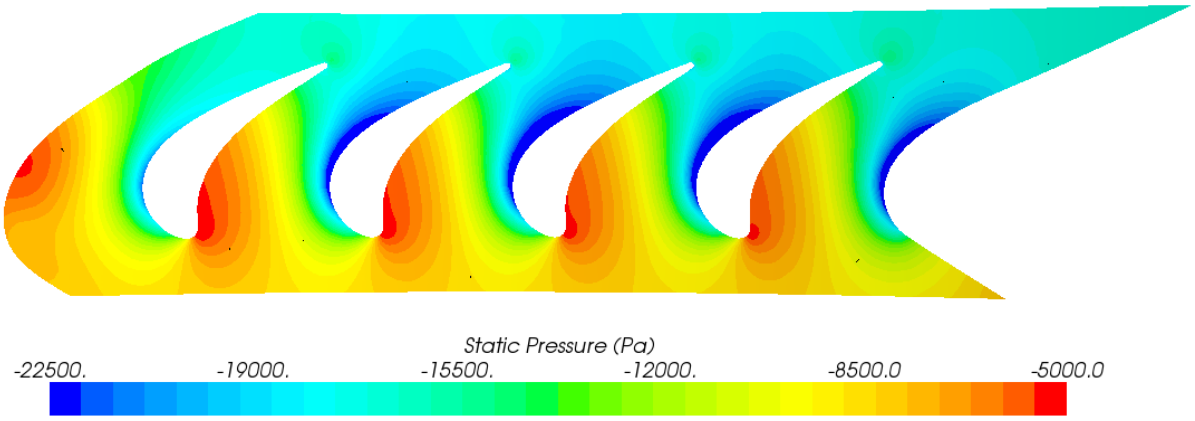

Figure 76: Stati pressure distribution on 50% radial cut, numerical simulation.

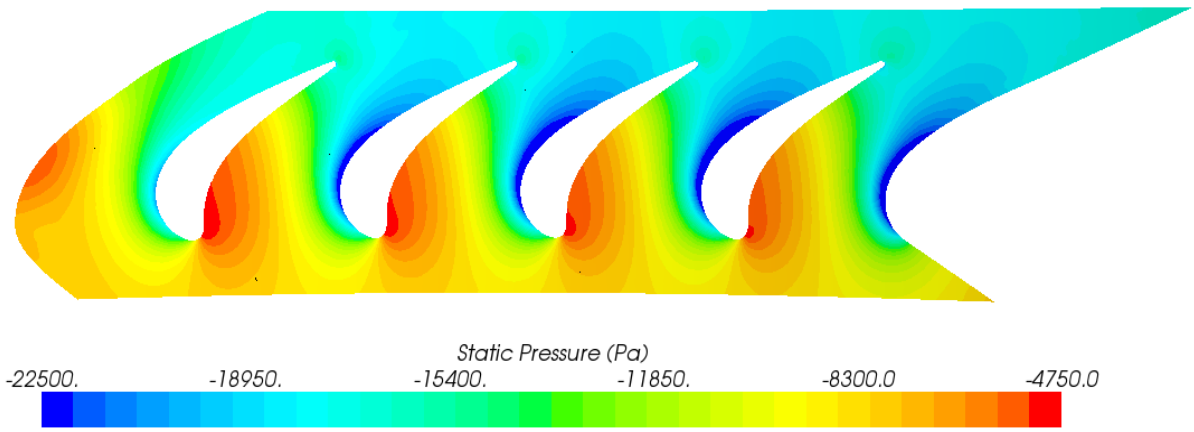

Figure 77: Static pressure distribution on 75% radial cut, numerical simulation.

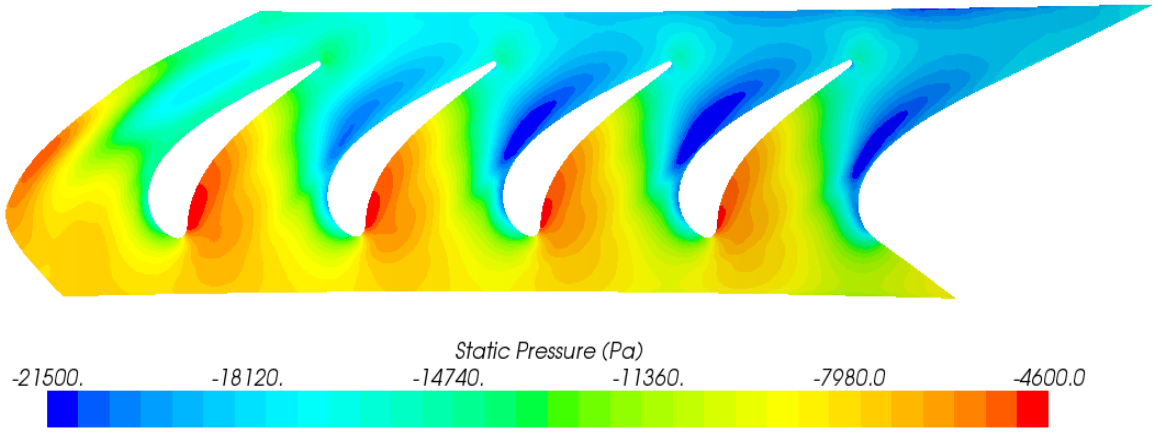

Figure 78: Static pressure distribution on the OD surface, numerical simulation.

5.3 Predictions of Pressure Distribution over a Blade Surface

A subject of current research at the CATER lab is determining the pressure distribution on the SS and PS of a blade surface. This has not yet successfully been completed, but this work will see to provide predictions to assist with this analysis. The values obtained here should be considered trends, but based on the previous data obtained, the static pressures at the exit will likely be much lower than shown in the simulation. First, lineplots will be shown at 0, 25,50,75, and 100% of span, where 0% is at the ID and 100% is at the OD. Then images will be shown to illustrate the pressure distribution over the entire blade surfaces. The pressure distribution over all the blades is shown for several reasons. First, it is beneficial to understand if all the blades are relatively periodic. Additionally, the program used does not have the ability to take cylindrical cross sections of only one blade, so any other choice would have resulted in less accurate data.

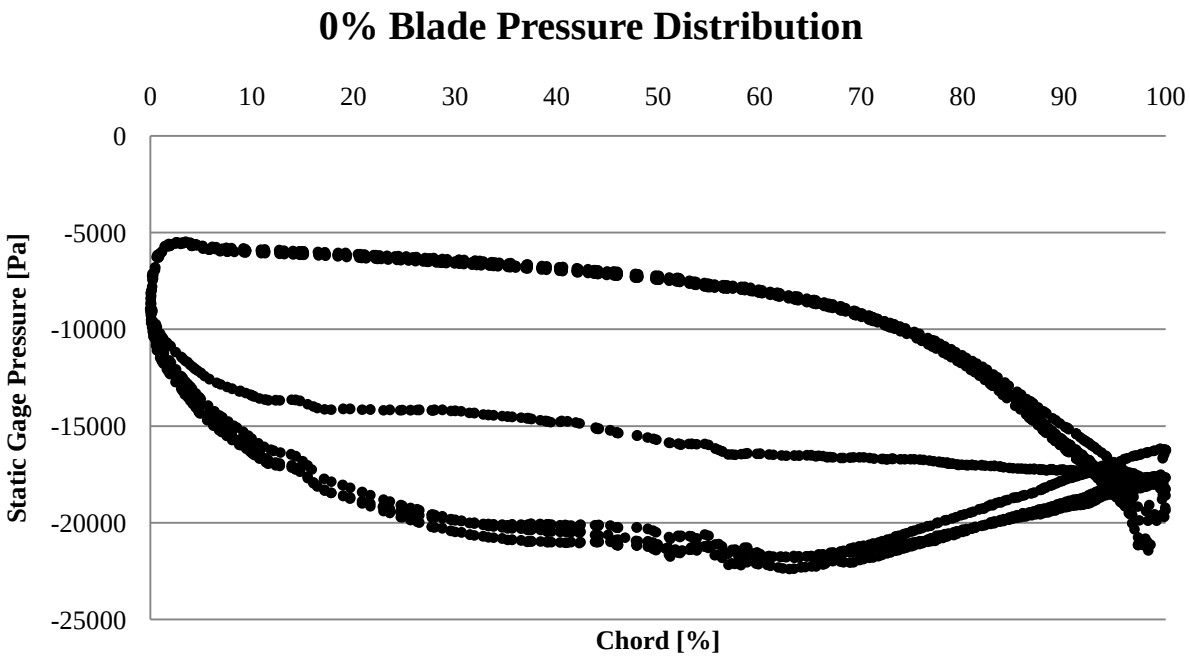

Figure 79: Static pressure distributions over the suction and pressure sides of the blade surface at 0% span.

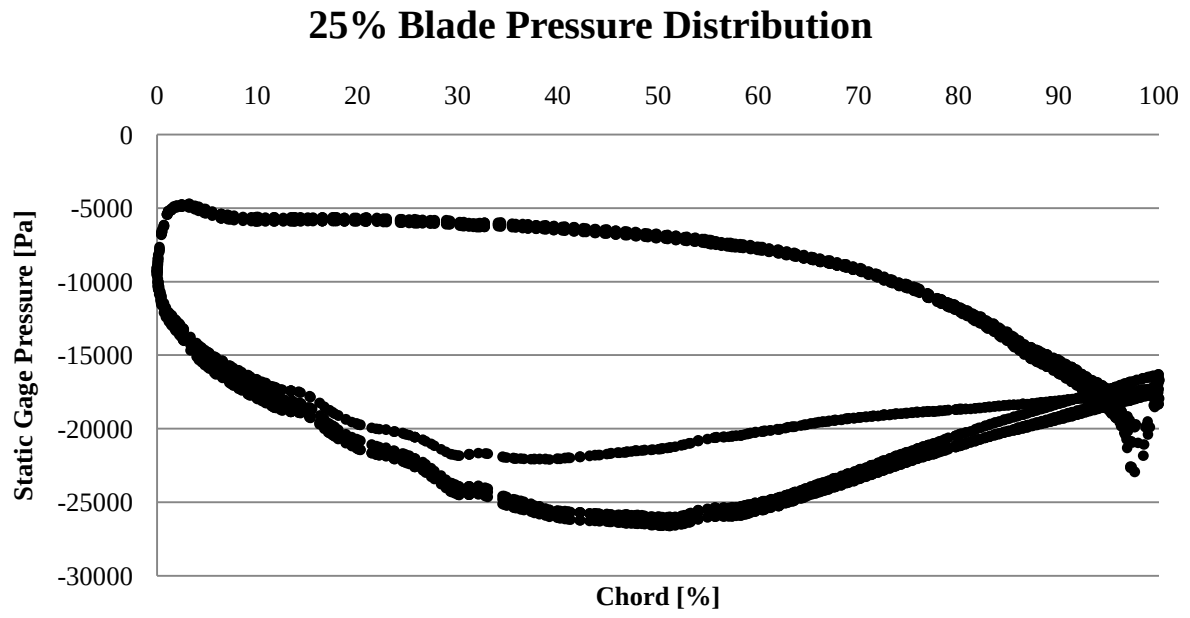

Figure 80: Static pressure distributions over the suction and pressure sides of the blade surface at 25% span.

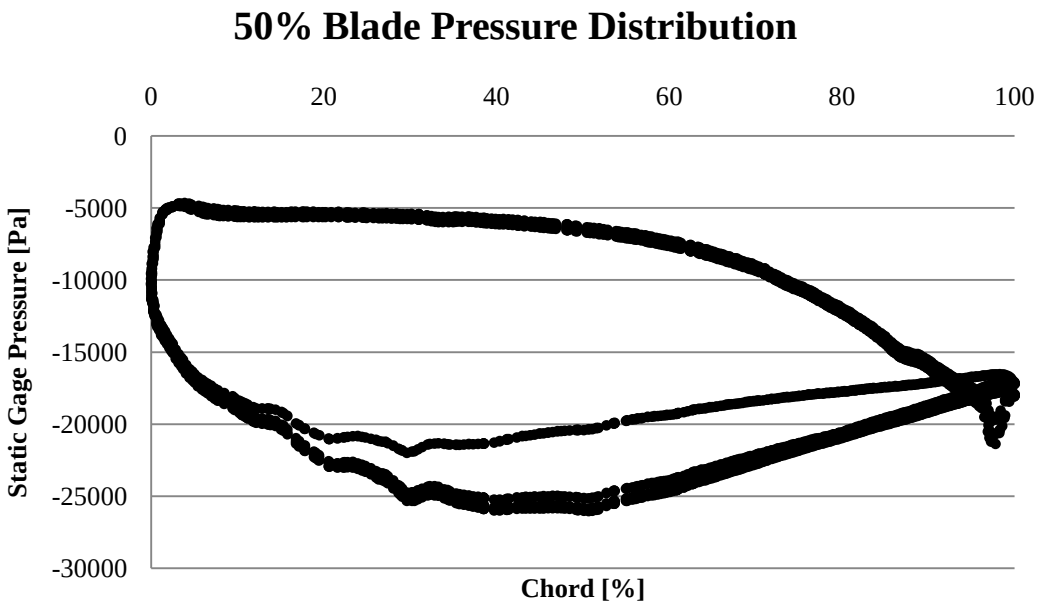

Figure 81: Static pressure distributions over the suction and pressure sides of the blade surface at 50% span.

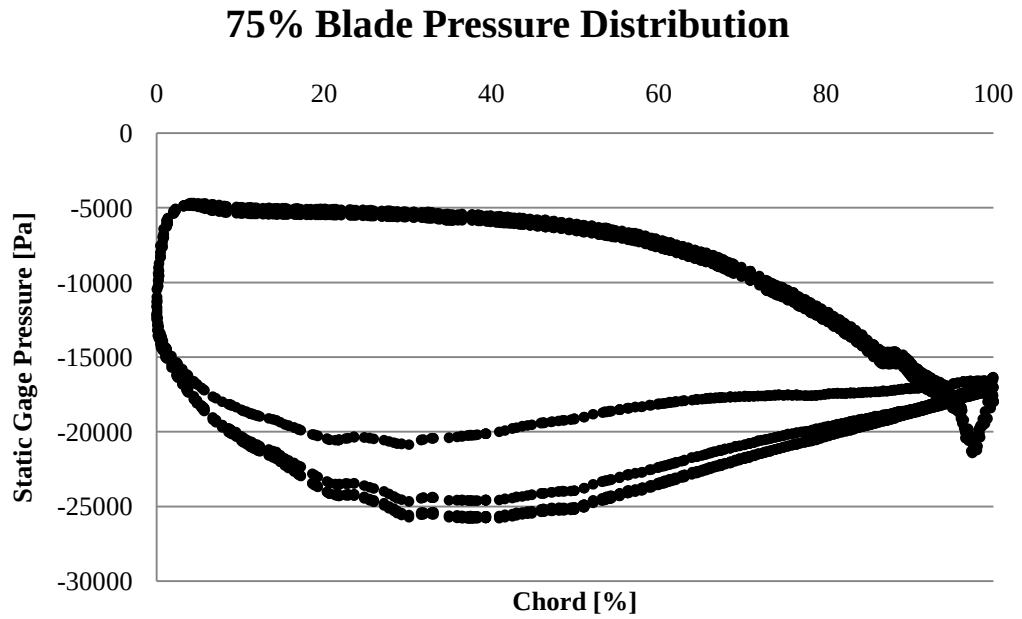

Figure 82: Static pressure distributions over the suction and pressure sides of the blade surface at 75% span.

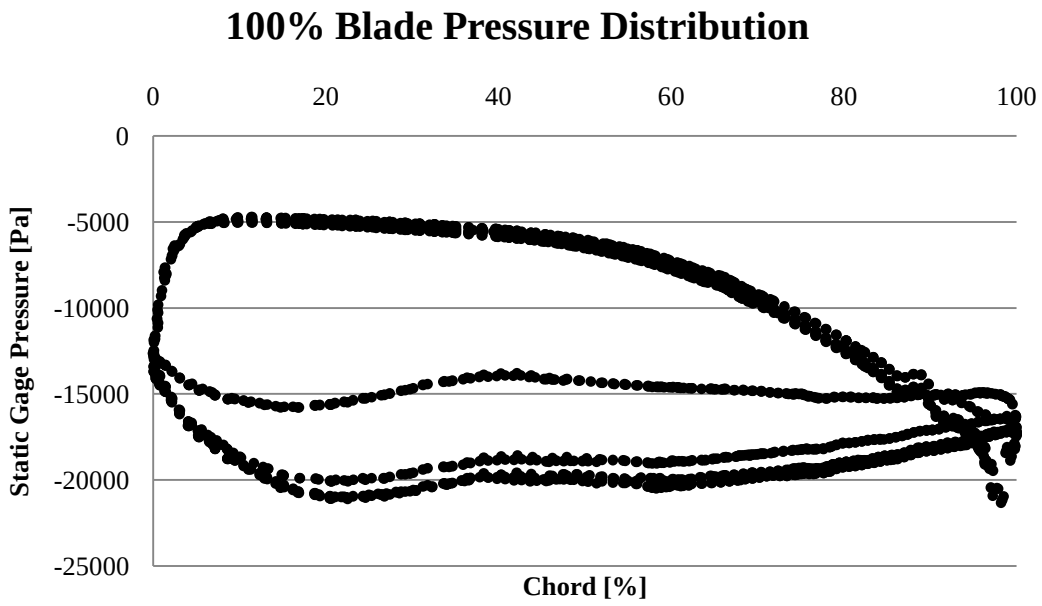

Figure 83: Static pressure distributions over the suction and pressure sides of the blade surface at 100% span.

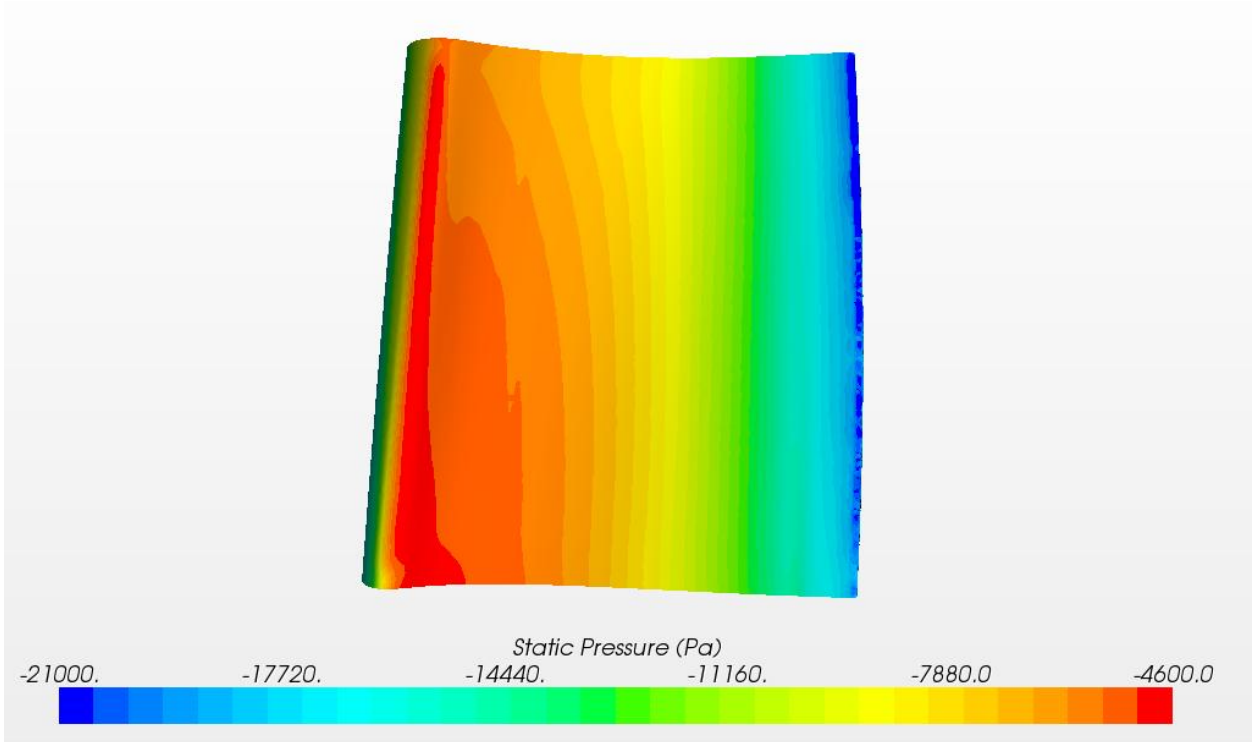

Figure 84: Static gage pressure over PS of blade.

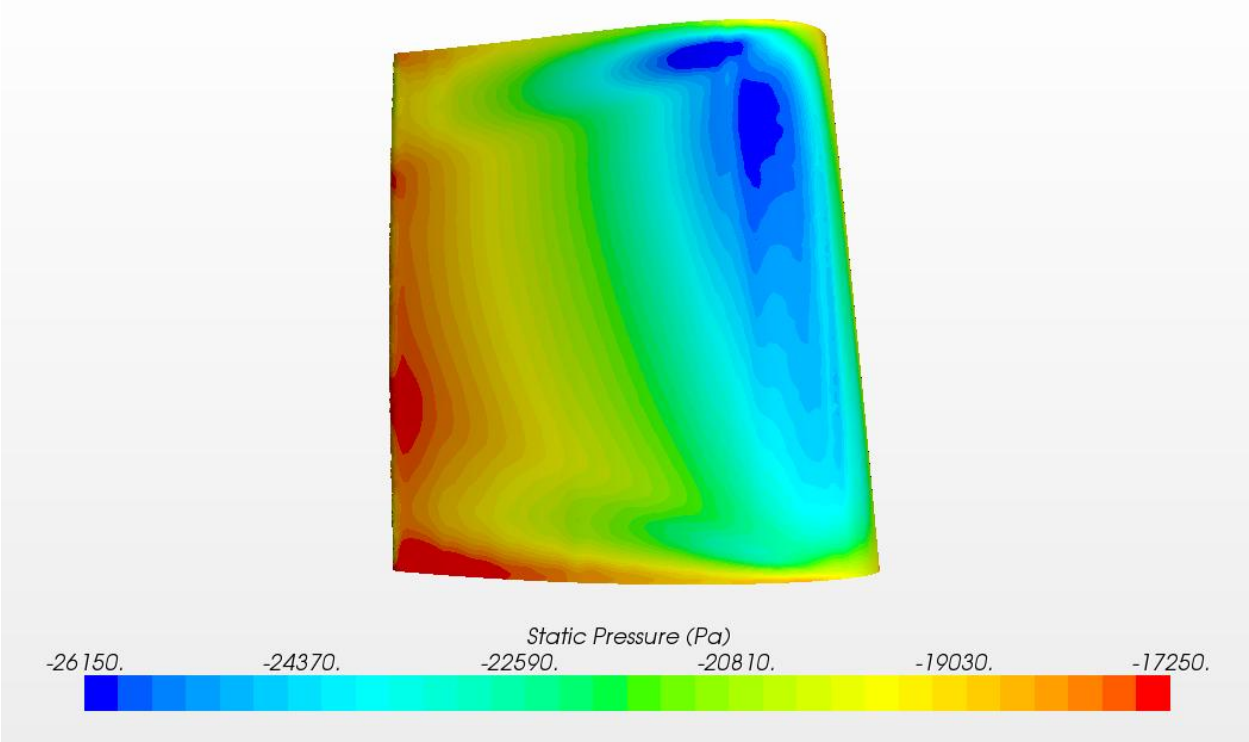

Figure 85: Static gage pressure over SS of blade.

5.4 Total Pressure Loss Comparisons

Another area of ongoing study in the CATER facility is investigating the total pressure losses in the experimental cascade to study secondary flows and how they are affected by film cooling. These numerical results will be compared to several works shown below such as Casey [1], Nguyen [20], and Friedrichs [9]. Casey performed an experimental study on loss in the E^3 experimental cascade and presented his study in terms of percent pressure loss, so his results will appear slightly different those others who used the total pressure loss coefficient. The definition used for this study is shown below where the $P_o$inlet and Poutlet are mass averaged over their respective flow areas. For Poutlet, this is the cascade exit and for $P_o$inlet this is the mainflow section before the coolant holes and coolant plenum inlet.

$$\zeta = \frac{P_o inlet - P_o local}{P_o inlet - Poutlet} \tag{11}$$

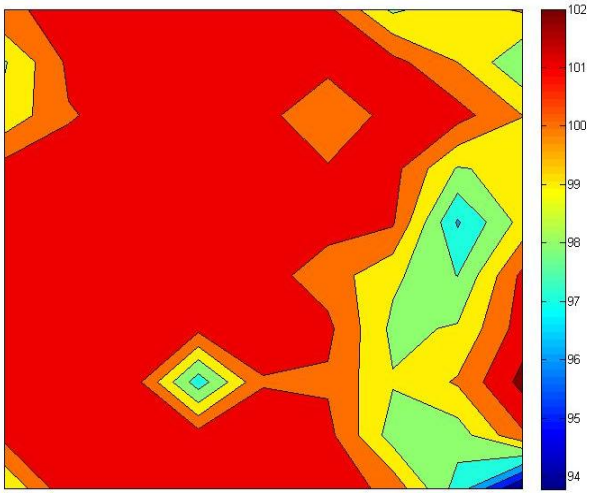

Figure 86: Total pressure map at cascade exit without film cooling [1].

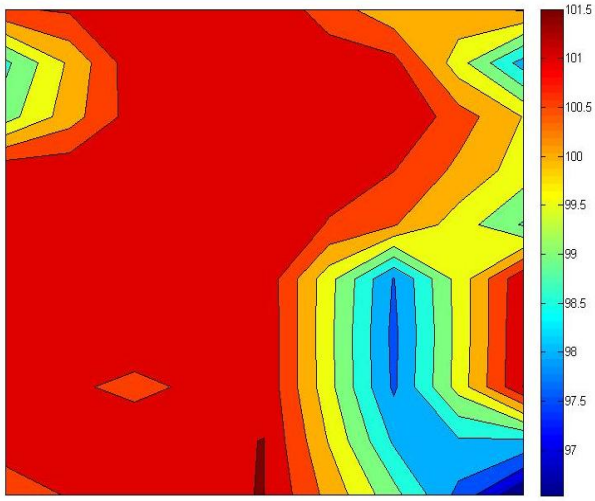

Figure 87: Total pressure map at cascade exit with film cooling, BR=0.3 [1].

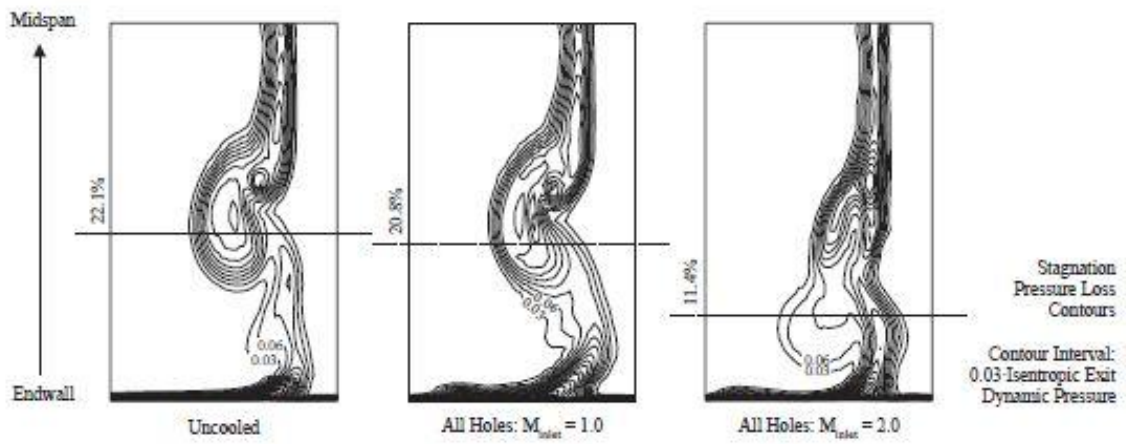

Figure 88: Friedrichs investigation of total pressure loss contours [9].

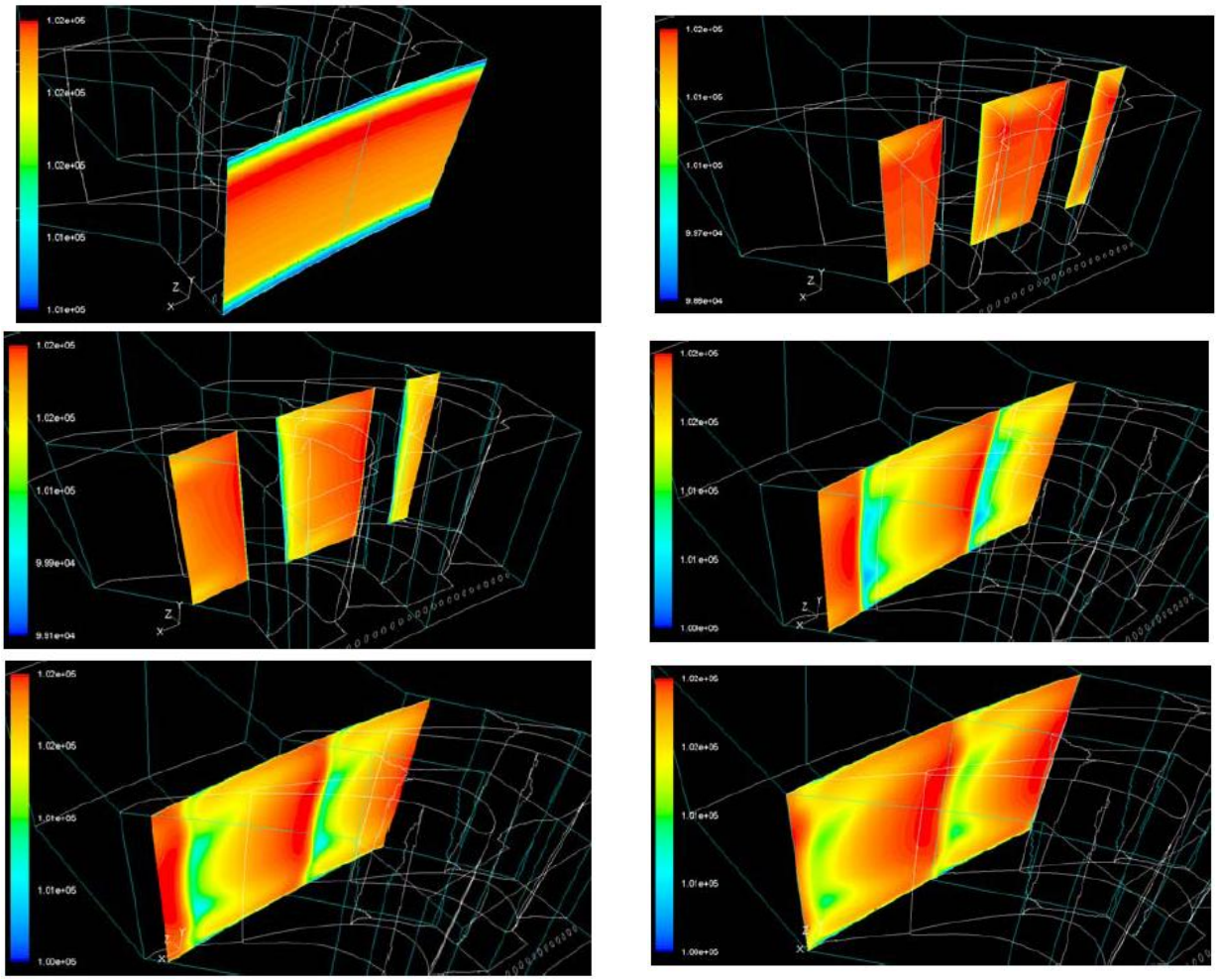

Figure 89: Various pressure loss images from Nguyen [20].

In comparison to the works of Casey, losses have been mapped at a similar location along the cascade and the results are shown below. It can be seen that these works are similar, though the experimental results seem to show another secondary flow in the bottom center of the passage that is not indicated by the numerical results, so this would be a good topic for future study.

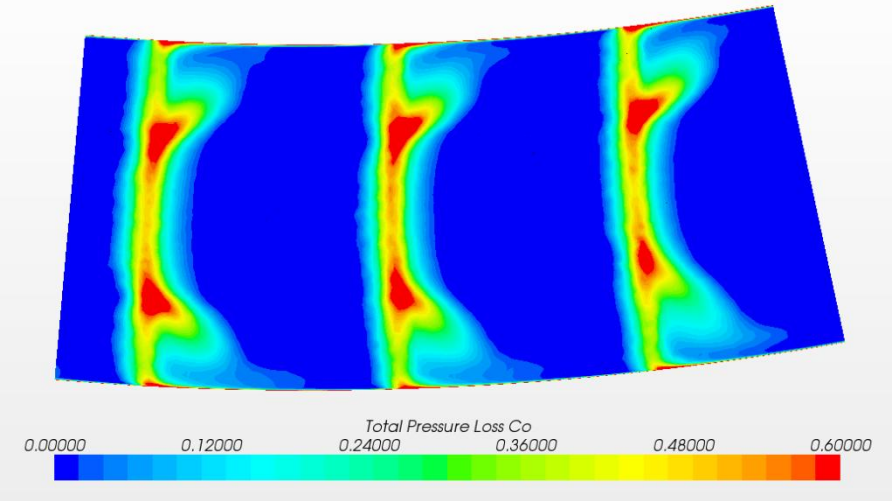

Figure 90: Total pressure loss coefficients at cascade exit.

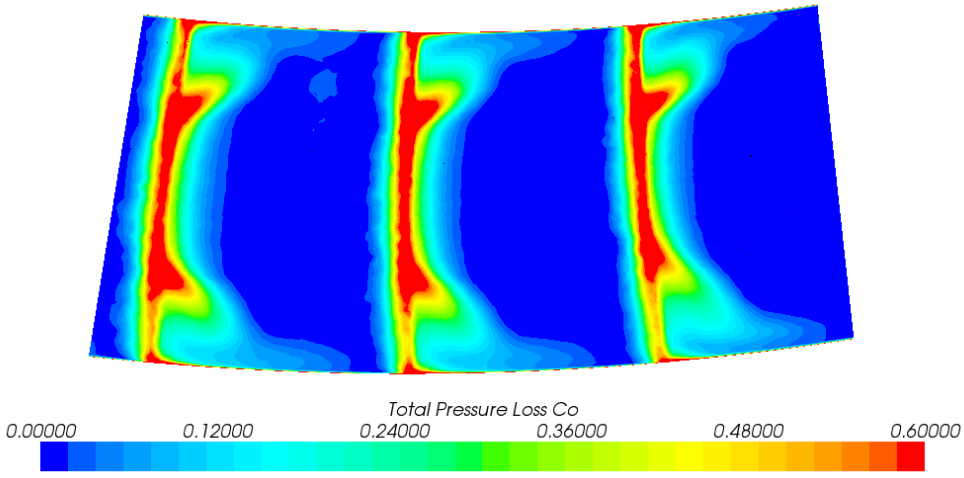

Figure 91: Total pressure loss coefficients at cascade exit with film cooling.

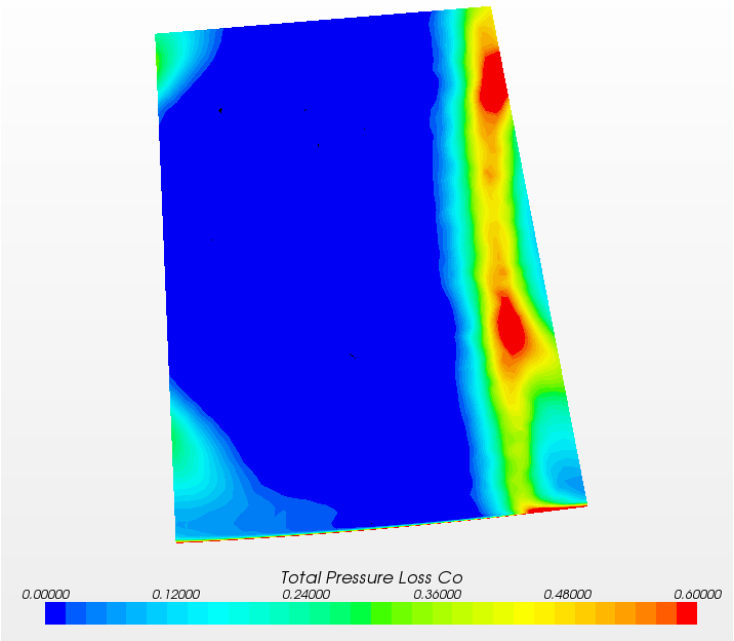

Figure 92: Cropped numerical results.

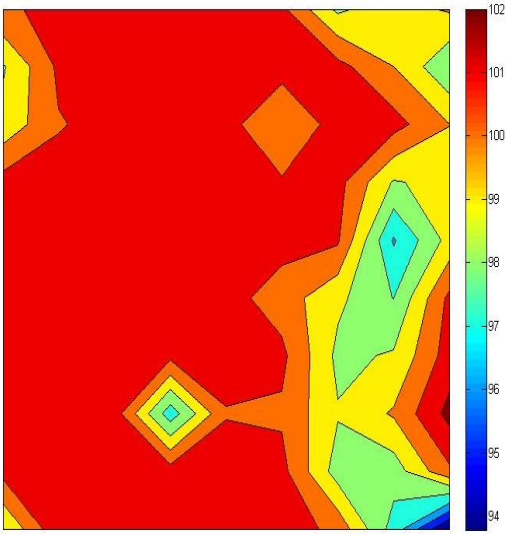

Figure 93: Results of Casey [1].

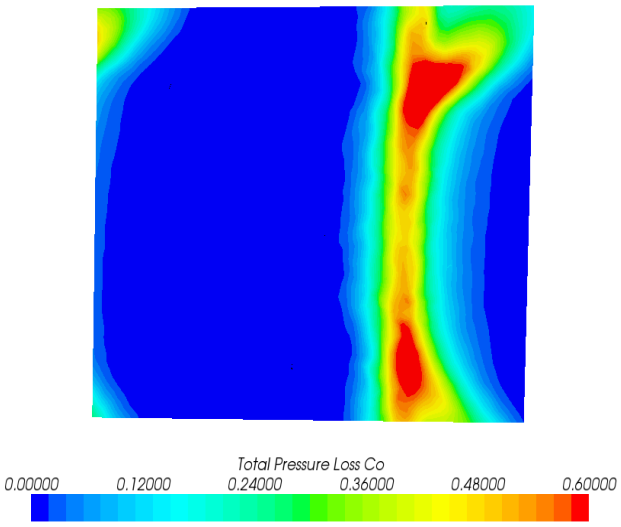

Figure 94: Cropped numerical results with film cooling.

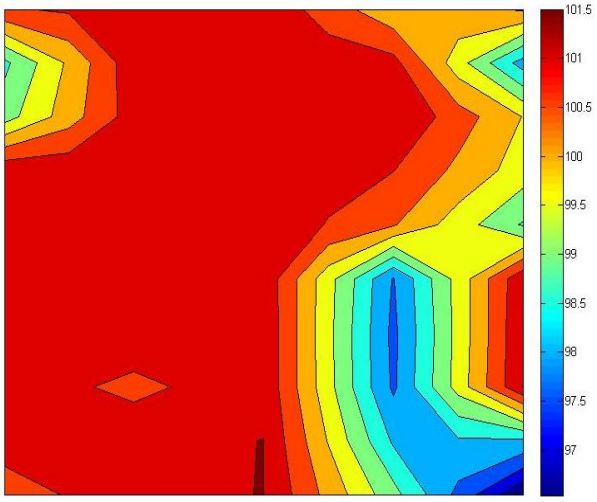

Figure 95: Results of Casey with film cooling [1].

The images above show comparisons to Casey [1]. It can be noted that the numerical results appear very similar, but the experimental results have significant differences. The cause of this is unknown because these images are biased toward the OD of the cascade where a BR of 0.5 should not

have been able to penetrate and cause any result. This issue should also be a topic of further study to validate this results and determine the physical mechanism creating this data.

The total pressure loss coefficient data was gathered for plane throughout the cascade for conditions with and without film cooling so that the secondary flows and th effects of film cooling on them can be observed. The development of the horseshoe vortex is very clear on the suction side of the blades and mirrors the work of Nguyen [1] and Friedrichs [9]. The passage vortex and pressure side horseshoe vortex are not very clear, so further studies should see whether they are being suppressed by a factor in the simulation.

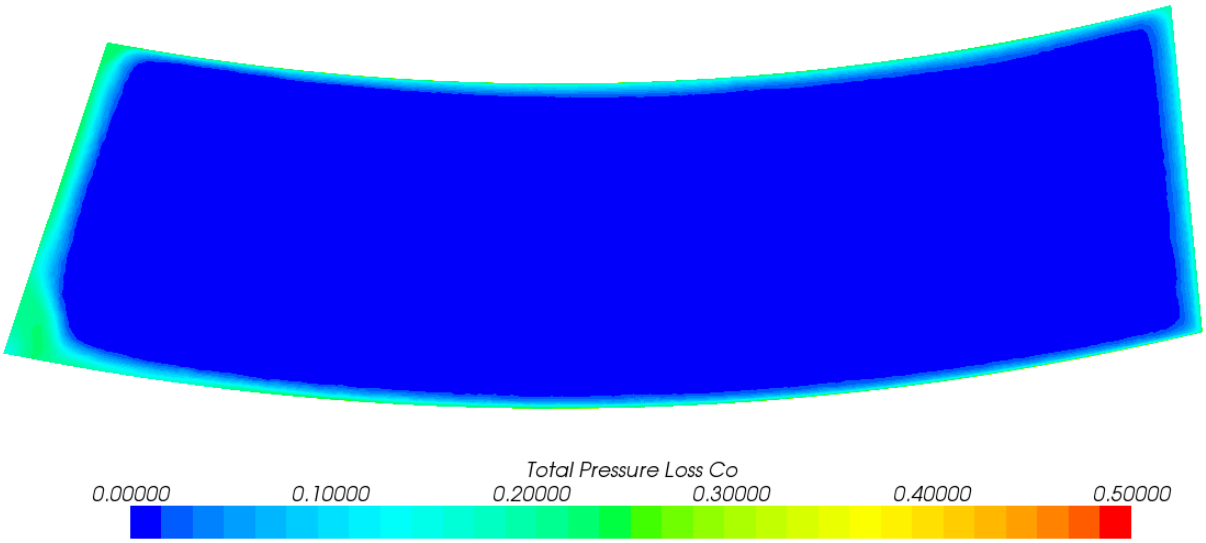

Figure 96: Total pressure loss coefficient upstream of blades, no film cooling.

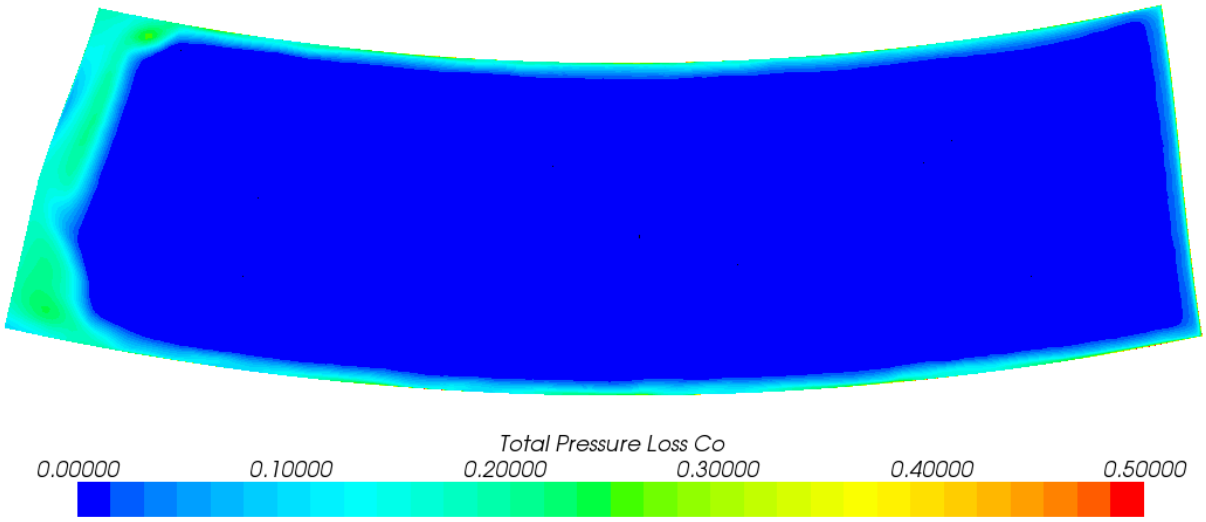

Figure 97: Total pressure loss coefficient at 0% chord, no film cooling.

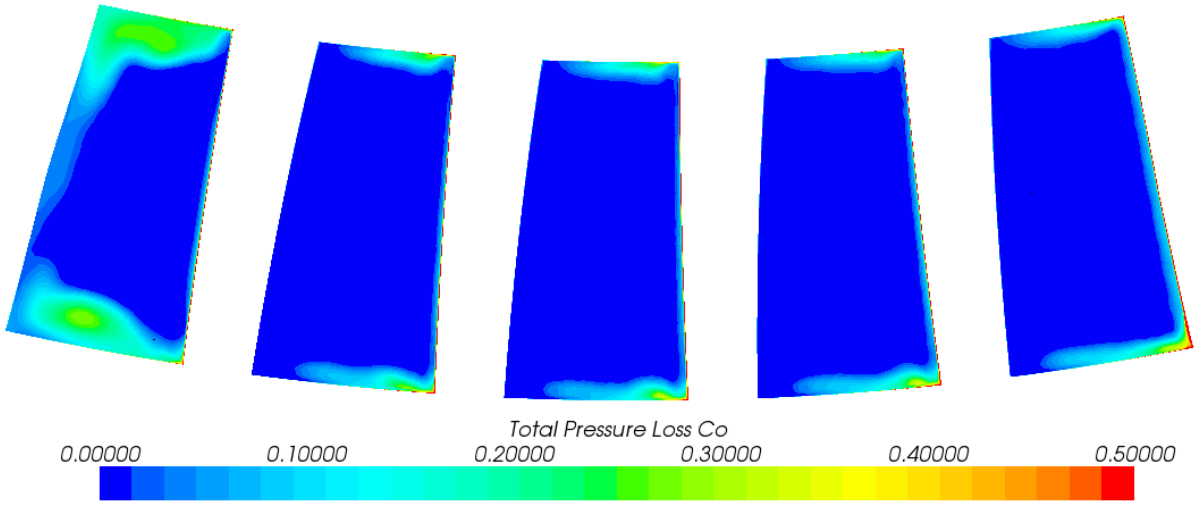

Figure 98: Total pressure loss coefficient at 25% chord, no film cooling.

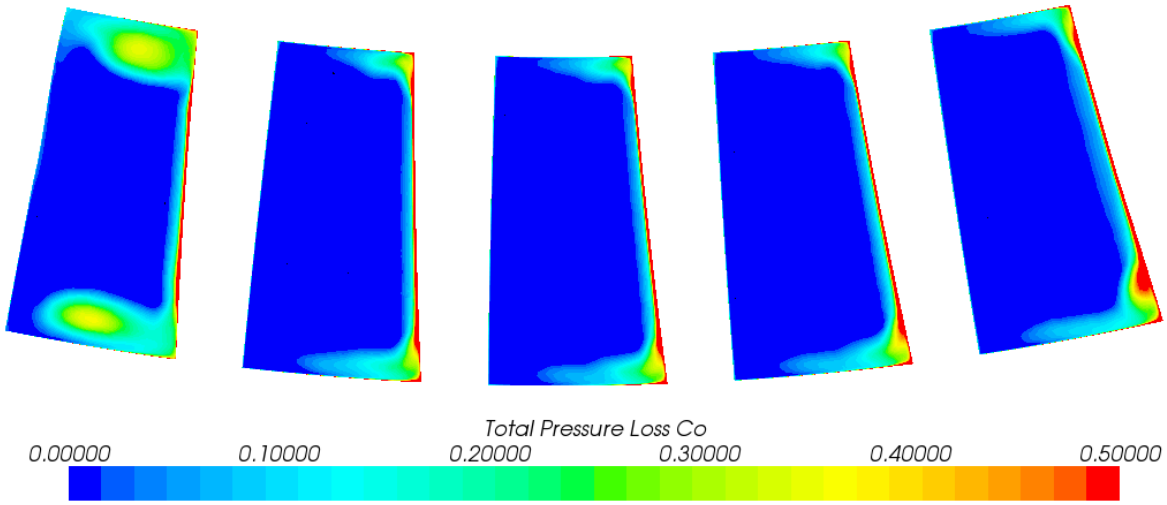

Figure 99: Total pressure loss coefficient at 50% chord, no film cooling.

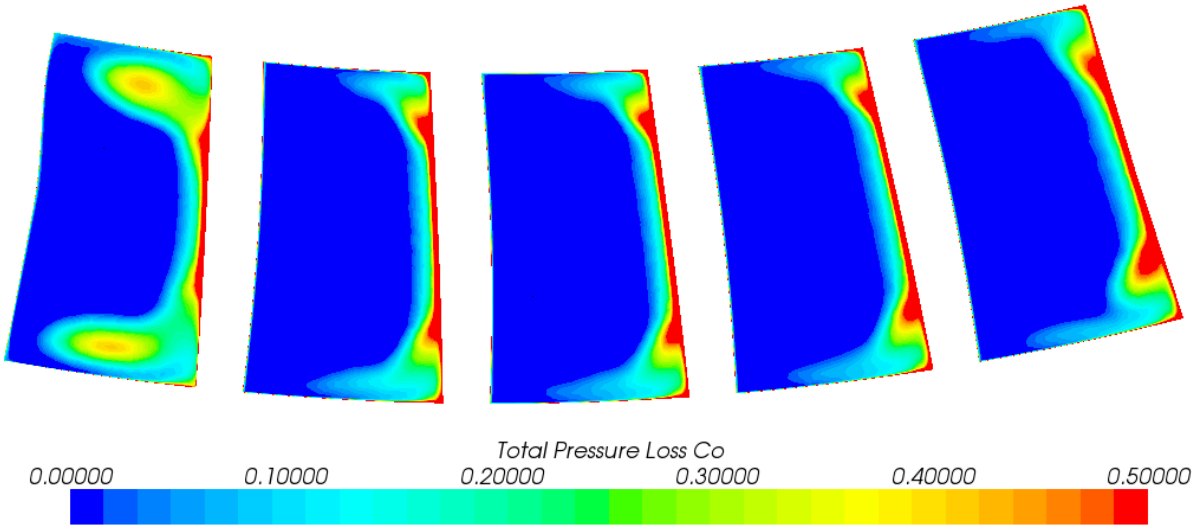

Figure 100: Total pressure loss coefficient at 75% chord, no film cooling.

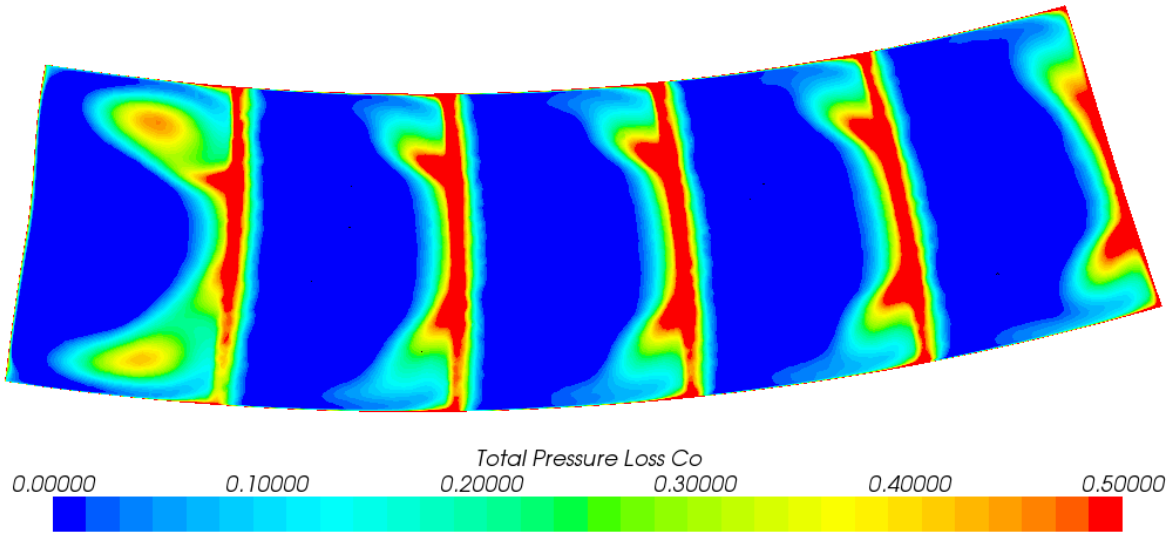

Figure 101: Total pressure loss coefficient at 100% chord, no film cooling.

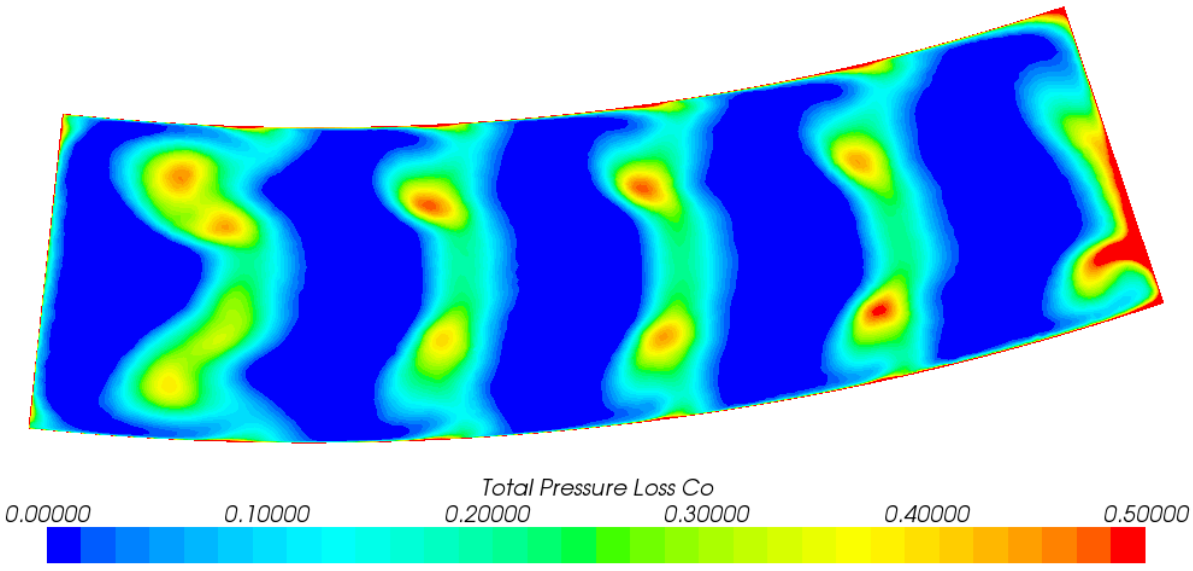

Figure 102: Total pressure loss coefficient downstream of blades, no film cooling.

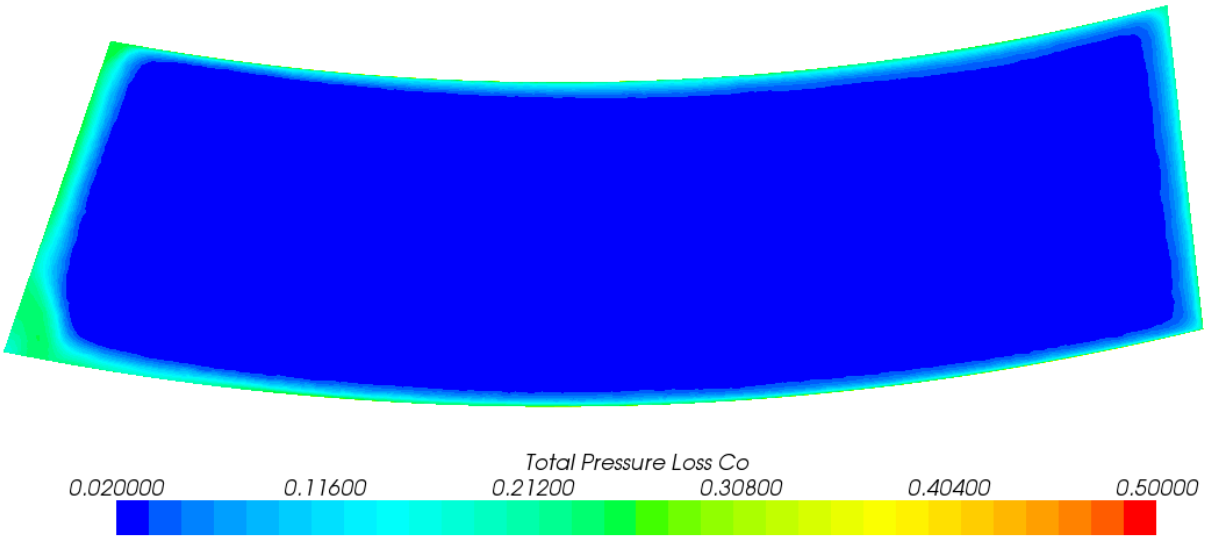

Figure 103: Total pressure loss coefficient upstream of cascade, with film cooling.

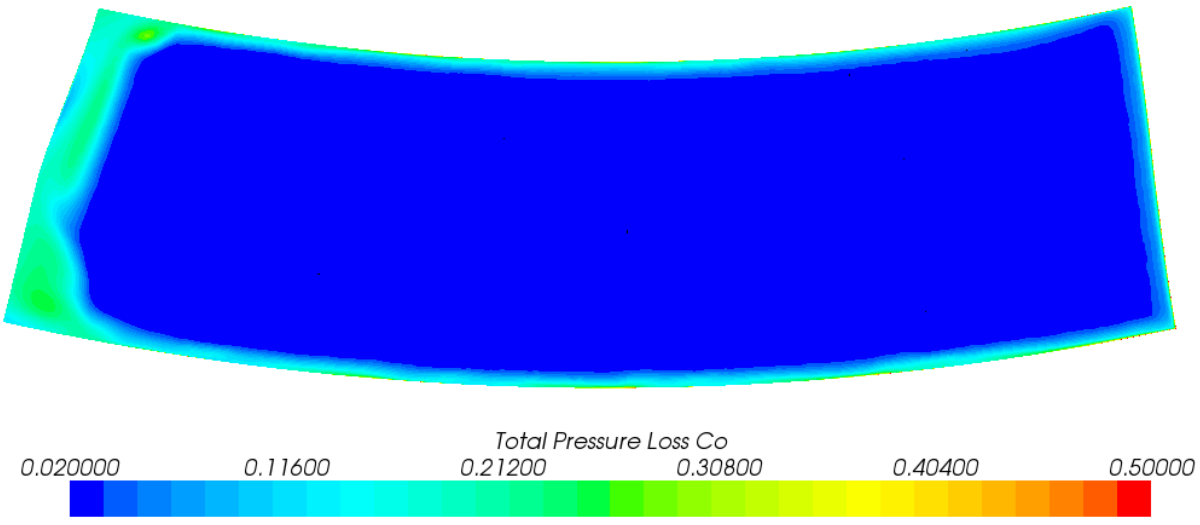

Figure 104: Total pressure loss coefficient at 0% chord, with film cooling.

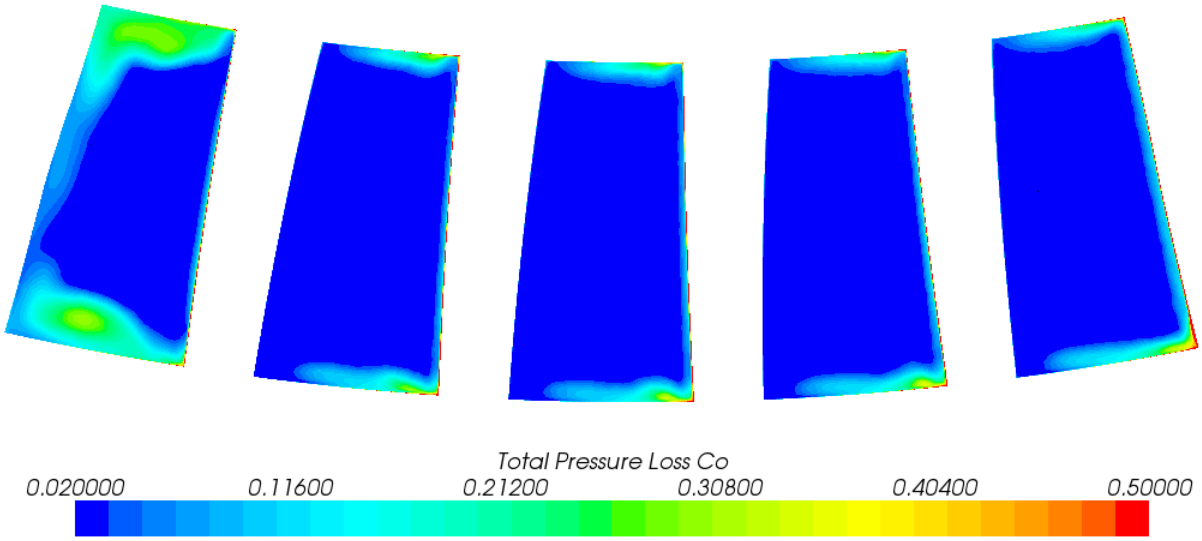

Figure 105: Total pressure loss coefficient at 25% chord, with film cooling.

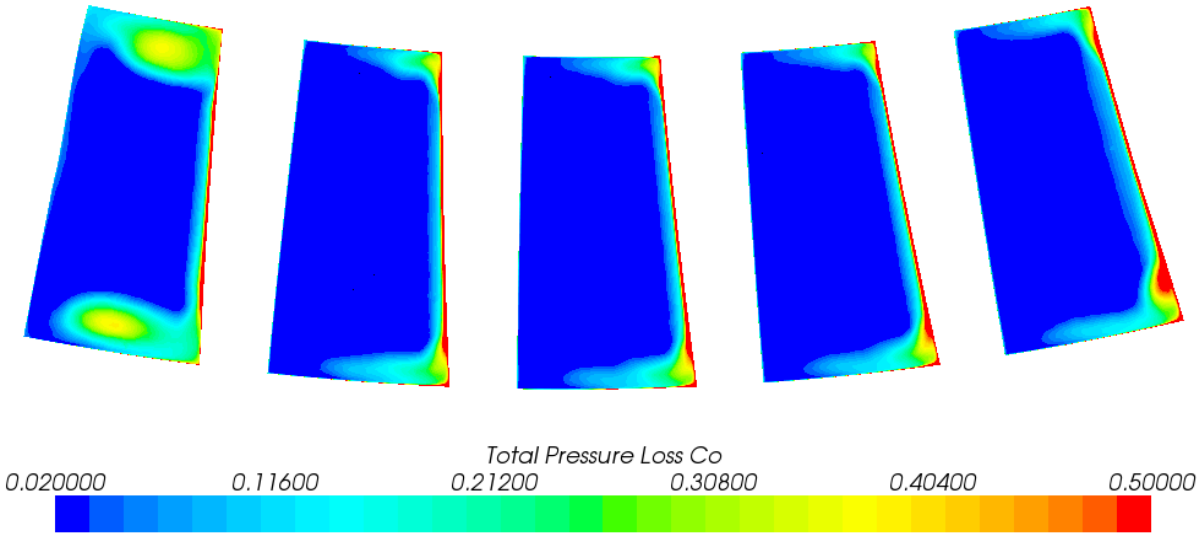

Figure 106: Total pressure loss coefficient at 50% chord, with film cooling.

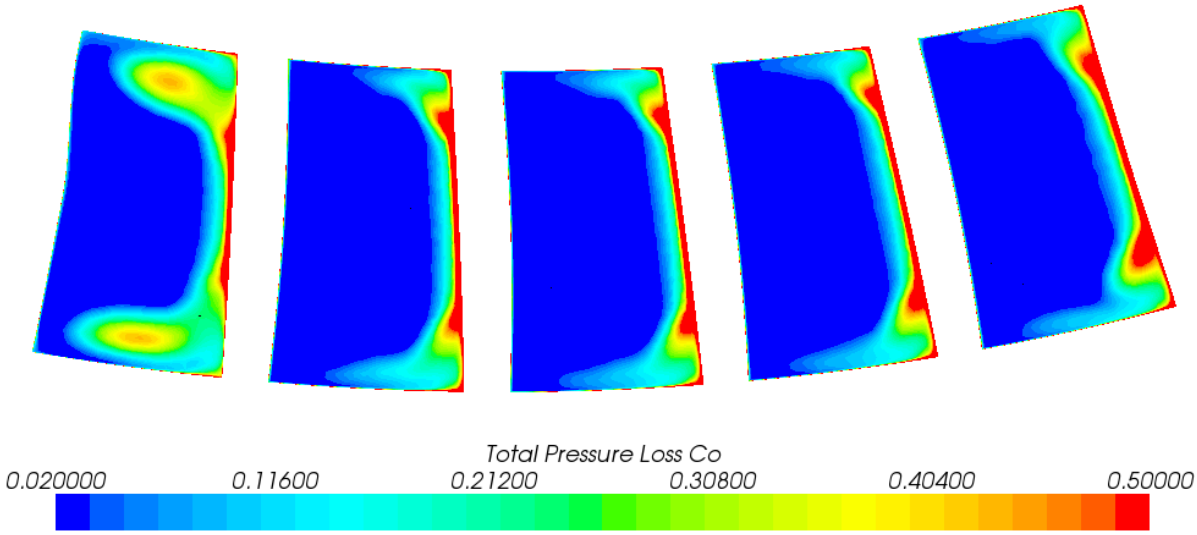

Figure 107: Total pressure loss coefficient at 75% chord, with film cooling.

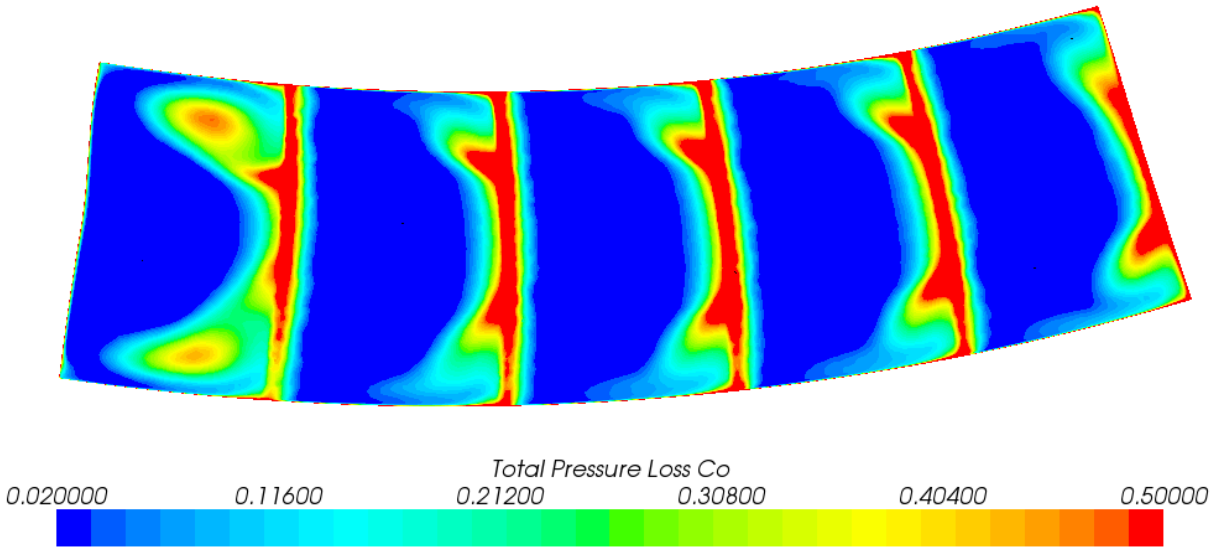

Figure 108: Total pressure loss coefficient at 100% chord, with film cooling.

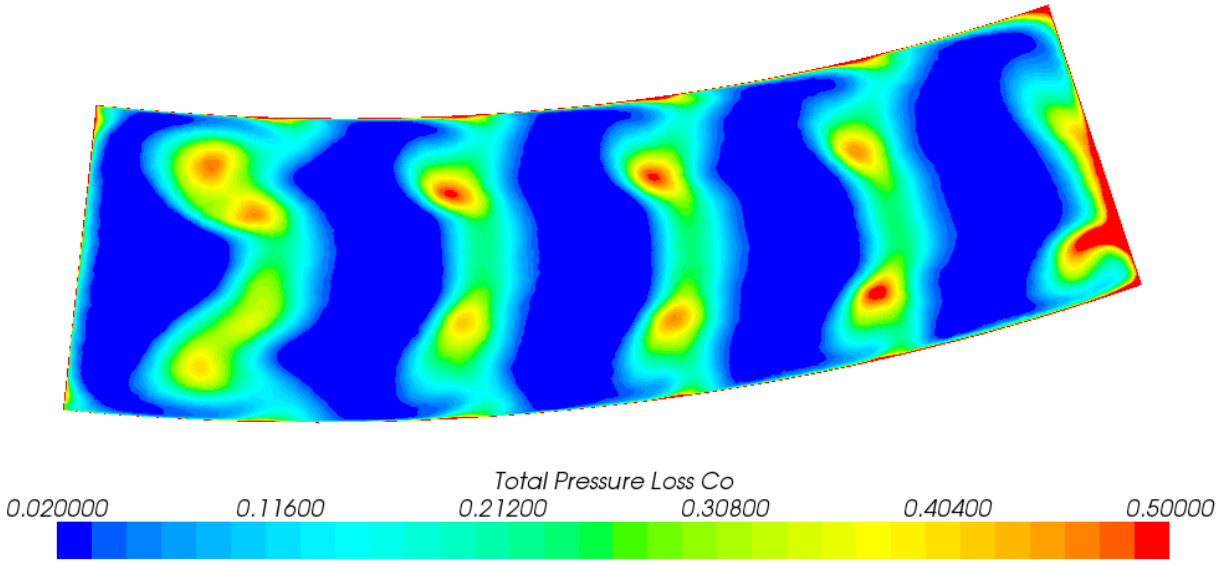

Figure 109: Total pressure loss coefficient downstream of cascade, with film cooling.

5.5 Film Cooling Effectiveness Comparison

Experiments were performed on the E^3 cascade to determine the endwall film cooling effectiveness of various blowing ratios, discussed in Casey [19]. Due to equipment limitations, only a blowing ratio of 0.5 has been tested so far, so that case was simulated in this thesis. This was the first time TSP had been implemented in the experimental rig and therefore these results are still somewhat rough. However, it can be seen from the results that the trends are very similar between the two cases and that the numerical simulation performs well. The inner diameters of the model where heat transfer occurs contain a much finer prism layer region than the rest of the model such that the smallest prism layer would be much less than 1 so that there were multiple cells within the y+ range of 0 to 1. This condition does makes the model much more difficult to mesh, but is required for accurate simulations of heat transfer. The graphs shown below plot the laterally averaged film cooling effectiveness. The numerical simulation has more access to chord locations upstream, so these is why the numerical graph has more data points. It can be seen that the trends are very similar, but that the numerical model seems to over-predict cooling effectiveness in the cascade at the entrance, but under-predict as the chord length increases. This pver-prediction is probably due to eddies and slight misalignments in the experimental cascade as well as the measurement uncertainties. The under-prediction at the exit is due to anomalous data obtained in the experimental work that should be validated before conclusions are drawn from this data. Also, the definition of chord length in the experimental version has an offset because the 0 chord mark is somewhat upstream of the cascade.

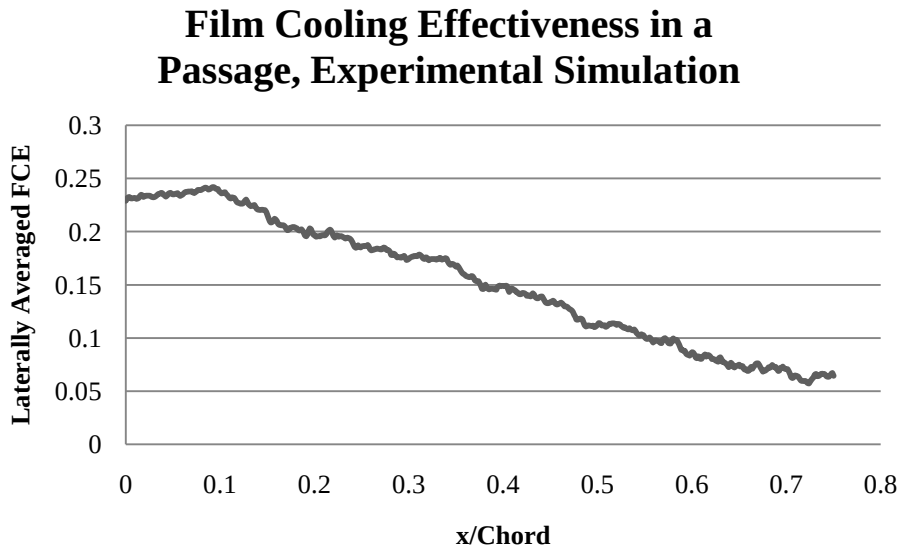

Figure 110: Numerical simulation of laterally averaged FCE in a passage [19].

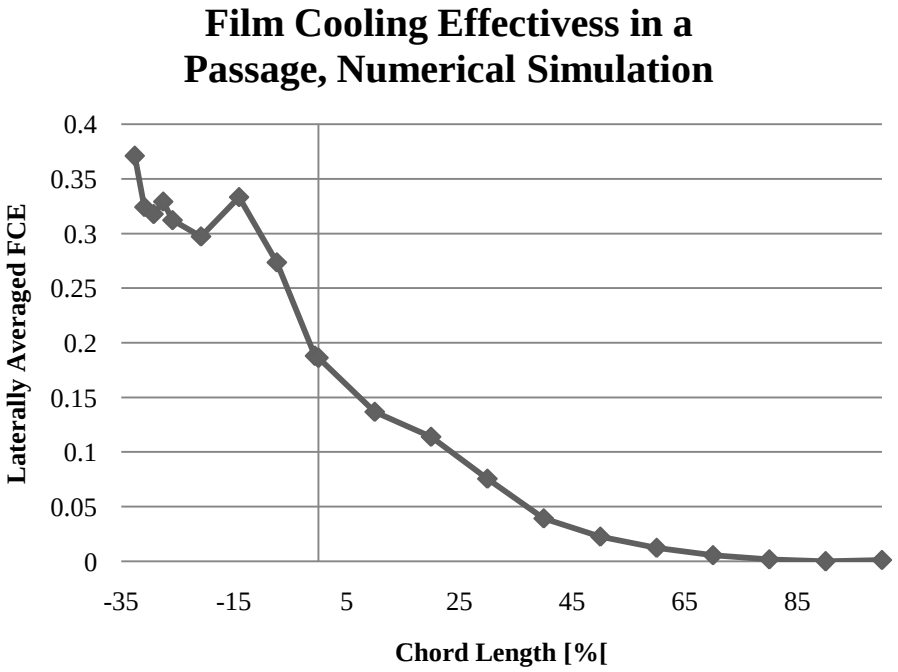

Figure 111: Numerical simulation of laterally averaged FCE in a passage.

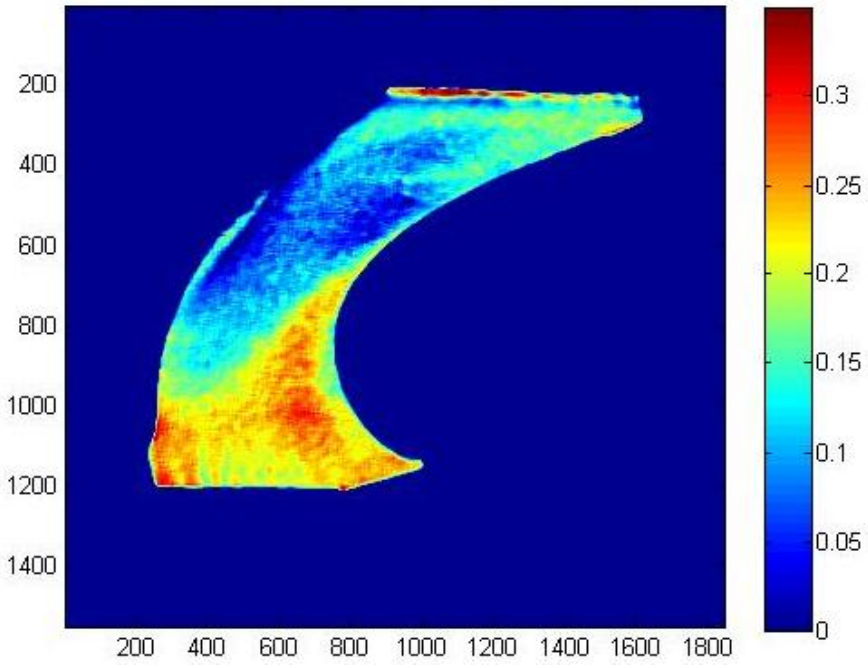

Figure 112: Experimental TSP data analysis of film cooling effectiveness at BR=0.5 [19].

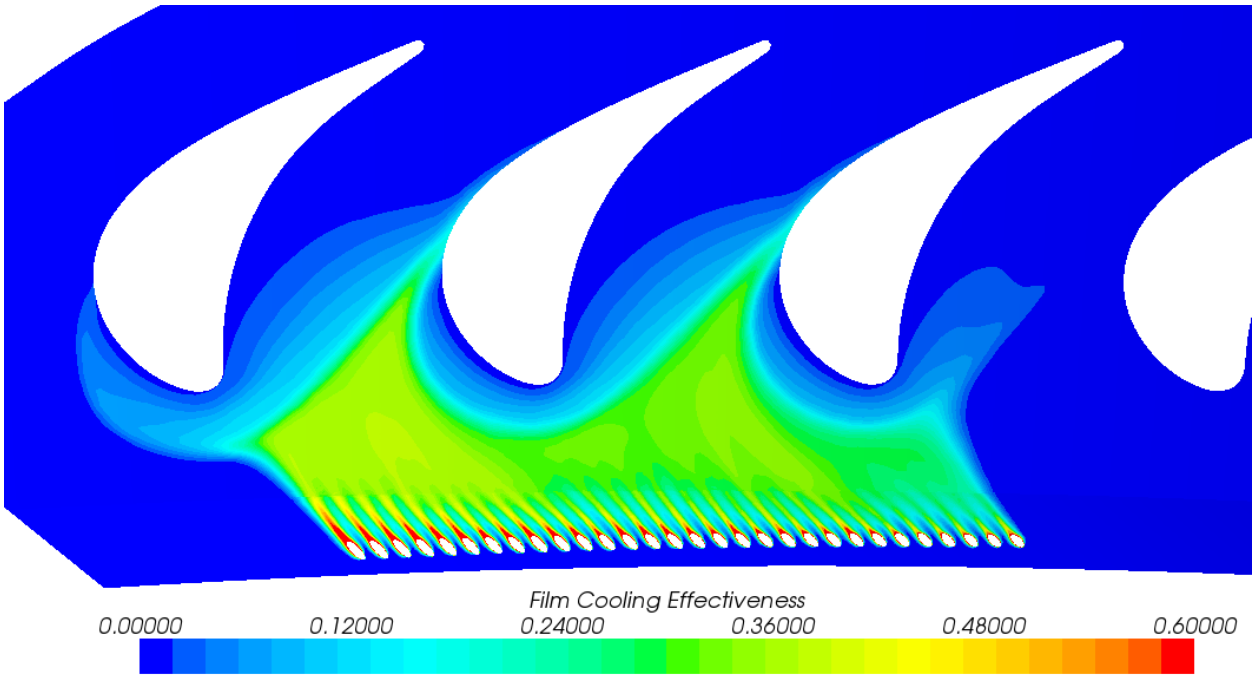

Figure 113: Numerical simulation of film cooling effectiveness at BR=0.5.

CHAPTER 6: CONCLUSIONS AND FUTURE RESEARCH

This work describes the experimental and numerical studies the author performed on the NASA-GE E^3 cascade at the CATER facility and represents all the data obtained since the inception of the project. This work is the first stage in obtaining an understanding of the cascade through experimental and numerical methods. The potential of this rig has not yet been realized because it is still in the process of being fully outfitted and validated. This work will assist with aerodynamic and heat transfer studies on the cascade for many years to come. It is directly applicable to the study of simple film cooling with various blowing ratios and other parameters, but is designed to be expanded to many other areas such as various film cooling geometries such as length/diameter, inclination angle, compound angle, and pitch/diameter. It will also be useful for variations such as purge cooling and trench cooling. The CATER facility is attempting to uses PSP to experimentally determine the pressure distribution over a blade and this thesis has provided resources for this comparison.

Future research can be done on the numerical model to validate and refine many of the initial assumptions made for this iteration of the model such as validating the inlet and outlet conditions numerically and conducting studies to validate these with experimental conditions. Additional measurements should be carried out on the experimental rig to validate the data presented here and then the numerical model should be customized to match these criteria as closely as possible. There are also some portions of the physical model that do not conform to

the ideal model of the test section. Ideally, these should be repaired, but alternatively, the numerical model could also be modeled to match these inaccuracies. These are thought to represent the variations in static pressure loss across the test section that was observed. These differences noted previously are probably due to small misalignments causing losses in the E^3 cascade and the probable differences in mass flow rates from the 3.85 kg/s value from Nguyen [20]. The mass flow through the test section is an important parameter to investigate as this controls many aspects of the numerical simulation. Additionally, little testing has been carried out on the cascade to study the vortex structure inside the passages and map the loss coefficients there. This is another important step for validating the numerical simulation.

When corrections have been made to the model such that it matches the data closely, then many different avenues are opened up for research. Aerodynamically, the static pressures on the endwalls and blades are important as are the total pressure in the passages. In terms of heat transfer, the film cooling effectiveness on the endwalls and blades are important subjects of research. These can all be studied with different types of cooling: discrete hole, purge, and trench with many possible different variations of geometry. This model will serve as a base to assist with validating, testing, and extracting data from many experimental works to come.

APPENDIX A: VALUES FOR DATA EXTRACTION

The purpose of this work is to validate a numerical model, provide comparisons for the current data, and be flexible in assisting future data collection. To accomplish this purpose, data must be able to be extracted at various planes. The values derived by the author will be presented here to assist with this. The calculation of boundary layer thickness was important and this tool from NASA was used in the estimation of y+ values: http://geolab.larc.nasa.gov/APPS/YPlus/

	[in]	[m]
Radius Inner:	38.19	0.970026
Radius Outer:	43.23	1.098042
Width of Cascade:	5.4	0.13716
To end of blades:	0.9	0.02286
To beginning of blades:	4.3	0.10922

	[deg]	[rad]
Total Angle of Cascade:	25	0.4363

	[in]	[m]
Cross-sectional Area:	89.53	0.05776
Perimeter:	45.61	1.15840
Hydraulic diameter:	7.85	0.19944

Nozzle Outlet Conditions for boundary layer estimates

Average speed:	74.6	m/s
Incoming temp:	303	K
Total pressure:	100.71	kPa
Speed of sound:	348.9	m/s
Mach Number:	0.214	
Total temp:	305.77	K
y+ of <1 estimate:	0.0000048	m
Distance to film holes:	0.0797	m
Re:	3.48E+05	
BL Thickness:	6.76E-04	m

The values used for coolant injection are shown below.

Density Mainflow Ave:	1.0908	kg/m^3
Velocity Mainflow Ave:	78.75	m/s
Blowing Ratio	0.5	
Density*Velocity Coolant	42.95	kg/m^2s
Cross-section Area Coolant	9.42E-05	m^2
Mass Flow Coolant	0.004048	kg/s
Temp Coolant	350	K
Temp Mainstream	300	K
Derived Static Pres.	93.92	kPa
Derived Coolant Dens.	0.93	kg/m^3
Derived Coolant Vel.	45.94	m/s
Density Ratio	0.86	

For proper data extraction, planes must be derived from the model. The first step is to define coordinate systems, specifically a cylindrical one. The coordinates should be created from the picking the points on the curve on the back end of the cascade through a tool, but these coordinates must be verified. The specifications should be close to this with respect to the original laboratory coordinate system that is created on import of a geometry, but it has been noted that they will differ slightly based on each individual file:

Radial direction:	[0.089219, -0.996012, -0.0674843 m]
Tangential direction:	[0.996012, .089219, 0]
Axial direction:	[0, 0, 1.0]
Origin:	[-0.02028899, 0.98694173, -0.0674843]

Next, planes must be derived from the model. The ones of significance are those that pass through the cascade and those that are downstream of the coolant holes. For the cascade, radial and z cuts must be made. The radial cuts should be made using the cylindrical tool and the specifications are shown below.

Origin: [0,0,0]
Direction: [0,0,1]
Radius: see values below

Cuts:	Radius [m]	Cuts:	Radius [m]
0%	0.970026	55%	1.0404348
5%	0.9764268	60%	1.0468356
10%	0.9828276	65%	1.0532364
15%	0.9892284	70%	1.0596372
20%	0.9956292	75%	1.066038
25%	1.00203	80%	1.0724388
30%	1.0084308	85%	1.0788396
35%	1.0148316	90%	1.0852404
40%	1.0212324	95%	1.0916412
45%	1.0276332	100%	1.098042
50%	1.034034		

Cuts must also be made in the z-direction of the cascade, which simply use the plane tool. The values are shown below. These were made more difficult because the locations are based on chord length instead of direct distance, so chord was measured in a solid model and points were evenly spaced on it and then the z distance between each point was calculated. The results are shown below.

Total z-length: 3.4"
Total chord length: 4.68"

Cut	Chord [in]	Z-lengths [in]	Z-distance [in]	Z-distance %	Cad location [in]	Cad location [m]
0%	0	0	0	0	4.3	0.10922
5%	0.234	0.1927	0.1927	5.68	4.107	0.10431
10%	0.468	0.2081	0.4008	11.82	3.898	0.09901
15%	0.702	0.2202	0.621	18.32	3.677	0.09340
20%	0.936	0.2297	0.8507	25.10	3.447	0.08755
25%	1.17	0.2355	1.0862	32.04	3.211	0.08155
30%	1.404	0.2329	1.3191	38.91	2.977	0.07562
35%	1.638	0.216	1.5351	45.28	2.760	0.07011
40%	1.872	0.1934	1.7285	50.99	2.566	0.06519
45%	2.106	0.1744	1.9029	56.13	2.391	0.06074
50%	2.34	0.1616	2.0645	60.90	2.229	0.05663
55%	2.574	0.1527	2.2172	65.41	2.076	0.05274
60%	2.808	0.1443	2.3615	69.66	1.931	0.04906
65%	3.042	0.1363	2.4978	73.68	1.795	0.04559
70%	3.276	0.1292	2.627	77.49	1.665	0.04230
75%	3.51	0.1242	2.7512	81.16	1.541	0.03913
80%	3.744	0.1216	2.8728	84.75	1.419	0.03603
85%	3.978	0.1219	2.9947	88.34	1.296	0.03293
90%	4.212	0.125	3.1197	92.03	1.171	0.02974
95%	4.446	0.1308	3.2505	95.89	1.040	0.02641
100%	4.68	0.1394	3.3899	100	0.9	0.02286

The film cooling distances also require derived geometry. For the purposes of this study, the distance was based on the chord length of the blade. In the passage, the FCE was plotted according to the z-direction cascade cuts shown above. Upstream of the passage, the FCE was based on the z/d distance and then converted to chord percentage to preserve constant measurement units. The results of the upstream calculations are shown below. As with the

previous cuts, units are in the z-direction and the origin is based on the cylindrical coordinate system based at the cascade exit.

Film Holes Location :	0.15	m
Cascade 0% Cut:	0.10922	m
Chord Length:	0.11887	m
Film Holes Diameter:	0.002	m

x/d	z-location [m]	Upstream z-distance [m]	Chord %
1	0.148	0.03878	-32.62
2	0.146	0.03678	-30.94
3	0.144	0.03478	-29.26
4	0.142	0.03278	-27.58
5	0.14	0.03078	-25.89
6	0.138	0.02878	-24.21
7	0.136	0.02678	-22.53
8	0.134	0.02478	-20.85
9	0.132	0.02278	-19.16
10	0.13	0.02078	-17.48
11	0.128	0.01878	-15.80
12	0.126	0.01678	-14.12
13	0.124	0.01478	-12.43
14	0.122	0.01278	-10.75
15	0.12	0.01078	-9.07
16	0.118	0.00878	-7.39
17	0.116	0.00678	-5.70
18	0.114	0.00478	-4.02
19	0.112	0.00278	-2.34
20	0.11	0.00078	-0.66

APPENDIX B: MATERIAL DATA SHEETS

The material data sheets for the parts of the test section manufactured at Mydea for the assistance of future research, especially for the understanding of temperature and stress limitations, which are significant when the wind tunnel is run in closed loop mode.

STRATASYS®

ABS

ABS is a strong, durable production-grade thermoplastic used across many industries. ABS is an ideal material for conceptual prototyping through design verification through direct digital manufacturing. The marriage of ABS with FDM technology gives you the ability to create Real Parts™ direct from digital files, in a variety of standard and custom colors. Refer to the FDM System Material Availability spec sheet for system availability and color options.

Mechanical Properties[1]	Test Method	Imperial	Metric
Tensile Strength, Type 1, 0.125	ASTM D638	3,200 psi	22 MPa
Tensile Modulus, Type 1, 0.125	ASTM D638	236,000 psi	1,627 MPa
Tensile Elongation, Type 1, 0.125	ASTM D638	6 %	6 %
Flexural Strength	ASTM D790	6,000 psi	41 MPa
Flexural Modulus	ASTM D790	266,000 psi	1,834 MPa
IZOD Impact, notched	ASTM D256	2 ft-lb/in	106.78 J/a
IZOD Impact, un-notched	ASTM D256	4 ft-lb/in	213.56 J/a

Thermal Properties	Test Method	Imperial	Metric
Heat Deflection Temperature @ 66 psi	ASTM D648	195° F	90° C
Heat Deflection Temperature @ 264 psi	ASTM D648	169° F	76° C
Glass Transition Temperature (Tg)	DMA (SSYS)	219° F	104° C
Coefficient of Thermal Expansion	ASTM D696	5.60E-05 in/in/F	- - - - -
Melt Point	- - - - - - - - -	Not Applicable[2]	Not Applicable[2]

Other	Test Method	Value
Specific Gravity	ASTM D792	1.05
Rockwell Hardness	ASTM D785	R105
Flame Classification	UL 94	HB
Dielectric Strength kV/mm	IEC 60112	32
Dielectric Constant @60Mhz	IEC 60250	2.4

Figure 114: Material data sheet for film cooling section.

WC-788 A/B
WATER CLEAR RIGID 84 SHORE D URETHANE CASTING SYSTEM

PRODUCT DESCRIPTION:

WC-788 A/B is an impact resistant, rigid, 84 Shore D aliphatic polyurethane that is commonly used to make clear or tinted castings of all kinds. Note: WC-788 A/B requires post-curing. Thin section casts, less than ½" thick, may require in mold post-curing. See post-cure instructions on page 2.

PRODUCT HIGHLIGHTS:

- Colorless with exceptional clarity
- Excellent impact strength
- 15 minute standard working time with six additional work speeds available
- No odor
- Good weatherability, non-yellowing all aliphatic
- Excellent heat resistance

PHYSICAL PROPERTIES:

Hardness, Shore D ASTM D-2240	84 ± 2
Density (g/cc) ASTM D-792	1.1
Cubic Inches Per Pound	26.2
Color/Appearance	Water clear/colorless
Tensile Strength, (psi) ASTM D-638	8,300
Tensile Modulus, (psi) ASTM D-638	2.7×10^5
Elongation, (%) ASTM D-638	20
Flexural Strength, (psi) ASTM D-790	11,200
Flexural Modulus, (psi) ASTM D-790	3.0×10^5
Shrinkage, (in./in.) linear (12"x ½ "x ½ ")	0.006
Izod Impact, notched (ft.-lb./in.) ASTM D-256	1.1
Heat Deflection Temperature, (@ 66 psi) ASTM D-648	175°F (79°C)
Index of Refraction ASTM D-542	1.49

Figure 115: Material data sheet for clear inner endwall.

POLYJET TECHNOLOGY > MATERIALS

FullCure™ 700 Series Photopolymer Materials

- Good impact strength
- No additional curing required
- Absorbs paint, can be machined, drilled, chrome-plated or used as a mold
- Elongation at break enables snap fit

Part of an expanded line of proprietary photopolymer resins, FullCure™ 700 Series are designed for precise jetting in super fine layers by PolyJet™ technology inside the Eden333 and 260 from Stratasys. Both model and non-toxic, gel-like support materials come in sealed, easy to handle 2kg cartridges easily replaced through a front-loading door.

Property	Standard Procedure	Value
Tensile Strength	D-638	42.3 MPa
Elongation at break	D-638	15%-25%
Modulus of Elasticity	D-638	2000 MPa
Flexural Strength	D790	70.6 MPa
Flexural Modulus	D790	1978 MPa
Izod Notched Impact	D256	25-38 J/m
Heat Distortion Temperature	D648@ 0.45Mpa (66psi)	110° F (43° C)
	@ 1.82Mpa (264psi)	115° F (46° C)
Compression Strength	D695	69.4 MPa
Rockwell	Scale M	81.0

Ash Content: The ash content of the FullCure 720 is < 0.01% at 1000° C **Resin Density:** Liquid model resin (RT) 1.092 gr/cc **Coefficient of Thermal Expansion:** @ 30-35°C: (34.6 ± 4.7) X 10-6 m/m°C @40-70°C: (60.8 ± 9.5) X 10-6 m/m°C @ 75-90°C: (104.4 ± 8.5) X 10-6 m/m°C @ 95-110°C (122.2 ± 4.0) X 10-6 m/m°C

For more information about Stratasys systems and materials, contact your representative or visit **www.stratasys.com**

DRIVE DESIGN. CONTROL RP.™ STRATASYS®

Figure 116: Material data sheet for film cooling coupon.

REFERENCES

[1] T. Casey, "The Aerodynamic Losses with the Addition of Film Cooling in a High-Speed Annular Cascade", H.I.M. thesis, University of Central Florida, Orlando, FL, 2010.

[2] R.J. Goldstein, E.R.G. Eckert, F.K. Tsou, A. Haji-Sheikh, "Film Cooling with Air and Helium Injection Through a Rearward-Facing Slot into a Supersonic Air Flow", AIAA Journal, Vol. 4, No. 6, June 1966 pp. 981-985.

[3] Cross-sectional view of turbine, [Online image], http://www.rchelisite.com/how_turbine_rc_ helicopters_work.php, Feb. 27, 2011.

[4] E.L. Knuth, "Mechanics of Film Cooling", Jet Propulsion, Vol. 25, No. 1, January 1955, pp. 16-25.

[5] R.J. Goldstein, E.R.G. Eckert, F. Burggraf, "Effects of Hole Geometry and Density on Three-Dimensional Film Cooling", International Journal of Heat and Mass Transfer, Vol. 17, 1974, pp. 595-607.

[6] L.S. Langston "Crossflows In A Turbine Cascade Passage", Journal of Engineering for Power, Vol. 102, Number 4, October 1980, pp. 866-874.

[7] A.D. Fitt, J.R. Ockendon, T.V. Jones, "Aerodynamics of slot-film cooling: theory and experiment", Journal of Fluid Mechanics, Vol. 160, Nov. 1985, pp. 15-27.

[8] S. Friedrichs, H.P. Hodson, W.N. Dawes, "Distribution of Film-Cooling Effectiveness on a Turbine Endwall Measured Using the Ammonia and Diazo Technique", Journal of Turbomachinery, Vol. 118, 1996, pp. 613-621.

[9] S. Friedrichs, H.P. Hodson, W.N. Dawes, “Aerodynamic Aspects of Endwall Film-Cooling”, Journal of Turbomachinery, Vol. 119, 1997, pp. 786-793.

[10] A.K. Sinha, D.G. Bogard, M.E. Crawford, "Film-Cooling Effectiveness Downstream of a Single Row of Holes With Variable Density Ratio", Journal of Turbomachinery, Vol. 113, July 1991, pp. 442-449.

[11] H.D. Ammari, N. Hay, D. Lampard, “The Effect of Density Ratio on the Heat Transfer Coefficient from a Film-Cooled Flat Plate”, Journal of Turbomachinery, Vol. 112, July 1990, pp.444-450.

[12] H.D. Ammari, N. Hay, D. Lampard, “Effect of Density Acceleration on the Heat Transfer Coefficient on a Film-Cooled Surface”, Journal of Turbomachinery, Vol. 113, July 1991, pp.464-471.

[13] J.P. Bons, C.D. MacArthur, R.B. Rivir, “The Effect of High Free-Stream Turbulence on Film Cooling Effectiveness”, Journal of Turbomachinery, Vol. 118, October 1996, pp.814-825.

[14] M. Gritsch, A. Schulz, S. Wittig, “Adiabatic Wall Effectiveness Measurements of Film-Cooling Holes with Expanded Exits”, Journal of Turbomachinery, Vol. 120, July 1998, pp.549-556.

[15] A. Kohli, D.G. Bogard, “Effects of Very High Freestream Turbulence on the Jet-Mainstream Interaction in a Film Cooling Flow”, Journal of Turbomachinery, Vol 120, October 1998, pp.785-790.

[16] C.M. Bell, P.M. Ligrani, W.A. Hull, C.M. Norton, “Film cooling subject to bulk flow pulsations: effects of blowing ration, freestream velocity, and pulsation frequency”, International Journal of Heat and Mass Transfer, Vol. 42, Issue 23, December 1999, pp.4334-4344.

[17] P. M. Ligrani, C. M. Bell, “Film cooling subject to bulk flow pulsations: effects of density ratio, hole length-to-diameter ratio, and pulsation frequency” International Journal of Heat and Mass Transfer, Vol. 44, Issue 10, May 2001, pp.2005-2009.

[18] C.Q. Nguyen, J Kullberg, W. McDonald, S.H. Ho, M. Ricklick, J.S. Kapat, "Numerical and Experimental Study of Trenched Film Hole Cooling for a Realistic Cascade with an Annular Endwall: Test Rig Construction and Preliminary Data", 48th AIAA Aerospace Sciences Meeting, Orlando, FL, Jan. 4-7, 2010.

[19] T. Casey, C.Q. Nguyen, J Kullberg, M. Ricklick, J.S. Kapat, "Numerical and Experimental Study of Film Cooling Effectiveness and Total Pressure Loss for a Realistic Cascade with an Annular Endwall", 49th AIAA Aerospace Sciences Meeting, Orlando, FL, Jan. 4-7, 2011.

[20] C.Q. Nguyen, "Interaction Between Secondary Flow & Film Cooling Jets of a Realistic Annular Airfoil Cascade (High Mach Number)", Ph.D. thesis, University of Central Florida, Orlando, FL, 2010.

[21] F.C. Kopper, R. Milanot, M. Vancot, "Experimental Investigation of Endwall Profiling in a Turbine Vane Cascade", AIAA Journal, Vol. 19, Issue 8, pp. 1033-1040

[22] Friedrich Kost, "Film-Cooled Turbine Endwall in a Transonic Flow Field: Part 1 - Aerodynamic Measurements", Journal of Turbomachinery, Vol. 123, No. 4, October 2001, pp. 709-719.

[23] Martin Nicklas, "Film-Cooled Turbine Endwall in a Transonic Flow Field: Part II - Heat Transfer and Film-Cooling Effectiveness", Journal of Turbomachinery, Vol. 123, No. 4, October 2001, pp. 720-729.

[24] Luzeng J. Zhang, Ruchira Sharma Jaiswal, "Turbine Nozzle Endwall Film Cooling Study Using Pressure Sensitive Paint", Journal of Turbomachinery, Vol. 123, No. 4, October 2001, pp.730-738.

[25] K.A. Thole, D.G. Knost, "Heat transfer and film-cooling for the endwall of a first stage turbine vane", International Journal of Heat and Mass Transfer, Vol. 48, Issues 25-26, December 2005, pp.5255-5269.

[26] M. Hung, P. Ding, P. Chen, "Effects of Injection Angle Orientation on Concave and Convex Surfaces Film Cooling", Journal of Experimental Thermal and Fluid Science, Vol. 33, Issue 2, January 2009, pp. 292-305.

[27] D.G. Bogard, K.A. Thole, "Gas Turbine Film Cooling", Journal of Propulsion and Power, Vol. 22, No. 2, March-April 2006, pp. 249-270

[28] L.P. Timko, "Energy Efficient Engine: High Pressure Turbine Component Test Performance Report", prepared for National Aeronautic and Space Administration, Jan. 1, 1984.

[29] R.D. Mehta, P. Bradshaw, "Technical Notes: Design rules for small low speed wind tunnels", The Aeronautical Journal of the Royal Aeronautical Society, November 1979, pp. 443-449.

[30] "Conventional Multi-Hole Probes", Aeroprobe Corporation, Mar. 1, 2011, http://www.aeroprobe.com/docs/Conventional-Probes-for-web.pdf.

[31] Diagram of five hole probe tip, [Online image], http://www-g.eng.cam.ac.uk/whittle/current-research/hph/pressure-probes/pressure-probes.html.

[32] Q. Lui, "Study of Heat Transfer Characteristics of Impinging Air Jet Using Pressure and Temperature Sensitive Luminescent Paint", Ph.D. thesis, University of Central Florida, Orlando, FL, 2006.